Quantitative Analysis of the Amorphous Phase and Multiple Polymorphs of Model Sulfa-Drugs; Sulfamerazine and Sulfathiazole

Pól MacFhionnghaile

PhD. Thesis

Supervisors: Dr. Andrea Erxleben, Prof. Patrick McArdle

National University of Ireland, Galway

Ollscoil na hÉireann, Gaillimh

Table of contents

Abstract

Polymorphic transformations are known to occur as a result of many factors, one of the most prominent being recrystallisation from different solutions. Though other factors have been known to induce polymorphic change, these can include environmental factors and mechanical/physical stress. During many manufacturing processes mechanical stress such as milling or compression can induce polymorphic transformation,[1] as well as environmental effects during storage such as changes in temperature or humidity.[2] In this body of work the solid state transformations of two model polymorphic drugs, sulfamerazine and sulfathiazole, were studied. For this accurate analytical methods were developed for comprehensive polymorphic analysis.

Previous studies have shown the effects of mechanical stress on the solid state chemistry of sulfamerazine. It has already been shown that compression during tabletting can cause transformation from sulfamerazine form I (FI) to form II (FII),[1] that cryo-milling can generate amorphous content,[3] and milling at room temperature can transform FI to FII.[4] In this work, methods to prepare bulk FII from FI were reviewed. Both forms I & II of sulfamerazine were monitored during milling at room temperature and low temperatures, achieving the first complete transformation to sulfamerazine's amorphous phase (FA). FA produced from cryo-milling both FI and FII at different time intervals were compared to determine the optimal method to prepare (FA) for multivariate analysis. This optimal method resulted in the most stable amorphous phase, while taking the least amount of time to prepare. FI, FII and FA were used to prepare binary and ternary mixtures for chemometric models using XRPD, NIR and IR spectroscopy. This gave a novel means to analysis and monitors the solid state transformations of sulfamerazine observed during the room temperature milling and cryo-milling of FI and FII. The shelf-life of FA was also monitored when stored under vacuum at 4^{o}C and room temperature using these calibration models.

For the work with sulfathiazole, low content analysis of different solid sates was used to determine the limitations of a number of analytical techniques such as XRPD, NIR and IR

spectroscopy. The analytical method that produced the most accurate calibrations was used in other studies. For the first time the amorphous phase of sulfathiazole was prepared via cryo-milling forms I and III. These produced purer samples of the amorphous phase when compared to samples prepared by the melt quench method. With a successful method to prepare pure samples of the amorphous phase, novel ternary studies containing the amorphous phase of sulfathiazole, and form I and form III were used to create ternary regression models from two different data sets, which were then compared. One ternary study was designed to focus on low content analysis, while the other was designed to focus on whole content analysis. The ternary system that gave the best results was then used to monitor the solid state transformations of forms I and III to the amorphous phase during cryo-milling.

Acknowledgments

I would first like to express my gratitude to Dr. Andrea Erxleben, Prof. Pat McArdle, and Dr. Yun Hu, who have guided me throughout my research with their expertise, encouragement, supervision, and patience. It has been a great pleasure and privilege to have had worked with such great people.

I would also like to thank the academic staff of the School of Chemistry, NUIG. Particularly to Dr. Leigh Jones and Dr. Alan Ryder for their discussions, welcoming attitudes and expressing their outlook.

My thanks go to the technical staff of NUIG's School of Chemistry, particularly to Marian Vignoles, Jim Cotter, Seamus Collier, Seamus Kellahan, Gerry Reilly, and Dermot McGrath. I find it difficult to express the aid and advice they gave me in solving problems, and their patience they showed me through many years of many demands.

I owe many thanks for the help that I have received from undergraduate students who have helped me throughout the years. Even though your work may of seemed underwhelming at the time, it did greatly help me. Two names that will stick in my mind (for the better) are James Basquill and Katarzyna Gniado, thank you for your amazing work.

Throughout the years of my research, I do not believe I've had to chance to adequately thank the many people that I have the luck to call friends. These people gave me support, have shown me patience, and distracted me from things I needed to be distracted from. With too many to thank I can only name a few. Firstly, I would like to thank my oldest and best friend Ciarán MacGinley, a true inspiration in kindness and new ways of thinking. To Fiona Griffin, I honestly have no idea how to express the thanks I owe you, but I'll start off with a simple 'thank you'. To Noel, Rob, Edel, Nora, and Cecelia I thank you for expanding 'philosophical views' as well as the many years of help and good times in the labs, I can honestly say I'll find it difficult to find better people to work with. To past member of the labs, Peter Dunne, Mairead Cruschel, and David Frain, thank you for introducing me into the life of a postgrad. I would like to express great thanks to Peadar Quinn, Ciaran Nixon, and Doug (aka Pa') Coleman for being

amazing people and great friends. I would like to thank Sarky for showing me the true meaning of Christmas. To all my friends I've meet growing up I thank you all, as there are too many of you to name. Favouring some over others I will mention Ciaran Diver, Marty, Conal, Eamon, Ray, and Kieran (Mac) McGee. To the many member of the FanSci Soc. NUIG, thank you for welcoming me and acting as hub of good friends when I first moved to Galway. Particularly to Garda Paraic Barrett, a good friend who's aspirations in life and work are humbling and deserve note of respect. To Dr. Alan Bergin, Wade Wilson, Ruth Campion, Kevin McCarthy, and Ray Flynn, thank you bringing an element of surprise to most weekends during my time in Bohermore. And to Bryan DeVany thank you for your patience and friendship in the last few months.

Lastly I would like to thank my family. To my mother (Margret), father (Owen), sister (Eilis), and the family of Padraig McGinley. To whom I owe the greatest thanks for my upbringing, my values and getting me where I am today. I only wish Sean and Vava were here to thank in person.

List of publications

Papers published

'Formation, physical stability, and quantification of process-induced disorder in cryomilled samples of a model polymorphic drug'; Yun Hu, Pól MacFhionnghaile, Vincent Caron, Lidia Tajber, Ann Marie Healy, Andrea Erxleben, Pat McArdle; *Journal of Pharmaceutical Science, 2013, 102(1) pp. 93-103*

'A comprehensive near infrared spectroscopic study of the limits of quantitative analysis of sulfathiazole polymorphism'; Pól MacFhionnghaile, Yun Hu, Pat McArdle, Andrea Erxleben; *Journal of Near Infrared Spectroscopy, 2013, 21(1), pp. 55-66*

Publications in preparation

'**Effects of Room Temperature and Cryo-milling on Sulfamerazine Polymorphs: a Quantitative Study';** Pól MacFhionnghaile, Katarzyna Gniado, Yun Hu, Pat Mc Ardle, Andrea Erxleben

Conference contributions

'Solid State Transformations of Sulfamerazine'; Oral presentation at the Irish Universities 64th Chemistry Research Colloquium; at Trinity College Dublin, Dublin, Ireland

'Ternary Analysis of Amorphous and Crystalline Sulfathiazole'; Oral presentation at PharSci 2011, University of Nottingham, Nottingham, UK

'Analysis of Amorphous and Crystalline Sulfamerazine'; Poster presented at CGOM10; University of Limerick, Limerick, Ireland.

'Analysis of Amorphous and Crystalline Sulfamerazine'; Poster presented at the Irish 64th Universities Chemistry Research Colloquium; University of Limerick, Limerick, Ireland.

'Quantification of the Amorphous and Crystalline Contents of Pharmaceutical Solids'; Poster presented at FACSS 2010; Raleigh, North Carolina, USA

Abbreviations

Analytical;

- **ss(as prefix);** Solid State
- **API;** Active Pharmaceutical Ingredient
- **IR;** Infrared
- **ATR-IR;** Attenuated Total Reflection - Infrared
- **UV;** Ultra Violet
- **NIR;** Near Infrared
- **PAT;** Process Analytical Technology
- **SEM;** Scanning Electron Microscope/Microscopy
- **NMR;** Nuclear Magnetic Resonance
- **DSC;** Differential Scanning Calorimetry
- **mDSC;** modulated Differential Scanning Calorimetry
- **T_g;** Glass transition temperature
- **T_c;** Temperature of crystallisation

Chemometric;

- **SNV;** Standard Normal Variate
- **MSC;** Mass/Multiplicative Scattering Correction/Correlation
- **OSC;** Orthogonal Signal Correlation
- **XRPD;** X-ray Powder Diffraction
- **HPLC;** High Pressure/Performance Liquid Chromatography
- **PC;** Principlal Component
- **PCA;** Principal Component Analysis
- **PCR;** Principal Component Regression
- **PLS;** Partial Least Squares
- **MCR;** Multiple Linear Regression
- **RMSEC;** Root Mean Square Error Calibration

- **RMSECV;** Root Mean Square Error Cross Validation
- **RMSEP;** Root Mean Square Error Prediction
- **LOD;** Limit of Detection
- **CCDC;** Cambridge Crystallographic Data Centre

Chapter One

Introduction

&

Theory

Crystalline solids

Crystalline materials, found throughout nature, can show variations in the arrangement of the molecules or ions in the crystal lattice. This is the result of the rearrangement of hydrogen bonding (H bonding) and other intermolecular forces, manifesting as changes to a variety of physical and chemical properties and a different crystalline lattice. The different crystal forms can be categorised into two main groups, true polymorphism, consisting of polymorphs and an amorphous phase, which are purely composed of the compound, or pseudo-polymorphs, such as solvates. This work focuses on preparation of different true polymorphs, and generation of quantitative methods used to monitor polymorphic transformations. Figure 1.1a & b shows how two different polymorphs, where both are made of the same Active Pharmaceutical Ingredient (API), can have entirely different molecular arrangements. IFigure 1.1c shows an API with no long range order or arrangement, and is thus called the amorphous phase, having no discernible shape. It can be clearly seen that even though these different forms are of the same API, they have unique structures, and will possess unique properties. Figures 1.1d - f illustrate polymorphs in which another component has been introduced, forming intermolecular interactions with the API, but not reacting with it. Figure 1.1d, shows when solvent molecules are incorporated into the crystal lattice creating a solvate, which can carry the added benefit of being more readily soluble in certain solvents. Co-crystals (figure 1.1e) consists of an API and one or more co-crystal formers which are solid at room temperature.

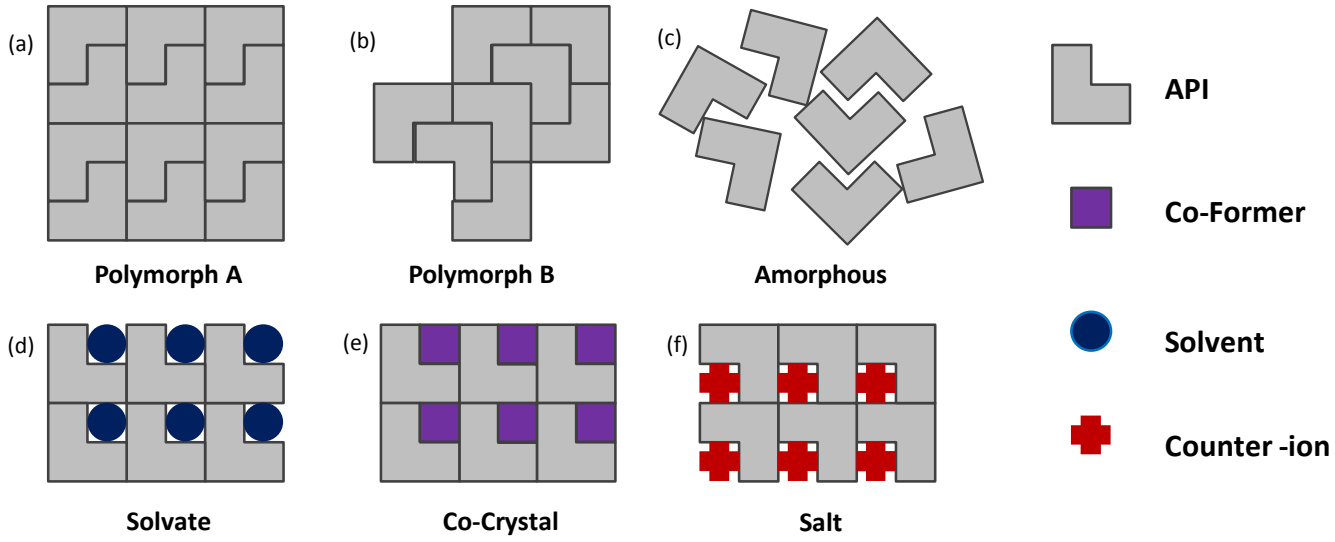

Fig. 1.1 Solid states of an API (a) one polymorph of an API, (b) another polymorph of the API, (c) the amorphous phase, (d) a solvate, (e) a co-crystal, and (f) a salt of the API

These enable a combination of desired API with other beneficial APIs, or excipients to enhance some physical or chemical properties of the drug. Figure 1.1f illustrates an API salt. This is usually a deprotonated API ionically bonded to a cation (or a protonated API to an anion) giving a salt which ideally will retain all the beneficial properties of the API, and can improve its solubility resulting from it being a salt. The different crystalline forms of an API differ primarily in hydrogen bonding (H bonding) and to a lesser extent other inter-molecular forces such as van der Waals forces and π-stacking. These changes in crystalline forms have great potential in altering the physical and chemical properties of an API, where its solubility, stability, and even bioavailability can be affected. This merits the study of the solid state structures of APIs as an essential investigation in the production of pharmaceuticals.[5] Furthermore, due to the relatively small energy that separates different polymorphs, polymorphic transformations of an API can occur during manufacturing processes or due to a range of environmental factors during storage, leading to the formation of an unwanted solid state form with undesirable physical or chemical properties.

One case exemplifying the problems associated with unstudied polymorphism of a compound is that of Ritonavir, an antiviral drug used in the treatment of AIDS. In this case polymorphic analysis was neglected and resulted in its withdrawal from the market when the polymorphic transformation of the pharmaceutically active polymorph to a less stable polymorph occurred. Because of this, Abbott had to revise the formulation of the drug to a gelcap instead of a semi-liquid capsule, costing them greatly in both time and money.[6] Due to the vast differences that exist between different polymorphs, patents can be awarded separately, even where one polymorph has already received regulatory approval, allowing the extension of a pharmaceutical's patent. In a well-known case, GlaxoSmithKline extended their patent of Zantac following the discovery of a new polymorph (type II) when the patent to older polymorph (type I) had expired. Calcipotriol is a vitamin D analogue and is used as API in pharmaceutical formulations against psoriasis. It exists as two pseudopolymorphs, the anhydrate and the monohydrate,[7] the latter of which, can be found in commercially available topical creams. Since the API monohydrate exhibits greater pharmaceutical potency, tracing of anhydrate crystals in the cream as well as the evaluation of their stability is needed to ensure a uniformly potent topical cream.[8, 9] These are just a few examples illustrating the necessity for pharmaceutical manufacturer to be aware of possible solid state transformations of an API

during production, and the penalties in neglecting it. Underscoring the statement of Walter McCrone, that

"every compound has different polymorphic forms, and that, in general, the number of forms known for a given compound is proportional to the time and money spent in research on that compound."[10]

When dealing with an API which has multiple crystalline phases, it is possible that solid state transformations occur without the addition of another component due a number of environmental factors during storage or manufacturing. This can include grinding / milling,[11] recrystallisation,[12] tabletting,[13] and even storage conditions.[2] Because of this the polymorphism of an API must be investigated, and an accurate means of analysis, identification, and knowledge of its crystallisation pathways are needed. The analysis of crystalline material is hindered by the fact that the analysis being conducted must be in the solid state. This limits the variety of methods that can be applied, ruling out many conventional methods of analysis, such as Ultra Violet-Visible Spectroscopy (UV-Vis), or any technique requiring the dissolution of the analyte. The focus of solid state analysis is to create an efficient and accurate, and if possible *in situ,* method of monitoring any changes that may occur to the solid state of an API. This has led the way for computational models for data analysis to be used to create regression models, which has been aided by the advancements in technology in recent years. This is particularly needed when dealing with the amorphous phase of an API, where recrystallisation can lead to a number of crystal forms.

Polymorphs

Polymorphism is a phenomenon where a compound may exist as a number of crystalline phases, deriving from changes in intermolecular bonding between molecules. Below is the definition as given by Walter McCrone;

"A polymorph is a solid crystalline phase of a given compound resulting from the possibility of at least two different arrangements of the molecules of that compound in the solid state. The molecule itself may be of different shape in the two polymorphs, but that is not necessary and, indeed, certain changes in shape (involving dynamic isomerism or tautomerism) involve formation of different molecules and hence do not constitute polymorphism."[14]

One of the earliest found observations of polymorphism is thought to be work conducted by Klaproth in 1788, where it was found that calcium carbonate can recrystallise as calcite, and aragonite. Humphrey Davy is regarded as the first to remark on the changes in physical and chemical properties resulting from different phases in 1809, in his work on diamond and graphite. However it was Mitscherlich who was the first to coin the phrase polymorphism in 1822 during his work on metal sulphates.[15] These led to the development of important theories on polymorphism in the latter half of the 19th century, one of the most prominent being Ostwalds step; Go further in Ostwalds rule, ref the diagrams, mention poltmorphs with forms

"The empirical observation that crystallisation from a solution occurs in steps in such a way that often thermodynamically unstable phases must first, be followed by the thermodynamically stable step"[16, 17]

Figure 1.2 shows the transformation of the least stable polymorph (Form a) to the most stable polymorph (Form d) by first crystallising to the other metastable polymorphs (Forms b and c).

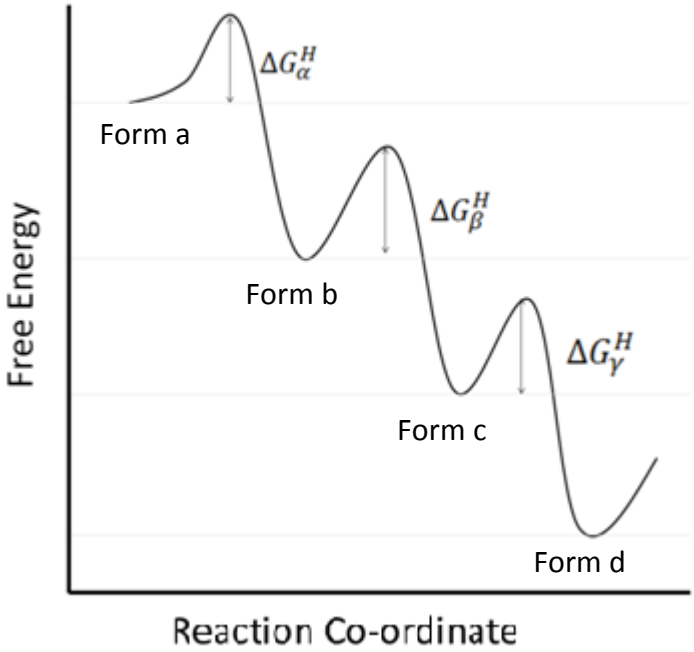

. **Fig. 1.2** Schematic representation of Ostwald's Rule of Stages with Form a being the least stable polymorph

Because polymorphism is the result of changes in intermolecular forces, the most prominent being H bonding, an array of effects can be observed. Table 1.1 shows the physical and chemical effects that can change due to polymorphism. Because these changes are so prevalent, it is necessary to distinguish between different polymorphs and to understand how they may arise. Polymorphic transformations can be induced using many practices, which include the solvent (or solvent mixture) used in crystallisation, the time taken for crystallisation, or the agitation of the mixture. The before mentioned methods are primarily used in the formulation of the API, but other factors such as mechanical stress and the storage environment must also be taken into consideration, seeing that they can also induce polymorphic change.

Packing properties	Molar volume and density
	Refractive index
	Conductivity: electrical and thermal
	Hygroscopicity
Thermodynamic properties	Melting and sublimation temperatures
	Internal or structural energy
	Enthalpy
	Heat capacity
	Entropy
	Free Energy and Chemical Potential
	Thermodynamic Activity
	Vapour Pressure
	Solubility
Spectroscopic properties	Electronic state transitions
	Vibrational state transitions
	Nuclear spin state transitions
Surface properties	Kinetic properties
	Rates of solid-state reactions
	Dissolution rate
	Stability
	Surface free energy
	Interfacial tensions
Mechanical properties	Crystal habit
	Hardness
	Tensile strength
	Compactibility, tabletting
	Handling, flow, and blending

Table 1.1 Property changes resulting from solid state changes

Another factor to be aware of is the existence of two thermodynamic types of polymorphs, the enantiotropy systems (which can allow reversible polymorphic transformation to occur under heating or cooling), and the monotropic systems (where transformations of these sorts are irreversible). This furthers the need for in depth analysis of an API's solid phases. Figure 1.3 illustrates the difference of thermal energy in enantiotropic and monotropic systems. Here it can be seen a transition can occur in the solid phase of the enantiotropic system where G (form 1) is isoenergetic (G form 2). In the monotropic system the solid melts (as can be seen by G (liquid) before the free energies of form 1 and 2 cross.

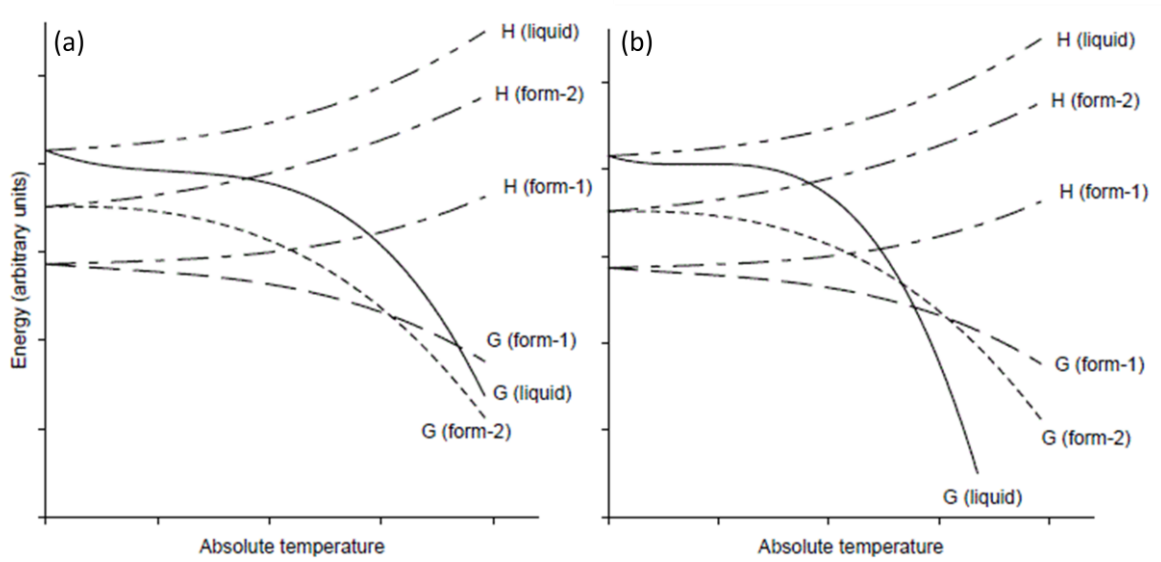

Fig. 1.3 The temperature dependence of the enthalpy (H) and free energy (G) for two polymorphic systems of (a) an enantiotropic system, and (b) monotropic system

The amorphous phase

The amorphous phase of a solid is regarded as a phase which possesses no long-range crystal order, typically exhibiting short range order in the order of a few molecules in dimensions. This gives way to a system with a higher surface free energy, which increases its molecular mobility, and changes many physical properties with regard to its crystalline counterparts. These can include increased solubility and bioavailability. Because of this, the amorphous phase can be highly sought after, but is regarded as the least stable state of true polymorphs, showing a decrease in melting point temperature, stability in accordance to Ostwald's step rule that the crystallisation of an unpredicted or undesired polymorph can occur from its recrystallisation. Also when dealing with amorphous materials, there are many subtle factors that can influence nucleation and crystallisation, giving way to a situation where the crystallisation of multiple polymorphs is possible, raising challenges when making predictions in its crystallisation. Despite its problems the amorphous phase of an API can be very beneficial, if it can be produced to be adequately stable. This leads to a desire to produce amorphous APIs and to examine their properties.

Below are a number of methods used to prepare amorphous materials.

- Mechanical milling
- Cryo-milling
- Tabletting
- Preparation from solvent (evaporation)
- Condensation
- Supercooling of melt (melt quench)
- Spray drying
- Freeze drying

The tendency for crystallisation is governed primarily by two factors; the degree of molecular mobility and the thermodynamic driving force of crystallisation. These factors can be manipulated to induce the generation of the amorphous phase. Many of the techniques listed above are found in the manufacturing of APIs as secondary manufacturing processes, where the chances of generating amorphous content (or inducing polymorphic transformation) can be

at their highest. Because the pharmaceutical industry uses many of these methods in secondary processes during the production of an API, a means to have a quality assured, homogenous and uniform product is needed.

As these procedures to generate amorphous content are found industrially, reliable methods are needed to indentify and monitor amorphisation during production. Due to its unique properties, resulting from a lack of crystallinity, amorphous content has many characteristic properties observable by differential scanning calorimetry (DSC) or X-ray powder diffraction (XRPD). One of the most important properties utilised in the analysis of amorphous content is its glass transition temperature (T_g). This is the temperature at which a compound in the amorphous phase can turn 'glassy'. The T_g is unique to the amorphous phase, and is observed as a thermal event by a slight change as a bump or kink in a DSC plot, showing either an increase or decrease in its the heat capacity (Figure 1.4). This however can be overlapped with other thermal events such as temperature of crystallisation, moisture being evaporated from the compound, etc.

Another property resulting from a lack of crystallinity can be found in the XRPD pattern, as an amorphous 'halo' or 'hump'. Here all diffraction peaks of a compound have deteriorated into a hump showing no peaks, due to its lack of crystalline properties.

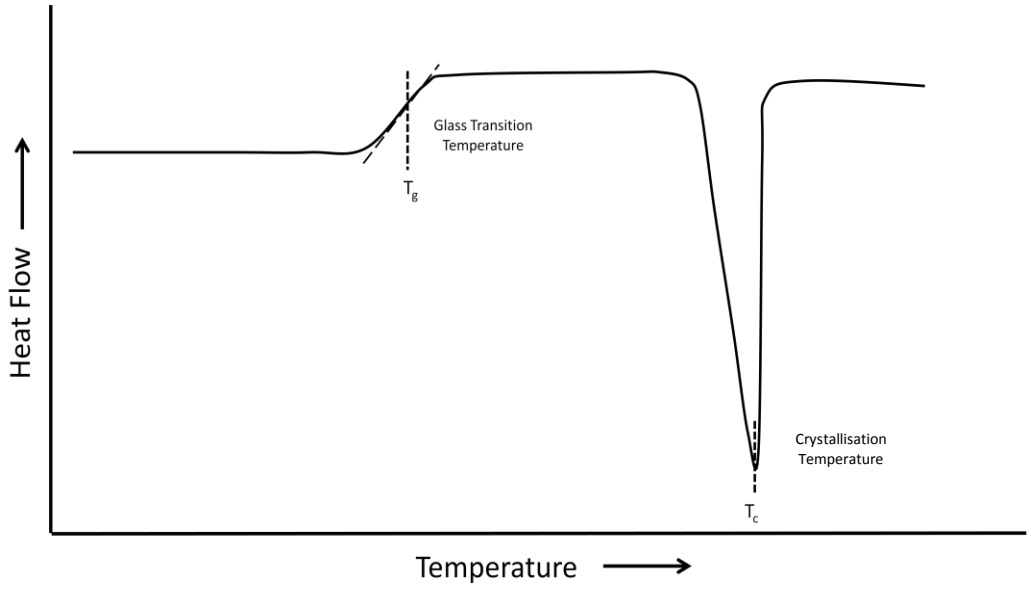

Fig. 1.4 Diagram representing the DSC pattern of an amorphous pharmaceutical

Analysis of solid state pharmaceuticals

Due to many physical and chemical properties brought about from changes in the solid state, many measurable effects can be observed by a multitude of analytical techniques. The main constraint of the analysis being that the material analysed must be in its solid phase, this rules out any type of solution analysis. In the manufacturing of pharmaceuticals, a quick, non-destructive, and preferably *in situ*, method is needed for the identification, detection, and the monitoring of any changes to a material's solid state.

As mentioned, X-ray diffraction, thermal analysis and visual techniques can be used in the analysis of amorphous content and polymorphs, and are considered the more traditional techniques used primarily in solid state analysis. Changes in the crystal lattice are detected by diffraction and can manifest as different crystal morphology, which can be observed visually. Changes in the crystal structure also result in notable changes in the melting point, a classical observation in thermal analysis. These methods were fundamental in solid state analysis during the earlier half of the 20th century. Though they have advanced with technology, they still utilise their fundamental principles, and are still in use in the solid state analysis. X-ray diffraction has become known as the gold standard in solid state analysis and thermal analysis has advanced as DSC and Thermal Gravimetric analysis (TGA). DSC and TGA can give more information about thermal events which may occur during the heating on the solid state of a pharmaceutical, and can be used to determine an API's sensitivity and susceptibility in absorbing atmospheric moisture. Visual analysis has advanced as microscopy, where more powerful optical microscopes can observe morphology in greater detail and the real-time crystallisation of materials from a range of solvents under different conditions. This can be done in greater detail using Scanning Electron Microscopy (SEM), giving a higher resolution on smaller objects, which can be coupled to some spectroscopic device, making it ideal in the analysis of particles.

The latter half of the 20th century brought about advancements in spectroscopy, giving rise to new methods of analysing solid state pharmaceuticals. This could be used to observe spectral differences resulting from differences in H bonding (and other intermolecular forces) in different crystalline forms. Advancements in spectroscopic techniques such as Infra-Red (IR),

Near Infra-red (NIR), Raman, ssNMR (solid state Nuclear Magnetic Resonance), and ssUV (solid state Ultra Violet), have been applied in the detection and identification of polymorphic materials with great success. Spectroscopic techniques such as NIR spectroscopy have been more readily applied in the manufacturing of pharmaceuticals due to their ease of use as an *in situ* analysis, being renowned as fast and reliable means of analysing an API's solid state.[18]

X-ray powder diffraction (XRPD)

One of the most prominent methods for the characterisation of solid state pharmaceuticals is X-ray diffraction, which can be divided into two techniques, single crystal diffraction, where a single crystal of pure compound is analysed and X-ray powder diffraction (XRPD), where a powdered sample of the material is analysed. Both techniques utilise the same concept, that each polymorph has its own unique unit cell parameters, density, crystal lattice, molecular conformation, and H bonding. This results in unique structural information, producing a characteristic diffraction pattern. Because of this X-ray diffraction has become the gold standard in crystalline quantification and characterisation. In both techniques of X-ray diffraction crystalline samples are irradiated with X-rays. This radiation is then diffracted depending on the crystal lattice (Figure 1.5). Single crystal diffraction gives very precise structural information that can be computed to give a model of the molecular arrangement in the crystal lattice. These models can then be used to predict the powder diffraction patterns. In X-ray powder diffraction, a flat level plane of the powder sample is exposed to X-rays. The sample is then rotated (relative to the X-ray source), changing the incident angle of the radiation source. The intensity of the diffracted beam changes with incident angle. Due to its lack crystalline characteristics amorphous content appears lacking in notable peaks, appear as an 'amorphous hump'.

In XRPD the sums of the combined integrals of all diffraction correlate with the content of the component,[19] whereas in the case of amorphous content it is the integral of the amorphous hump that correlates with its content. This makes it possible to quantify different components in mixtures.[20, 21] Any XRPD pattern can be verified from a theoretical pattern produced from information from the single crystal diffraction data, which can be obtained from a number of websites. This is of great benefit in identifying powdered samples.

While X-ray single crystal diffraction can give greater information of a crystallised API, it is generally not used in industry. This is because a high degree of expertise, the need of pure stable crystals, and can only analyse a single crystal at a time.

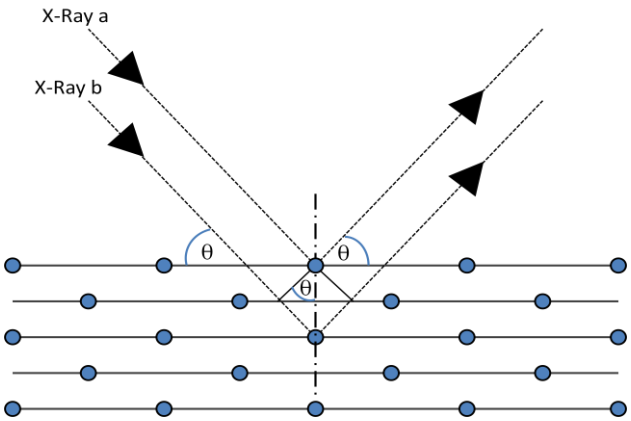

Fig. 1.5 Representation of X-ray diffraction on a crystalline structure

Though XRPD is regarded as the gold standard in crystalline detection it does have a number of shortcomings. Disadvantages of XRPD include its high noise to peak ratio, varying Bragg angles, and preferred orientation. The high noise to peak ratio is, in itself self-explanatory. High background noise is a consequence of background radiation, which can interfere with the interpretation of peak height and area. When this is accompanied by a change in baseline due to amorphous content the error in quantification can greatly increase. Sensitivity to sample packing in XRPD can result in varying Bragg angles, distorting the crystalline powder pattern. Preferred orientation presents itself as an intensity increase of one or more peaks (Figure 1.6), and a decrease in all others. This is the result of the tendency of plate or needle like crystals not to adopt random orientations when packed into the sample holder. XRPD is rarely used industrially due to its cost, sample preparation, time taken for analysis, and its integration to *in situ* analytical systems.

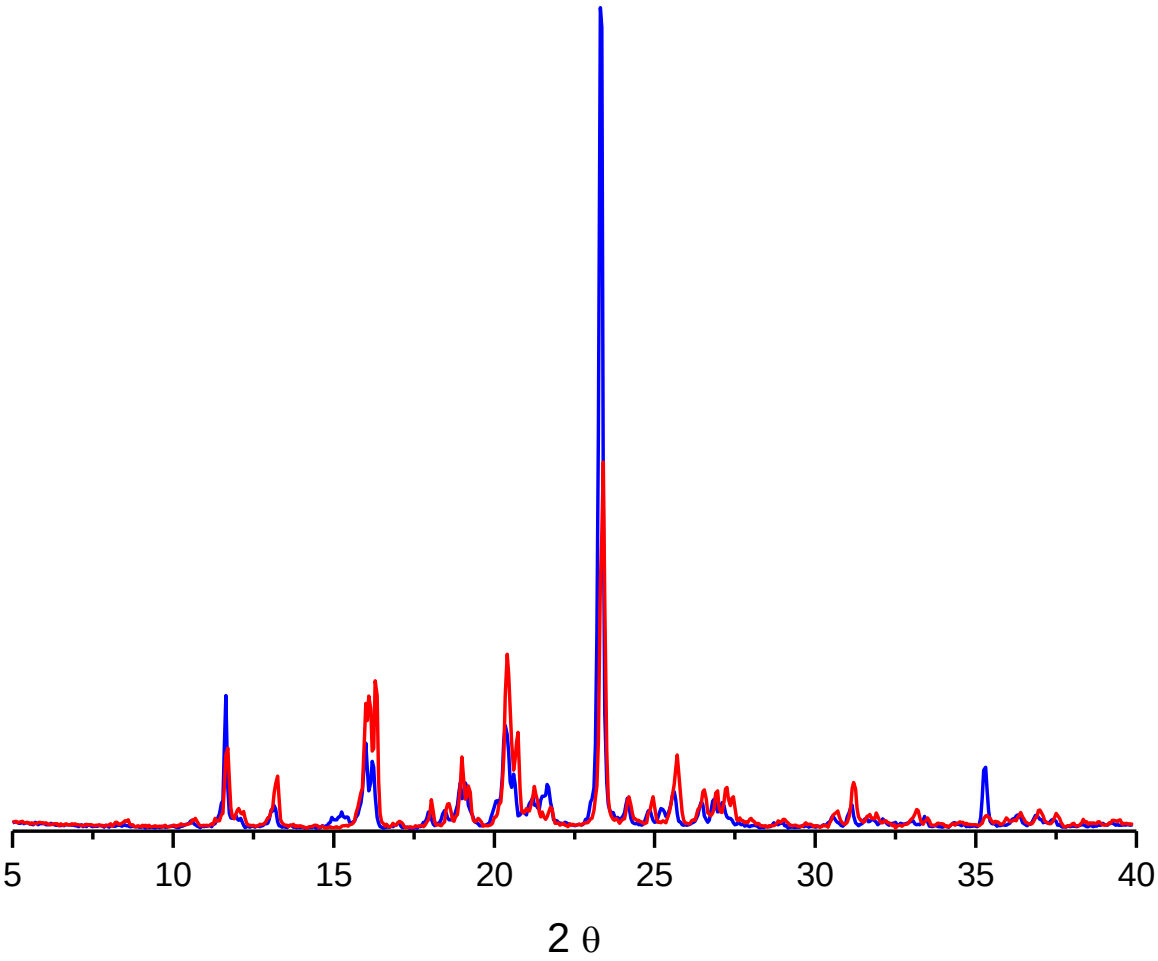

Fig. 1.6 Different XRPD patterns of sulfathiazole form V resulting from preferred orientation

Vibrational spectroscopy in solid state analysis

Spectroscopy has become a prominent means of solid state analysis, which has developed through the decades with the emergence of new apparatus designs, particularly those for solid state analysis. Advances in technology have allowed instruments to become faster and more accurate and can be coupled with computational devices used to process data. In dealing with the analysis of polymorphs and amorphous content, it is worth keeping in mind that no chemical bonds are formed or broken, all changes are structural, brought about by intermolecular forces (H bonding, van der Waals forces, etc.). Due to changes in H bonding from different molecular arrangements, many chemical bonds can become affected by a polymorphic phase change or amorphisation. Vibrational spectroscopy is the result of energy (in the form of radiation) being absorbed, by certain vibrational movements in a molecule, i.e. stretching, bending or wagging of chemical bonds, causing periodic modes (or vibrational modes). Due to the change in bond lengths between different polymorphs, the radiation being absorbed by each polymorph is different, resulting in unique spectra for different polymorphs.

Sampling methods in spectroscopy have also changed over time, allowing the development of sampling methods that improve the accuracy of the analysis, e.g. sampling methods that do not require the addition of diluents or the preparation of KBr pellets. Analytical systems have gone from a solution mediated sample equipment (such as Ultra Violet-visible (UV-vis), Nuclear Magnetic Resonance (NMR), or solution IR), towards systems allowing for solid state analysis (solid state UV analysis (ssUV-vis), solid state NMR (ssNMR), and attenuated total reflectance Infra-red spectroscopy (ATR-IR). This overcomes having to process the sample as a solution, losing any solid state characteristic and resulting in impossible analysis of a compound's polymorphism. This has brought about an influx of new methods that give further insight to the chemistry of solid state materials.

Infra-red spectroscopy

Infra-red (IR) spectroscopy is the classical method used to study fundamental molecular vibrations. Here radiation is absorbed by vibrating chemical bonds in the infra-red region of the electromagnetic spectrum. In IR spectroscopy the radiation is too low in energy to induce an electronic transition, as would happen using UV spectroscopy, but instead is absorbed depending on different vibrational or rotation states of the chemical bonds of a molecule. The molecular vibrations or rotations must create a net change in dipole moment to be observed in infra-red spectroscopy (to be IR active). If the frequency of the radiation matches the vibrational frequency of the molecule then radiation will be absorbed, causing a change in the amplitude of molecular vibration, potentially allowing for the identification of chemical groups and molecular functional groups.

The nature of infra-red spectroscopy is dependent on a net change in dipole moment. A limited number of vibrations can occur resulting from bending or stretching, which can be calculated using the equations;

for linear molecules

$$3N - 5 \qquad \text{Eq. 1}$$

and, for non-linear molecules

$$3N - 6 \qquad \text{Eq. 2}$$

where N is the number of atoms in the molecule. Figure 1.7 (top) illustrates the normal modes of stretching for water (H_2O), which being a bent molecule having 3 N numbers of atoms, and thus having three vibrational modes. ν_1, ν_2, and ν_3 are the first, second and third vibrational states respectively. As can be seen, intermolecular forces can influence both the degree and type of vibration a molecule can possesses (Figure 1.7 bottom). This alters a molecule's centre of gravity, changing its dipole moment, making it IR active. But if these changes were to be made to make more symmetrical molecules, any stretching or bending of the molecule that

does not bring about change in the dipole moment will not be IR active (such as the first two vibrational modes of acetylene).

Due to the effect of hydrogen bonding on the IR spectrum, polymorphism and changes in the crystallinity of a pharmaceutical can be observed accurately. This makes IR spectroscopy a reliable method for the identification and characterisation of solid state pharmaceutical when used in conjunction with suitable sampling methods (such as ATR-IR).[22]

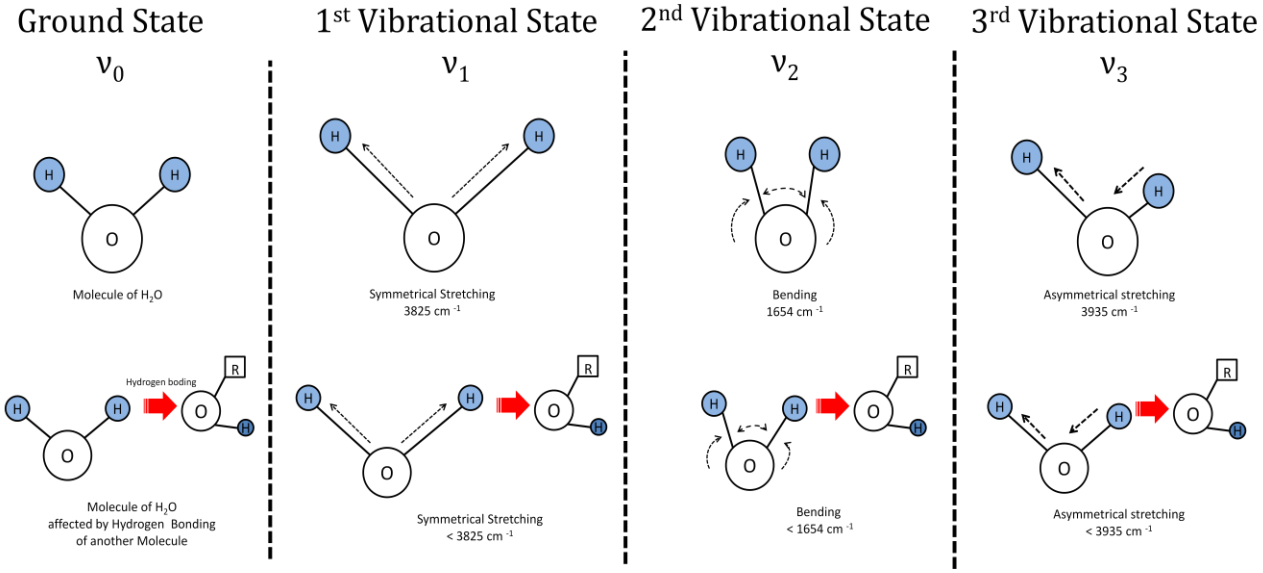

Fig. 1.7 Representation of the IR active vibrational states of water (top) and the effects of hydrogen bonding on the vibration states (bottom)

Although IR spectroscopy is predominately used in qualitative analysis, it has also shown great success when used in quantitative analysis, demonstrating its accuracy and sensitivity resulting from changes in the solid structure of a compound. Because of the sensitivity of IR analysis difficulties can also emerge, particularly during sample preparation. When dealing with an ATR-IR spectrometer, force is applied to the material over the sample plate. Even with the same applied force this can give varying degrees of absorbance, making calibrations difficult, and reducing the robustness of good calibration models. Also many ATR-IR require applied pressure on the sample during analysis, which can induce a polymorphic transformation, reducing the reliability of IR spectroscopy.

Near infra-red spectroscopy

While IR spectroscopy is widely used for qualitative analysis and identification from the structural change, near infra-red (NIR) spectroscopy has predominately been used for quantitative analysis. NIR absorption is due to combination bands and vibrational overtones. The first overtone ($\nu_0 \rightarrow \nu_2$) shows the highest intensity, the second overtone ($\nu_0 \rightarrow \nu_3$) showing less intensity and the third overtone ($\nu_0 \rightarrow \nu_4$) showing even less intensity. For each succession the intensity of the overtone decreases by one order of magnitude (Figure 1.8). These are known as forbidden transitions and result in relatively low peak absorption and the notable broad peaks of NIR spectra. This also limits the qualitative power of NIR spectroscopy, where the absorption bands arise from overtone combinations of C-H, O-H, or N-H stretching modes.

The dependence of NIR spectroscopy on C-H, O-H, and N-H bonds makes it a prime means of analysis in the study of solid state pharmaceuticals, due to the fact that the majority of pharmaceuticals contain N-H and O-H hydrogen bond donating functional groups. Even with its relatively low absorption, the signal to noise ratio of NIR spectroscopy is high. This stems from an intense radiation source, and sensitive detectors giving a high degree of accuracy when applied in combination with chemometric techniques. Because of this NIR spectroscopy has been utilised in many industries as a Process Analytical Technology (PAT) tool, most prominently in food quality and pharmaceuticals, due to its ease of use, its efficiency, and non-destructive sample preparation.

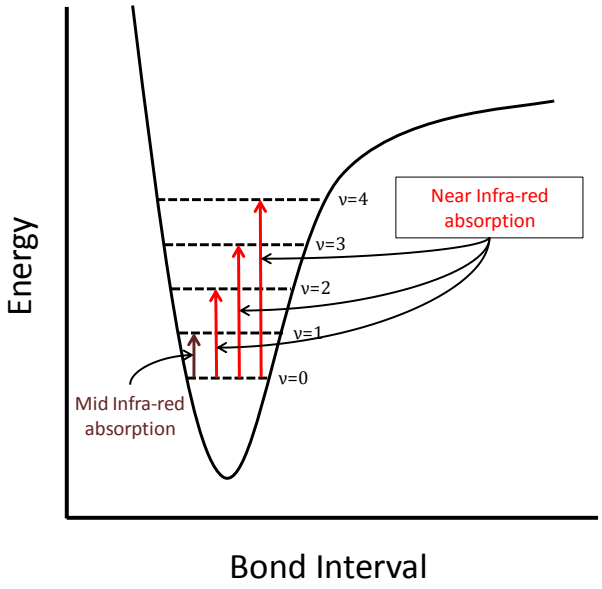

Fig. 1.8 Representation of the energy excitation in NIR spectroscopy

Raman spectroscopy

Raman spectroscopy is based on inelastic backscattering of radiation (usually from a monochromatic source). The Raman Effect originates from the distortion of the electron cloud of a molecule in an electric field which leads to an induced electric dipole moment. The distortion of the electron cloud brings about changes in the molecular polarisability.

There are two ways this radiation scattering can occur

1. Rayleigh scattering (or elastic scattering): scattered photons which have the same energy (frequency) as the incident photons.
2. Raman scattering (inelastic scattering):

The ease with which the electron cloud can be distorted is the molecular polarisability. The molecular vibration can change the polarisability, which results in three types of back scattering (Figure 1.9);

Raman scattering: excitation to a virtual energy state, relaxation and change of vibrational energy

Stoke lines: Scattered photons which have lower energy than incident photons.

Anti-Stokes lines: scattered photons which have higher energy than incident photons (scattering from vibrationally excited molecules)

In academic research, Raman spectroscopy has been used in the solid state analysis of crystalline materials for decades and has recently become industrially viable. In academia, the research and development of Raman spectroscopy met a number of challenging obstacles, needing an elaborate instrumental system set up for experimental analysis. But through the years it has been greatly developed to the point that it can be used as a hand held model. For years Raman spectroscopy was deemed unwelcomed in the pharmaceutical industry, due to the high level of instrumental knowledge needed, price, apparatus set up using varying lasers giving different spectra, problems with fluorescence, and its sample set up. Recently with

lowering costs, simple methodology related to new instruments and an array of variation (where transmission Raman can penetrate tablets)[23], and its application to SEM to analyse samples in the μm range, Raman spectroscopy is now becoming commonplace in industry.

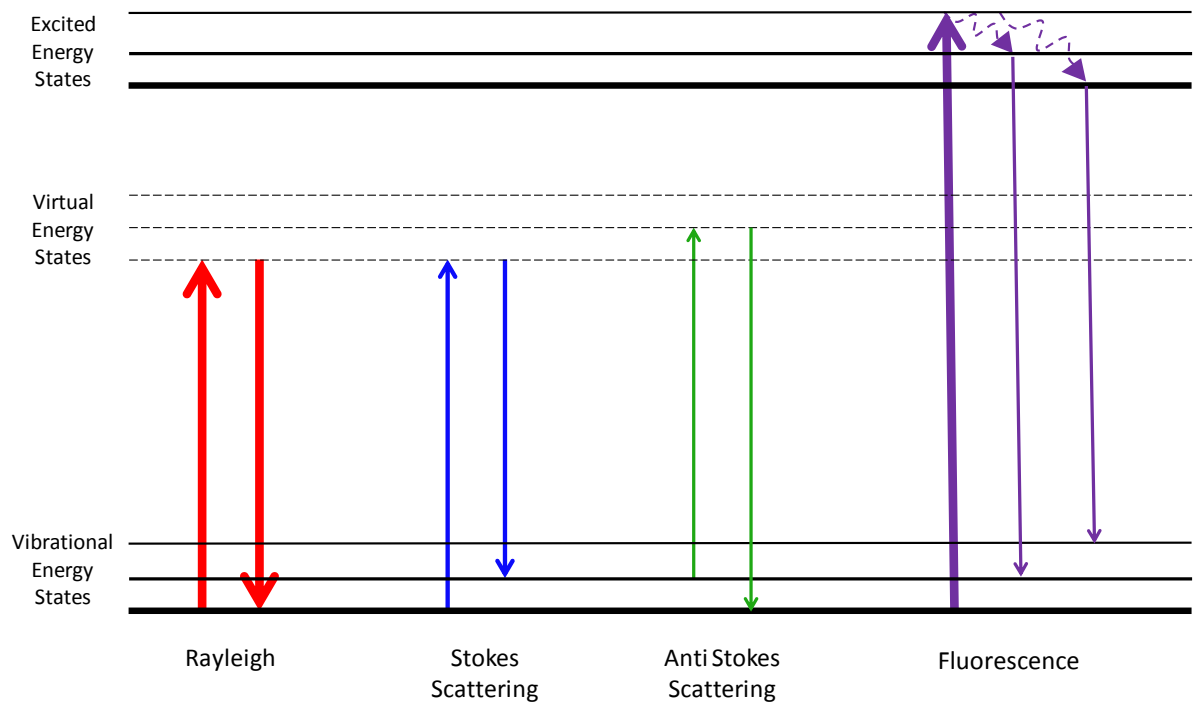

Fig. 1.9 Representation of the energy excitation, causing Rayleigh, Stoke and anti-Stokes scatter, and fluorescence that can occur in Raman spectroscopy

Thermal analysis

Thermal analysis is one of the oldest means of polymorphic characterisation, as each solid phase of a compound has its own unique melting point. Because different solid phases must have a specific unit energy resulting from specific lattice energy, the energy needed to induce a thermal event (such as melting, or enantiotropic transformations) is characteristic to each specific solid phase. Thermal analysis has expanded to include and measure a multitude of thermal events. These include solid state transformations such as the glass transition, polymorphic transformation, or the release of water or solvent of crystallisation during heating. The most widely used techniques in thermal analysis are differential scanning calorimetry (DSC), Thermal Gravimetric Analysis (TGA), solution calorimetry, and isothermal calorimetry.

Differential scanning calorimetry (DSC)

DSC is a destructive method of analysis requiring only microgram amounts of samples. It measures the energy needed to change the temperature of the sample in relation to sample weight. Using DSC gives a greater understanding of the physical changes a polymorph undergoes during heating. It can show the glass transition temperature, and both exo- and endo-thermic events. Depending on the experimental set up and software used, thermic events may appear differently. It is generally regarded that endo-thermic events appear as peaks in the DSC graphs, indicating energy is needed for the event to occur. This includes the solid-solid transformations of a meta-stable form. Exo-thermic events appear as dips. These are indicative of energy being released which can also be seen during solid-solid transformation where crystallisation occurs forming a more stable polymorph, if the polymorphs are enantropically related. In amorphous pharmaceuticals and relatively small molecules, the glass transition can be seen as a slight step change.

The rate at which the sample is heated can have a great effect on the DSC analysis and can result in some thermal events overlapping and masking other thermal events. Though this is often considered a hindrance, it can also be beneficial, providing information about the

transformation kinetics, and can be resolved by changing the heating rate during the analysis. Other attributes that can offset DSC analysis include the presence of impurities, and the heat flow for the evaporation of solvents or atmospheric moisture. Despite its inability to be used *in situ* and its destructive nature, it has become regarded as a highly informative means of analysis instrument in the characterisation and identification of polymorphs.

Though DSC is primarily seen as a qualitative means of analysis, it has also been used in quantitative studies, indentifying and quantifying different polymorphic mixtures.[24] DSC can also be coupled with NIR and Raman spectroscopy to give a more advanced insight to the chemistry of a polymorph undergoing thermal transformations

Thermogravimetric analysis (TGA)

While thermogravimetric analysis cannot be directly used in the study of pure polymorphs (on the basis that polymorphic transitions do not involve a change in mass) it is worth while noting its accuracy in characterising solvates of drugs and their excipients, and in investigating the resulting difference in the absorption of atmospheric moisture brought about by changes in the material's solid phase. [25] Thermogravimetric analysis (TGA) measures mass as a function of temperature, thereby observing changes in mass as components of material are released (usually in the form of a solvent). As such it can play a central role in determining the stoichiometry of solvates and hydrates, where the mass change due to the expulsion of the solvents and water can be calculated. This also gives an indication of the type and degree of the bonding involved.

Experiments have also shown great accuracy in determining a the ability of a material to absorb moisture.[26] This can give critical information when studying the polymorphism of pharmaceuticals, due to the fact that moisture can induce unwanted crystallisation. TGA can determine the amount of moisture absorbed. It can also be used to examine thermal degradation, although this is not an application that has been widely used within the pharmaceutical field as it is not advisable to extrapolate such data to room temperature. With

this TGA has a limited scope, but can give an insight into some physical properties of polymorphic materials.

Microscopy

Although visual analysis of a polymorph may seem trivial, it is an established and reliable means of polymorphic analysis, where crystals can be observed to take on new shapes (Figure 1.10). Using microscopy, changes in crystal growth can be monitored under a number of different conditions. One of the most common applications is the use of optical microscopy, or scanning electron microscopy (SEM) to monitor the crystallisation of different polymorphs using various solvents, in different temperatures or changing other environmental conditions. Using SEM physical characteristics of a polymorph's surface can be monitored to the point where dents, fissures or pits can be seen to act as nucleating points for new polymorphs.[27] It is common to couple microscopy (both optical and SEM) with spectroscopy, allowing spectral analysis to be conducted on precise regions of a particle.[28, 29]

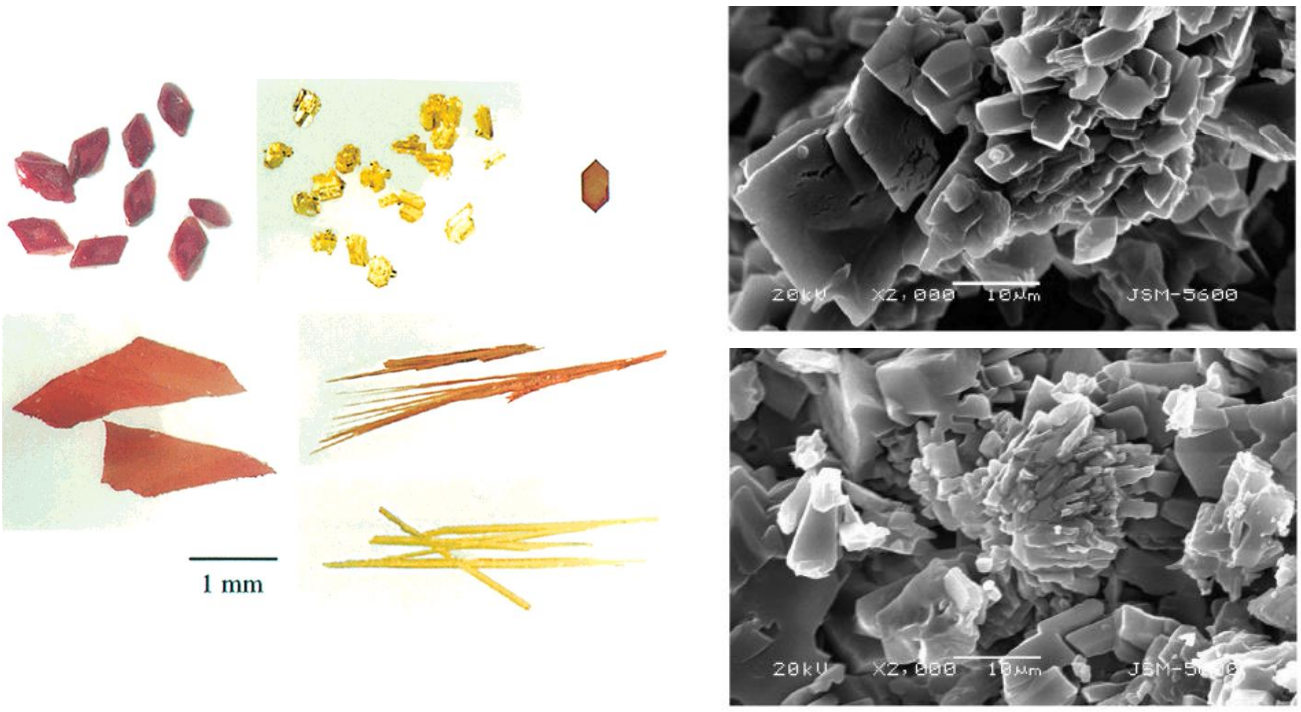

Fig. 1.10 Polymorphism of 5-methyl-2-[(2-nitrophenyl) amino]-3-thiophenecarbonitrile, also known as ROY (Red, Orange, Yellow) using visual microscopy (left) and Scanning Electron Microscopy (SEM) (right)

Chemometrics

Chemometrics is the use of mathematical and statistical methods for experiment design and information extraction, and here is focused on information extraction methods by means of classification and regression models. This allows a computational system that can process data characterising information relating to those samples analysed. This allows analytical data to be processed using mathematical algorithms, which may be used to create a model to classify or quantify materials. This can be done using either classical linear methods, or using multivariate methods using latent variables (or principal components). This has been implemented for characterising and quantifying samples by pre-treating analytical data to create regression models containing multiple components, with increased accuracy, robustness, and precision. The models can then be used to study factors that may influence the sample, such as environmental factors, or alternatively to quantify one or more components.

Whereas two decades ago the practice of multivariate analysis was a demanding chore for any computer, due to advanced technology in computational devices it can now be used in mobile devices, and desktop computers. Data can be analysed in real time, allowing the implementation of *in situ* process analytical technologies (PATs). Certain analytical techniques have been coupled to chemoinformatic processes in an industrial setting. Raman, IR and NIR spectroscopy are commonly chosen in such processes, as they are quick and accurate. Other analytical methods, such as DSC and XRPD, are also used in conjunction with chemoinformatics, but due to the time needed to conduct the analysis, their destructive nature and the required sample preparation, these methods are inappropriate for *in situ* analysis in the manufacturing of pharmaceuticals. However, they can still be used in off line analysis. Here chemoinformatics shall be discussed under two headings, multivariate analysis and data pre-treatments.

Multivariate analysis

Here mathematical and statistical concepts are applied to find relationships between different measurements corresponding to different components. Multivariate analysis, used as a means of calibration and characterisation is regarded as the area of chemoinformatics that has attracted the most interest by many (Martains and Naes 1989, Sundberg 1999).[30, 31] As mentioned before multivariate analysis can be utilized for regression analysis (such as Partial Least Square (PLS) or Multiple Linear Regression (MLR)), and discriminative (Principal component Analysis (PCA)) (Figure 1.11). Regression analysis can be used to construct calibration models for the quantitative analysis of samples of unknown concentrations, and can at times be used to classify components. Whereas the different clusters obtained from discriminative analysis can be classified into separate groups. Both are powerful tools that can give great insight to a system.

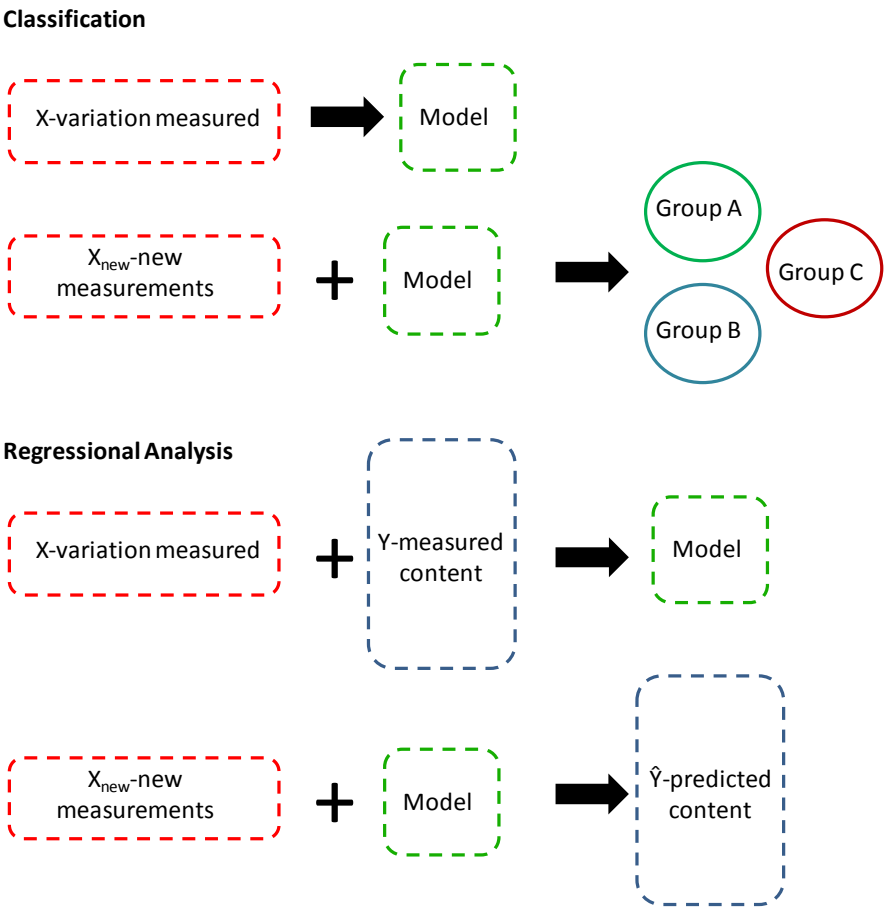

Fig. 1.11 Two most utilised methods in chemometrics, classification (top) and regression analysis (bottom)

Principal component analysis (Discriminant)

One of the first and most widely used applications of multivariate analysis is Principal Component Analysis (PCA). PCA was developed in 1901 by Karl Pearson,[32] and acts as an introduction to other multivariate systems. PCA, over the decades, has been used in both discriminant analysis and for cluster analysis, showing greater potential in cluster analysis using higher class variance, by allowing different perspective of the data to better cluster samples.[31] PCA works by a method where recognisable information corresponding to the variation of multiple components is projected onto a multidimensional table, consisting of a smaller number of latent variables called Principal Components (PC). Each PC explains a certain amount of information with the first PC containing the most information and showing a reduction of information with each successive principal component. This is known as the projection method, in which the variance of an object can be plotted. A hyperplane can be fitted and used to extract information, which can be plotted on a simpler set of variations. This allows for partially hidden data to be more confidently interpreted when dealing with complex data sets, and can be used to expose variation in a spectral data resulting from adulterations or degradation. These principles of projection are fundamental for all multivariate systems.

In PCA samples can only be interpreted when plotted in multi-dimensional space. Figure 1.12 below describes the projection of data in multi-dimensional space. For human perception this must be limited to three spatial dimensions of differing variations to be plotted on the hyperplane, though this can be higher. If a sample possess excessive complexity it can be confined to a system where it can be coordinated in a lower dimension of space, while retaining the information resulting from its own complexity, where variation from its proposed or predicted coordinate can be exposed resulting from its higher complexity. In brief, samples containing similar information or variation should have similar spatial coordinates and cluster together, whereas adulterated samples will show greater complexity and thus greater variation when plotted and processed.

Though terms such as systematic variation and responses are generally used throughout literature, this study will refer to spectroscopic terminology. Here variation will refer to

changes between spectra. Systematic variation indicates characteristic changes in spectra that relate to the response, which will refer to the content of a component.

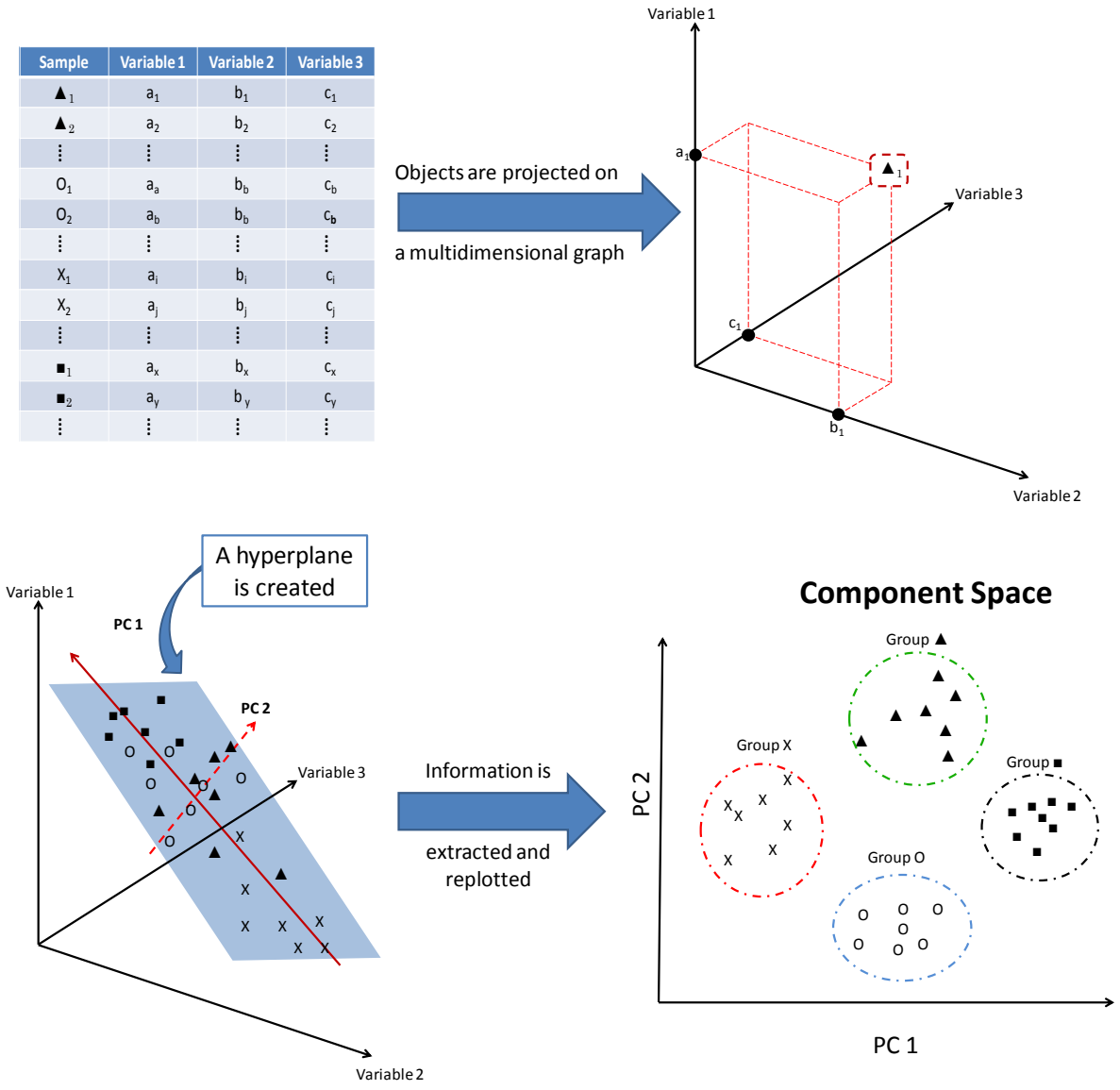

Fig. 1.12 Replotting of raw data for Principal Component Analysis

Well-defined changes in the spectrum of a known component unique to the component can be used to extract information relative to that component, allowing the grouping of other samples with spectra showing similarities with the extracted information. If certain regions of the spectra are shown to have little if any systematic variation related to the spectra, they are considered uninterruptable information (or error). PCA extracts the large systematic variations, while excluding noise, allowing a clearer interpretation of the measurements made with regard to a certain component.

This is represented by the equation;

$$X = TP^T + E \qquad \text{Eq.3}$$

where **T** is the score matrix, **P** is the loading matrix, being the structured part of the data, and **E** is the Error matrix. The score matrix (scores) describes properties of a sample and allows samples to be categorised into clusters. The scores can be plotted on a multidimensional graph using the PCs as new variables, giving each component a specific coordination. The loading matrix (loadings) describes the relationship between multiple sets of different variables. This can be plotted for the interpretation of data, showing the regions of a spectrum that best relate to a specific component.

The deviation of a sample from a cluster is determined by its residual variation or leverage. Residual variation is a measure of how well a sample fits a model with regard to the other samples, or how well a measured spectrum fits other spectra relating to a specific component. Samples with a high residual variation are poorly described by the model, which nevertheless fits the other samples quite well. The leverage is the distance of a projected sample (i.e. its model approximation) to the centred plane (the hyperplane). Samples with high leverages have a stronger influence on the model than other samples (Figure 1.13).

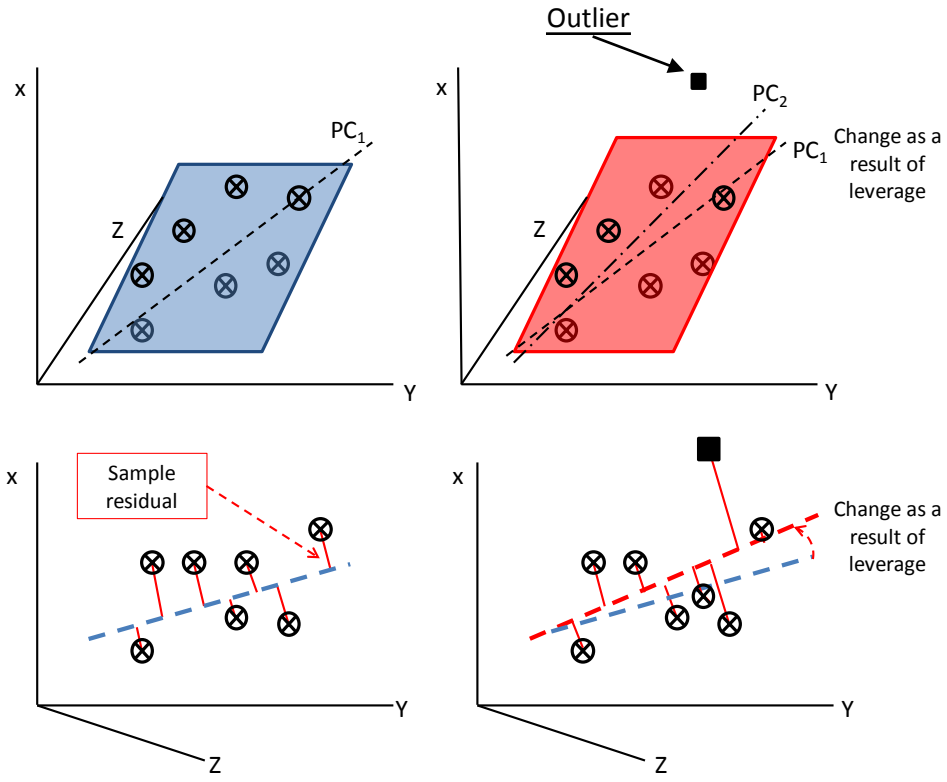

Fig. 1.13 The effects of leverage from an outlier on the PC axis

This can be problematic in the case of an outlier possessing a high degree of leverage and may change a model, thus reducing its accuracy and precision.

PCA can be used in spectral analysis by treating the spectra as data to be processed, where characteristic peaks are translated to variations measured in observable data, the different spectral variation related to the different components. This spectral variation '**X**' is then translated into a score and loading matrix (as shown by the equation 3). The spectra showing similarities resulting from their characteristic peaks are clustered together when plotted. Patterns are extracted and used to create a hyperplane, and to determine the principal components. Samples of greater complexity can be represented by a higher number of principal components. This creates a system showing spectral similarities, which can be plotted in relation to the existing cluster. This allows samples to be separated into clusters by residual variations, and be limited in its classification by their leverage. The degree of leverage which is allowed can be inputted or calculated internally by the giving software. This can create a system where some variation in samples may be allowed, regarded as background interference, and does not hinder its classification as a particular component. This allows the accurate classification of spectra even with slight differences in baseline and background noise. Whereas samples showing greater variation may be found to be outside these limits of

background interference and are considered outliers. These outliers are not classified as the pure component. As expected this has greater relevance in qualitative analysis than in quantitative analysis.

Regression analysis

While classification can be a descriptive method, regression analysis establishes a relationship between variations that occur in a data set to a corresponding response. This means that spectral variation can be quantified with regard to concentration or content (known as the Y-variables or response). This creates a regression model which can be used to measure change. There are many techniques in regression analysis which can be implemented in the study of polymorphic mixtures. Multiple Linear Regression (MLR) is a classical example which relates one single response to a small number of variables. This allows the peak intensity at selected wavenumbers to be used in the quantification of a component. Due to MLR having issues with collinearity between variables, model coefficients or expressions may not be interpretable, where the model may fail.

Though MLR has its drawbacks, the core concepts have been subjected to many improvements and deviations, creating different regression methods. This also led to other more sophisticated methods of regression analysis such as Partial Least Square (PLS) and Principal Component Regression (PCR). Many comparisons of PCR and PLS have been made, and it has been reported that PLS should in theory predict better. This is because PLS requires fewer latent variables than PCR.[33] Because of better correlations with the **y** variable are sought in determining the scores values, PLS loadings may be more easier to interpret, and handle nonlinearities better than PCR.[34] Because of this, PLS regression has been chosen as the main means of multivariate analysis in this body of work.

PLS regression

PLS performs a data compression similar to PCA finding a linear regression model by projecting observed variables against known responses, i.e. the observed spectra is projected against known concentration. This generates a model that allows for quantification of the system and the prediction of unknowns. This is achieved by simultaneously establishing a relationship between the **X** variable (eg spectra) and **Y** responses (concentration) creating a collinearity, and

giving rise to an interpretable relationship between variables where multiple **Y** responses can be analysed. This allows the analysis of multiple component mixtures.

The PLS method utilises many aspects used by PCA. Whereas PCA creates clusters from the data provided, PLS can go further. PLS analysis can relate information obtained from creating score plot **'X'**, where the score data **'t'** is correlated to the **Y** responses creating a loading plot. This replots the systematic variations of spectra as score data and correlates it to specific quantities of different components. This is known as the **Y**-loadings, having **'q'** data. The **'q'** data is then related with the **'t'** data which is then used to create a new score plot, **Y**-score, with data **'u'**, much the way PCA correlates spectra to their content. This should allow changes in the varying spectra to correspond to the **Y** responses (the content of a given sample). The data sets **'u'** and **'t'** are then correlated giving a correlation between spectra and content. This is illustrated in figure 1.14 and equations 4& 5.

$$X = TP^T + E \qquad \text{Eq. 4}$$

$$Y = TQ^T + F \qquad \text{Eq. 5}$$

PLS can be applied to more than one variable to response relationship, meaning multiple variations of **X** (multiple regions of different spectra) can be related to one of multiple responses **Y** (one of several components). This means that certain variations in different regions of a spectrum can be related to a specific response or component. These detected variations in a spectrum can be related to a specific factor, such as an environmental effect or its content.

Models generated from PLS regression methods must be tested and evaluated by measuring their accuracy and precision. The test for this estimation include the Root Mean Square of Error Calibration (RMSEC), Cross Validation (RMSECV), Prediction (RMSEP), standard deviation and the Limit of Detection (LOD), as shown in equations 6-11.

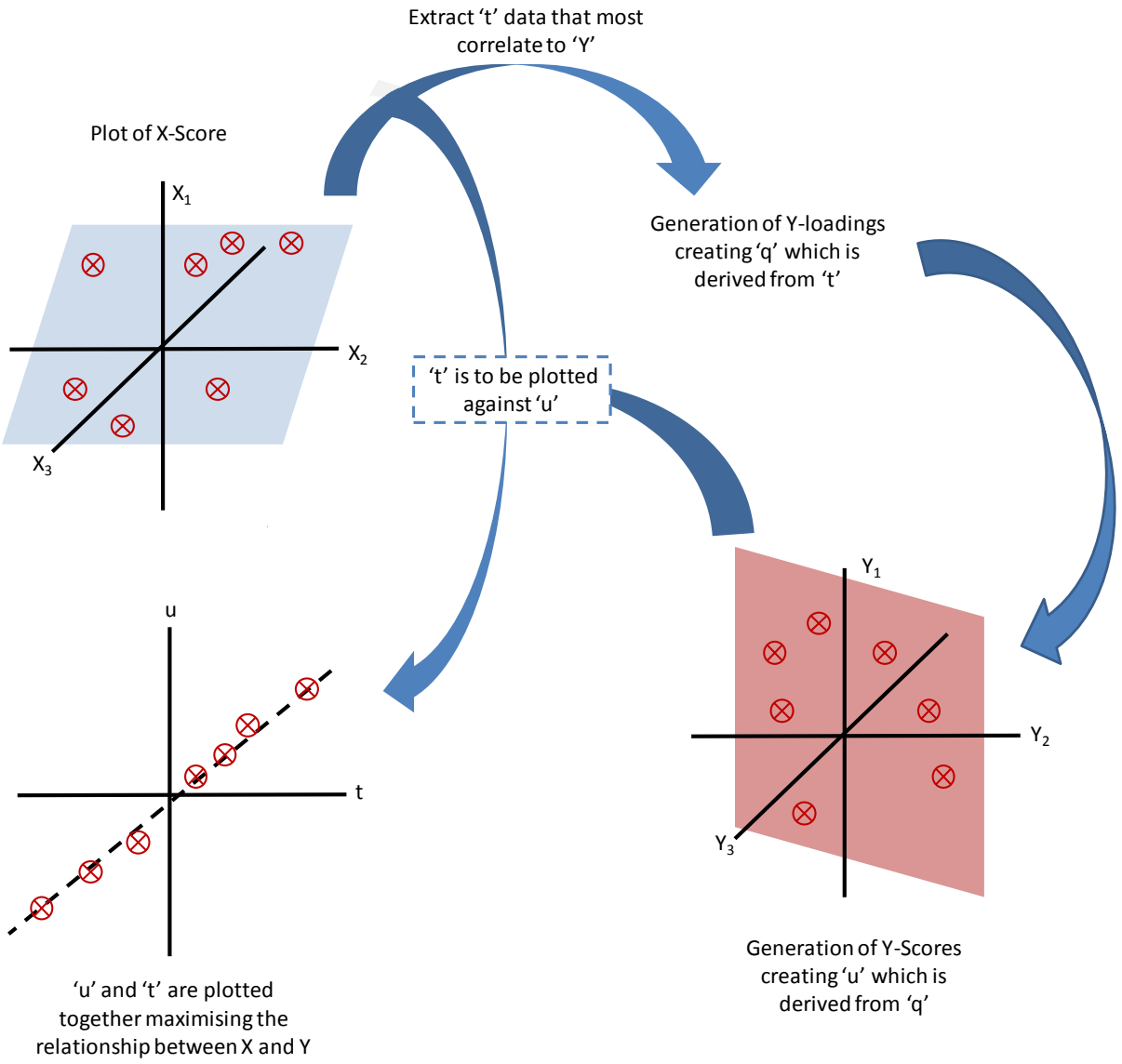

Fig. 1.14 The transformation of raw data throughout PLS analysis

The RMSEC value exposes how well the data points fit the regression line. For the RMSECV, the cross-validation method can use the same data used in building the calibration model, to validate its accuracy. In the cross-validation method some samples are left out and the remaining samples are used to create a calibration model. The samples left out are then plotted on the calibration model created. This is then related to another model created removing and replotting another set of samples. Each point is removed and replotted systematically until each point is removed and replotted to a new calibration model, and the RMSE measured from all replotted calibration models are averaged and this is taken as the

RMSECV. Where both RMSEC and RMSECV can be measured internally, the RMSEP needs an external data set to measure a model's ability to make predictions. The RMSEP is calculated by projecting a new data set spanning the range of the calibration model. The deviation of the new data set from the calibration model is calculated as the RMSEP. The standard deviation is calculated by measuring the deviation of 'blank samples', or those of known concentration, from the calibration model. These deviations are standardised, giving the standard deviation (Equations 9 & 10). The limit of detection (LOD) is calculated as three times the standard deviation (Equation 11).

$$RMSEC = \sqrt{\sum_{i=1}^{N} \frac{(\hat{y}_i - y_i)^2}{(N - A - 1)}} \quad \text{Eq. 6}$$

$$RMSECV = \sqrt{\sum_{i=1}^{N} \frac{(\hat{y}_{CV,i} - y_i)^2}{(N)}} \quad \text{Eq. 7}$$

$$RMSEP = \sqrt{\sum_{i=1}^{N} \frac{(\hat{y}_i - y_i)^2}{(N_p)}} \quad \text{Eq. 8}$$

$$\sigma = \sqrt{\frac{1}{N} \sum_{i=1}^{N} (x_i - \mu)^2} \quad \text{Eq. 9}$$

,

where $\mu = \frac{1}{N} \sum_{i=1}^{N} p_i x_i$ Eq. 10

, and LOD = 3σ (of blank samples) Eq. 11

This has created a systematic approach to evaluate multivariate analysis where the calibration model can be scrutinised, and if need be improved upon. Figure 1.15 shows a

commonly accepted flow chart used in creating calibration models. In this chart “Raw data” represents all information obtained experimentally, which is then split into variation (**X**), used to calibrate measured variation against the response(**Y**). This can be applied to chemical analysis, such as changes in spectral information can be taken as the variation **X**, and the response **Y** refer to the concentration. The calibration data is usually modified by pre-processing the raw data in an attempt to remove baseline offsets, scattering effects, and other distortions, and can also improve the signal to noise ratio, and enhance collinearity of the data. This modified data ($\mathbf{X_{mod}}$), is used with **Y** to create a model (such as PLS, or MLR), here known as model 1. This model generates information used to determine a model’s accuracy. This includes the regression coefficient (R^2), RMSEC, and RMSECV if an internal validation system such as full cross-validation is used. When these figures are satisfactory the model must be assessed by predicting known samples, giving information such as RMSEP. Here a prediction set of samples of known content ($\mathbf{X_p}$ + $\mathbf{Y_p}$) are applied to the model and used to measure the model’s precision and accuracy in predicting over the range of the calibration model. So the prediction of sample with the spectrum $\mathbf{X_p}$ through the model should result in the predicted concentration of $\hat{\mathbf{Y}}_\mathbf{p}$, which should be equal to the known concentration $\mathbf{Y_p}$, this signifies a successful model where its standard deviation and limits of detection can be measured from blanks.

As can be seen, the model is dependent on the data used to create the model. If poor results are found in any of the RMSEC, RMSECV, RMSEP, the standard deviation, or limit of detection, the model must be optimised often by replacing outlying data.

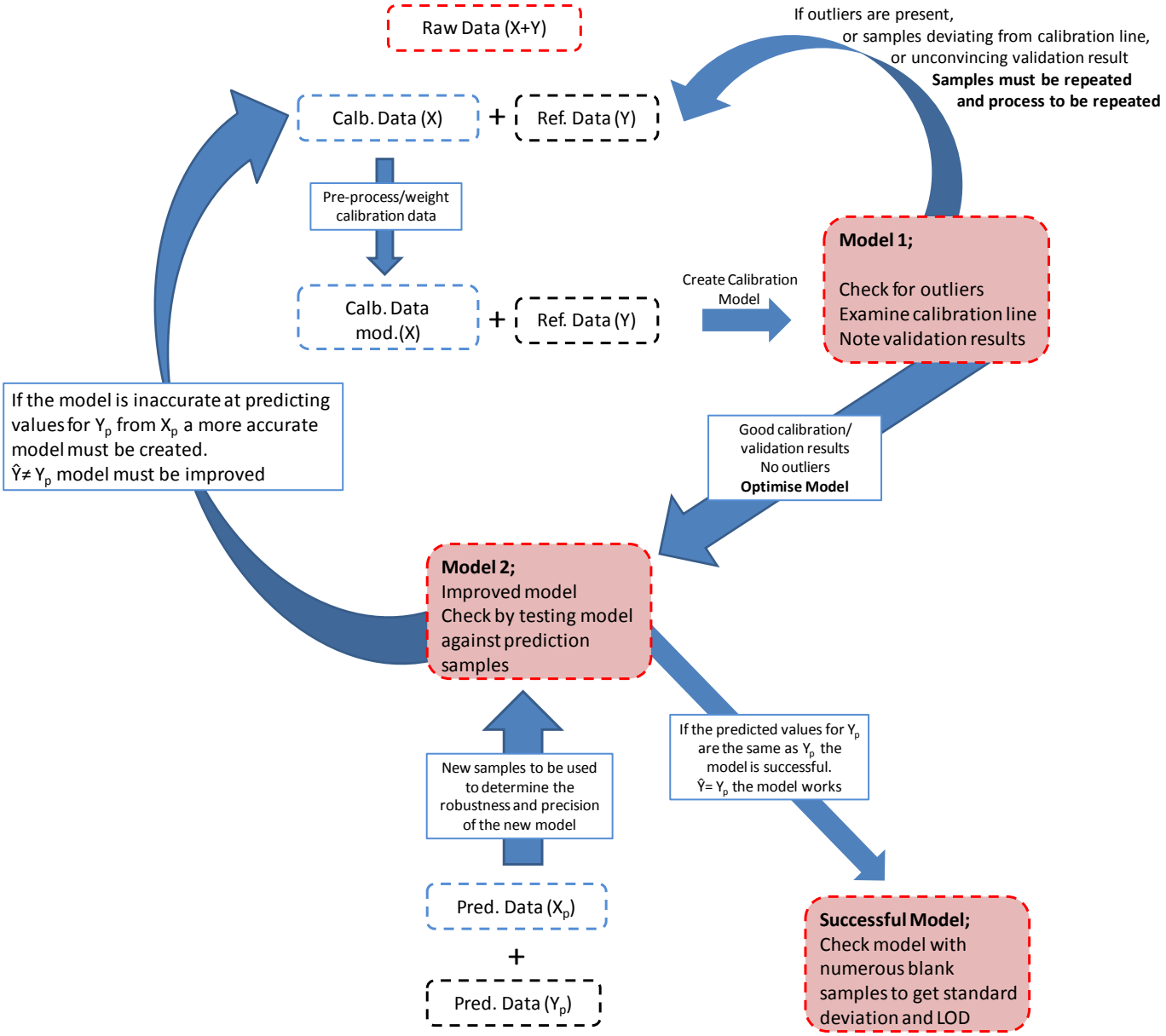

Fig. 1.15 Process chart in creating a successful PLS model. Here X data should be considered to be the spectra having content Y

Pre-processing

Pre-processing algorithms remove non-linearities and effects of uncorrelated sources from spectral variance, such as particle size and shape, and background noise. This may increase the performance of the calibration model. The most common pre-processing methods are discussed here; Smoothing, Multiplicative Scatter Correction (MSC), Standard Normal Variate (SNV), the 1st & 2nd Derivatives, and Orthogonal Signal Correction (OSC).[35]

To illustrate the transformations that occur during pre-processing, changes to the XRPD patterns, IR and NIR spectra of the three forms of sulfamerazine (Forms I, II, and the amorphous phase), and an average mixture (33:33:33 of all three components) will be shown in the examples below (Figure 1.16).

Raw data;

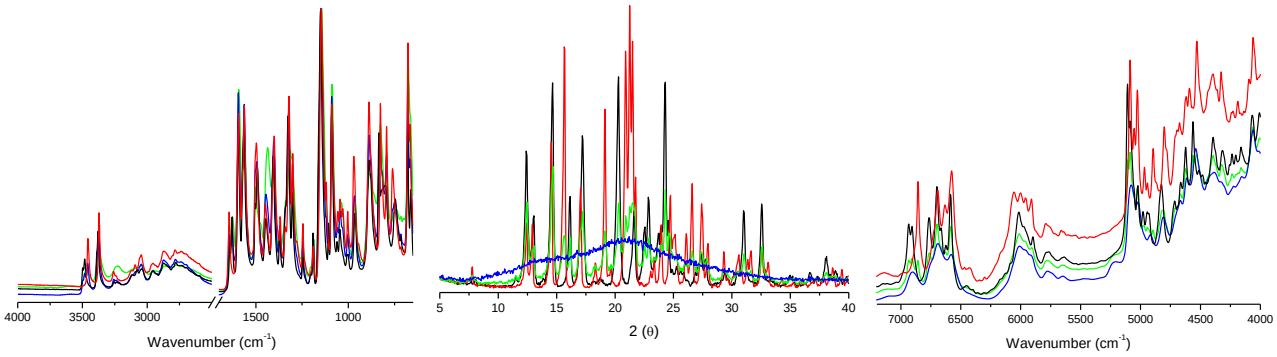

Fig. 1.16 Raw IR spectra (left), XRPD patterns (middle), and NIR spectra (right) of sulfamerazine form I (black) and II (red), the amorphous phase (blue), and the average of the three components (green)

Smoothing

This is a row-orientated transformation which reduces background noise without reducing the variance. In smoothing, a data point is averaged over a segment of surrounding data points. The original data point is then replaced by the average of the segment, creating a smoothing effect. The degree of smoothing is chosen by the size of the segment chosen. This allows a 'box-car' transformation of single samples to be altered independently, leading to its popularity in recent decades, and its use in imaging. Many methods of smoothing in chemometrics are

based on this technique, such as moving average, Savitzky-Golay, median filter, and Gaussian filter.

Moving average

Moving average works by replacing an observed data point with that of an average value over a segmented range of data, as shown in the equation 12.

$$x_{mod} = \frac{x_1 + x_2 + \cdots + x_{i-1} + x_i}{i} \qquad \text{Eq. 12}$$

where $\mathbf{x_{mod}}$ is the modified data point from the moving average smoothing, and **i** is the range of the segment chosen. The range of the segment greatly effects $\mathbf{x_{mod}}$. This is demonstrated in figure 1.17, where the background noise of the X-ray diffraction patterns are smoothed, reducing the effects of background noise.

Moving average smoothed data;

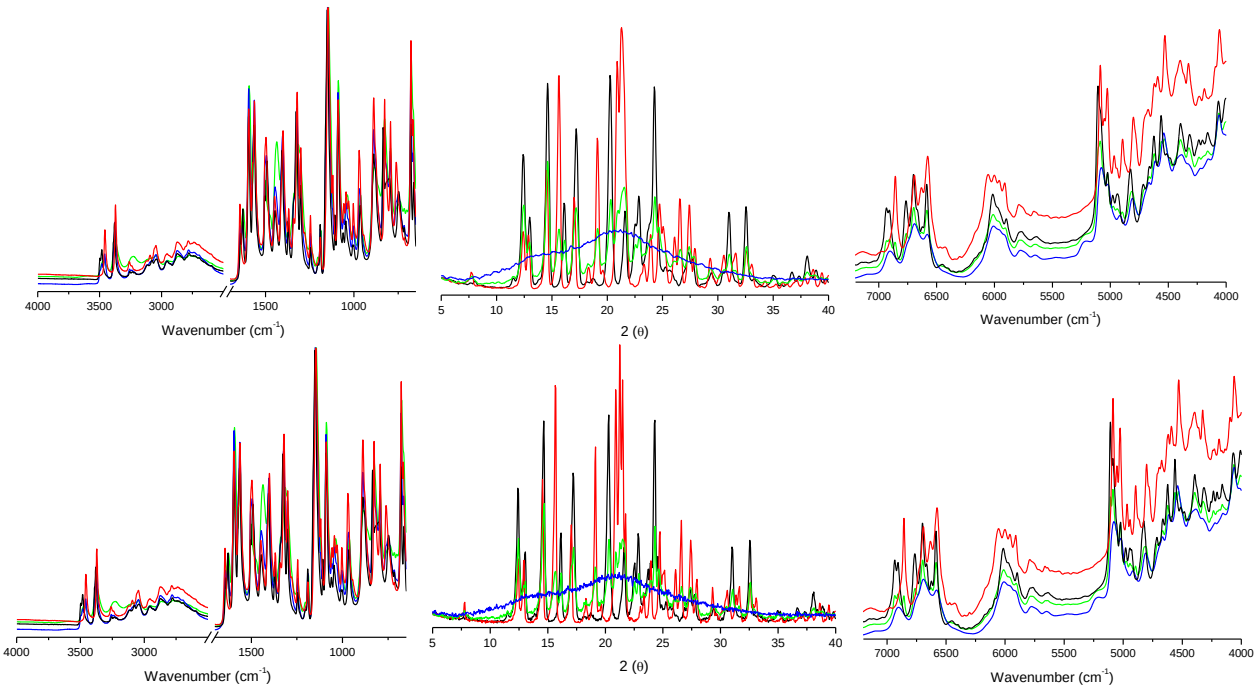

Fig. 1.17 The effects of moving average smoothed, choosing 5 segments (Top), on raw data (Bottom)

Savitzky-Golay smoothing

Savitzky-Golay smoothing operates similarly to the moving average method. However, the average value is replaced with a polynomial fit. This allows both the length of the smoothing segment and the polynomial order of the algorithm to be chosen. This replaces the original data point with a data point that has more regular variation than that of moving average, and with removed noise while retaining the chemical information. This makes it one of the most widely used methods of smoothing in chemoinformatics. Savitzky and Golay's paper is one of the most cited papers of Analytical Chemistry.[36, 37]

Savitzky-Golay smoothed data;

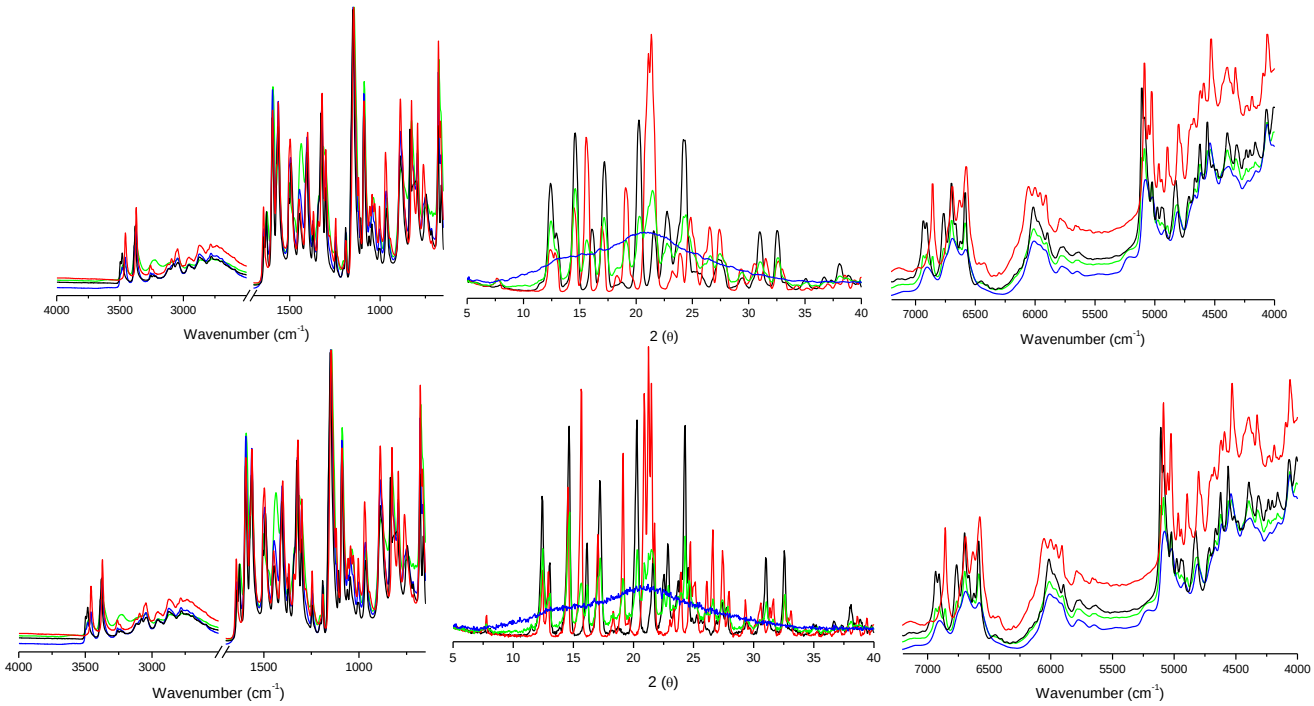

Fig. 1.18 The effects of Savitzky-Golay average smoothed (Top), choosing 9 smoothing points on raw data (Bottom)

Gaussian filter smoothing

Gaussian filtering is another example of smoothing. It smoothes the data by coupling it with a Gaussian function. Here a coefficient determined by a Gaussian function and a median filter replaces the original data points with a new data point which is weighted by a moving average and a median of its neighbouring data points. The number of data points from which to take the median is chosen as the segment size. It should be noted that the segment size must be an odd number.

Gaussian filter smoothed data;

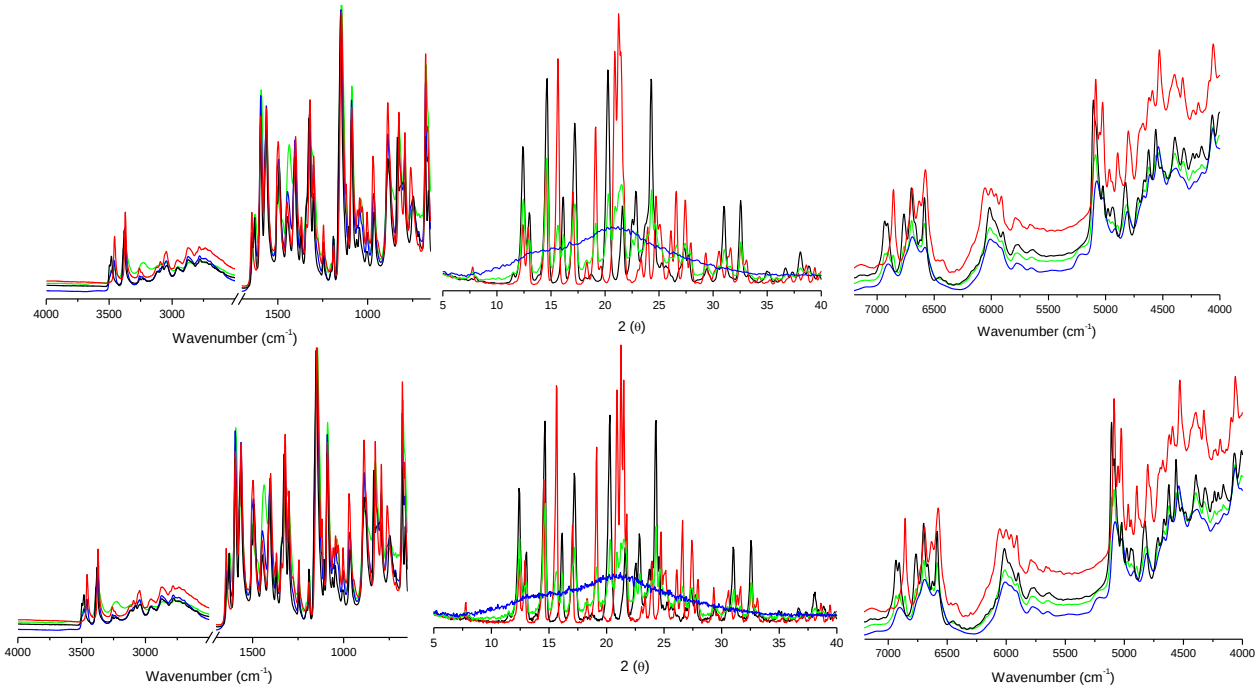

Fig. 1.19 The effects of Gaussian filter average smoothed choosing 9 smoothing points (Top), on raw data (Bottom)

Multiplicative scatter correction (MSC)

Scattering is the result of randomly emitted radiation from a sample, which deviates from its expected trajectories, and gives inaccurate readings during analysis. This is particular true for powdered samples where the size, uniformity, and surface area vary, increasing the scattering effects, inducing background noise and baseline offset. MSC is an algorithm used to negate, or correct, these scattering effects. In MSC the spectra are treated as vector rows $\mathbf{x_i}$, where $\mathbf{x_i}$ is normalised by regressing it against the average spectrum $\mathbf{m_k}$, where the average spectrum is obtained by using equations 13 and 14:

Eq. 13

$$m_k = \sum x_{ik}/N$$

so that:

$$x_{ik} = a_i + b_i m_k + e_{ik} \qquad \text{Eq. 14}$$

where $\mathbf{a_i}$ is the intercept, $\mathbf{b_i}$ is the multiplicative constant, and $\mathbf{e_{ik}}$ is the error. Now a corrected spectrum $\mathbf{x_{i,mod}}$ can be calculated by subtracting the intercept, and multiplicative constant, thus correcting baseline offset, and reducing noise:

$$x_{i,mod} = (x_i - a_i)/b_i \qquad \text{Eq. 15}$$

This is a simple technique to orthogonalise the spectra (variation, **X**), against a measurable factor (response, **Y**), such as concentration, by correlating the vectors, $\mathbf{a_i}$ & $\mathbf{b_i}$, to '**Y**'. However, there is a risk that information may be lost from the spectra (**X**). Because of this the same algorithm used to create $\mathbf{x_{i,mod}}$ must be applied to all data used for predictions, giving the prediction data the same calculated net effect.

MSC data;

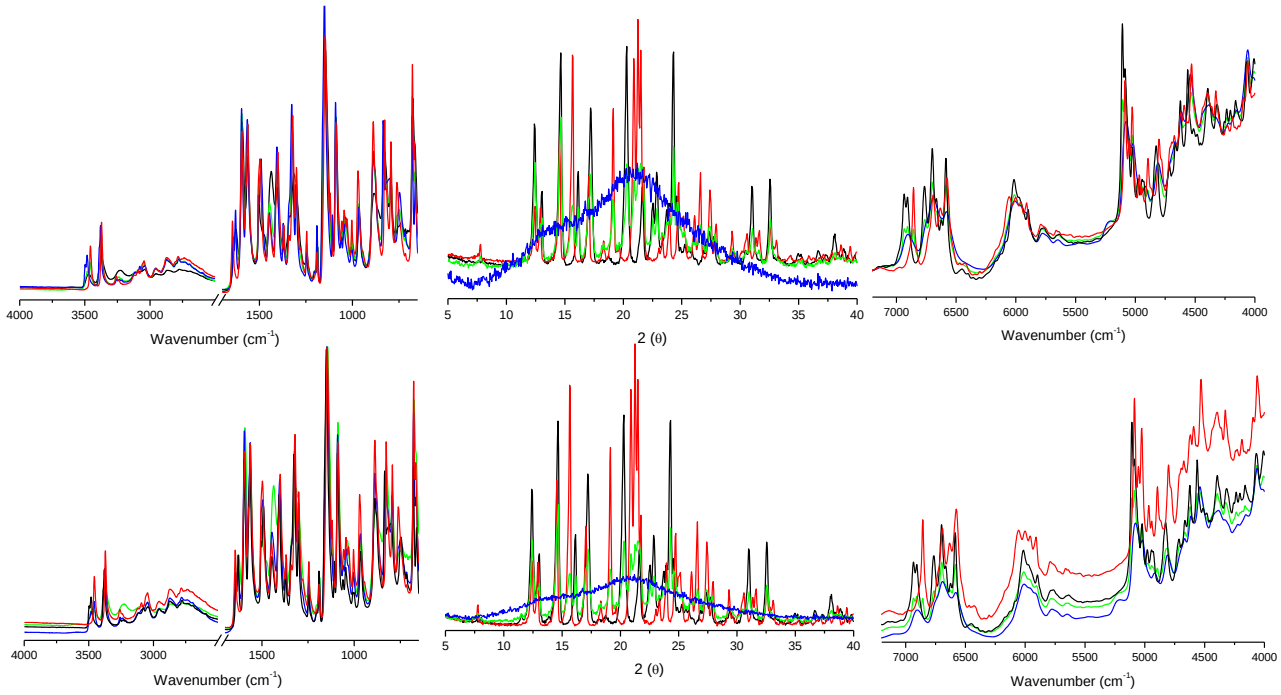

Fig. 1.20 The effects of MSC transformation (Top) on raw data (Bottom)

Standard normal variate (SNV)

Much like MSC, SNV is an algorithm that transforms a row of data 'variation $\mathbf{X_i}$' to remove multiplicative scattering effects, and reduce baseline offset of spectra resulting from non-uniform particle size and surface area. Each individual spectrum is scaled and centred depending on the mean of $\mathbf{X_i}$ and its standard deviation ($\boldsymbol{\sigma X_i}$):

$$x_{i,mod} = \frac{x_i - (mean\ X_i)}{\sigma X_i} \qquad \text{Eq. 16}$$

here each spectrum is centered on zero, where it varies in a new vertical scale from -2 to +2. Each spectrum is standardised by itself, which means it does not use the mean spectrum of the data set (as in the case of MSC), so that each transformation of a spectrum is independent of the other spectra.

There is some debate on which is the more beneficial algorithm to use, MSC or SNV.[38] Some point out that SNV works independently on each spectrum, whereas MSC derives the corrected spectrum from other spectra of the data set, which can bias the new corrected spectrum using MSC, leading to inaccurate predictions.[38] It has also been noted that SNV can decrease measureable absorption, which affects the model's precision. Both SNV and MSC are equated similarities in calculating where in MSC $\mathbf{a_i}$ and $\mathbf{b_i}$ are calculated, instead of the average and standard deviation of the $\mathbf{i^{th}}$ row of X respectively in SNV. Both SNV and MSC were chosen and compared throughout this body of work.

SNV data;

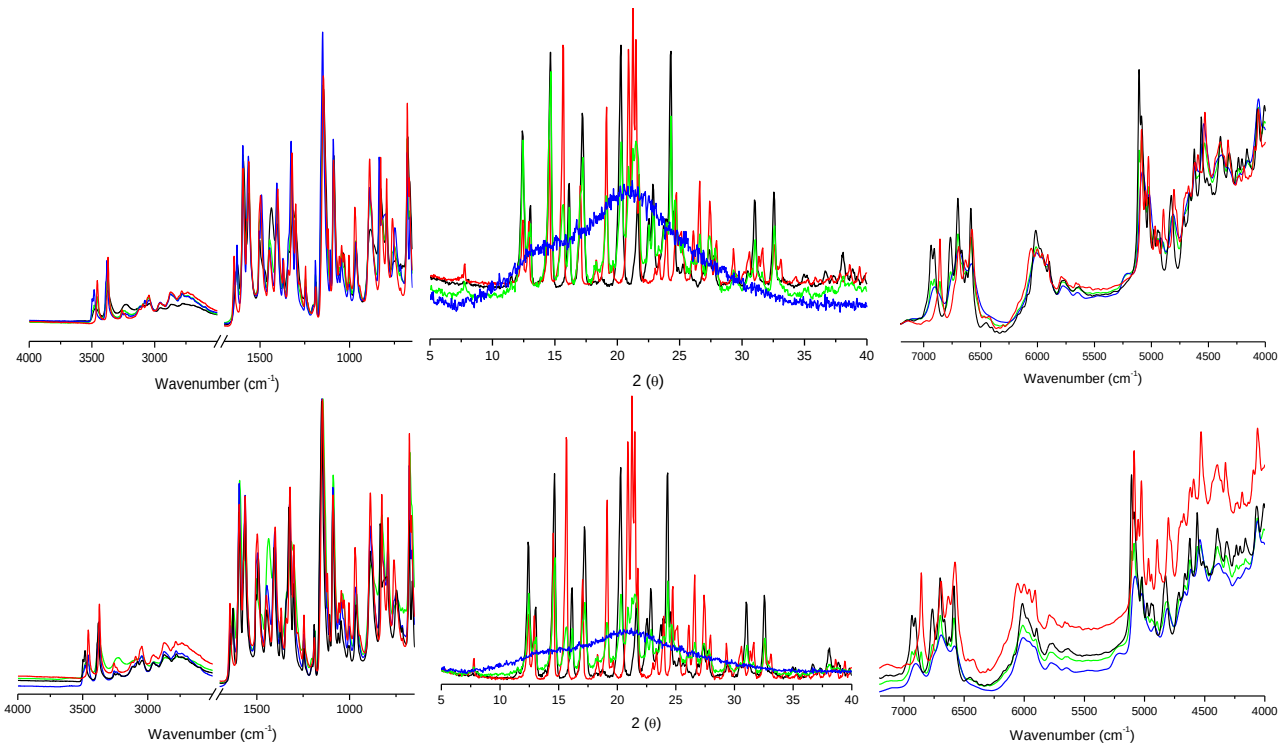

Fig. 1.21 The effects of SNV transformation (Top) on raw data (Bellow)

1st & 2nd Derivatives

There are many benefits in using derivatives in chemoinformatics. Due to the nature of derivatives, where the rate of change is measured, baseline offset is corrected. This also makes it easier in resolving any peak overlap, identifying different components, and removing non-chemical effects from the variation data set. Even though higher order derivatives can be used, The 1st and 2nd derivatives are usually adequate for chemoinformatics, where higher order derivatives (3rd derivative or above) can result in inaccuracies and can greatly reduce the robustness of any calibration models created, though the 4th derivative has been successfully used in quantitative and discriminative analysis discriminative analysis.[39] Derivatives are commonly combined with other algorithms to incorporate smoothing effects; these include Savitzky-Golay derivatives, Norris-Gap derivatives, and Gap-Segment, which use different techniques to compute the derivatives of spectral and X-ray diffraction data.

Norris-Gap derivatives

A Norris-Gap derivative is a type of Gap-Segment derivative where the segment size is 1, and therefore does not smooth the data during the derivation. Instead smoothening of the spectrum prior to the derivation is achieved by averaging over a given number of data points in the spectrum. Here the variations are averaged separately over 1 segment on each side of the data point. The original data point is then replaced with the difference of the two averages, creating an estimate of the derivative at that point.

Norris-Gap 1st and 2nd derivative data;

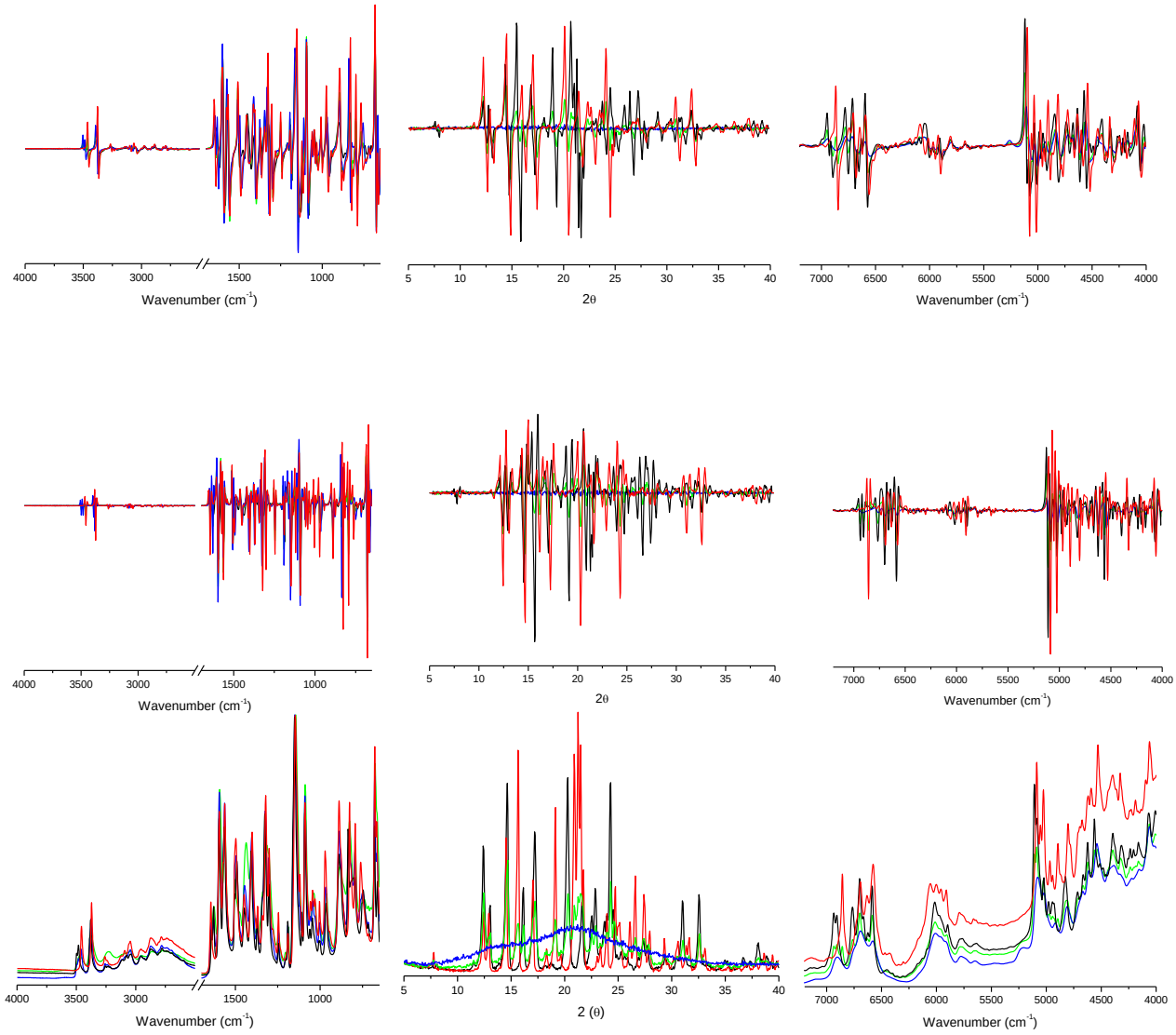

Fig. 1.22 The effects of Norris-Gap 1st (Top) and 2nd (Middle) transformation on raw data (Bottom)

Gap-Segment derivative

Gap-Segment derivative calculates the derivative of a variable with the application of a gap factor and smoothing factor. This results in the distortion of spectral or X-ray diffraction data, where the rate of changes are monitored, but with a corrected baseline. This gives the benefit of having a smoothing effect reduce the interference from background noise. The gap derivative at a data point is calculated as the difference of two averages. Where one segment on each side of the data point is averaged separately, these two segments are separated by a gap, where the data point is the midpoint. The derivative of the data point is calculated as the difference of the two averages of the two segments. This can lead to an issue that if too large a segment is chosen, the resolution of the peaks may decrease, and if the segment chosen is too narrow, to the degree where it is half the band width and will appear as noise.

Gap-Segment 1st and 2nd derivative data;

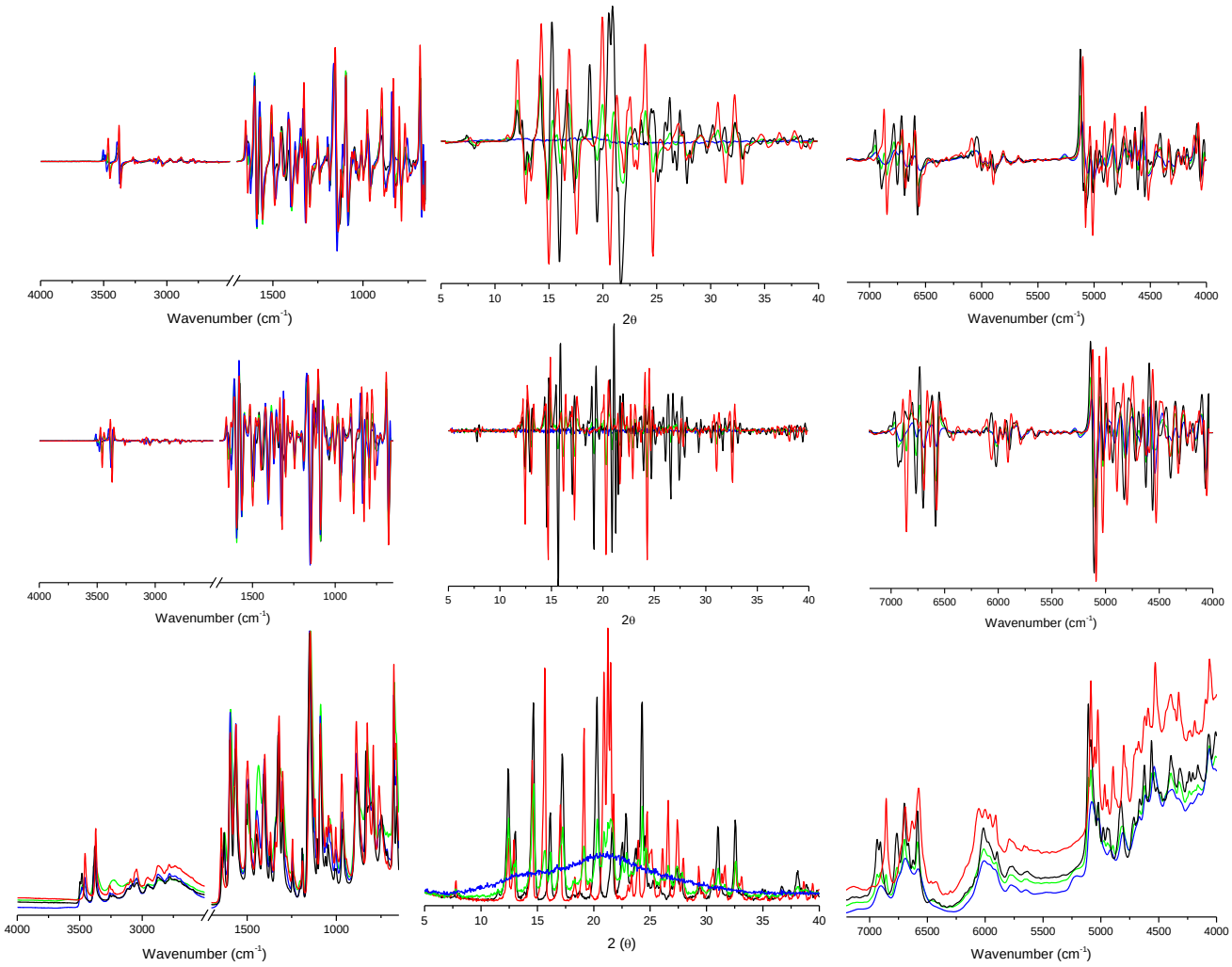

Fig. 1.23 The effects of Gap-Segment 1st (Top) and 2nd (Middle) transformation on raw data (Bottom)

Savitzky-Golay derivatives

This algorithm models a small region/segment of data (estimated by the number of adjacent variables) using a polynomial function. The use of least squares regression is used for a derivative of the polynomial to be calculated. With the baseline offset corrected the derivative can now be smoothed, giving a corrected pattern or spectrum with reduced background noise. A higher degree of polynomial can fit better to the data, giving a more precise derivative, however noise sensitivity will increase.

Savitzky-Golay 1st and 2nd derivative;

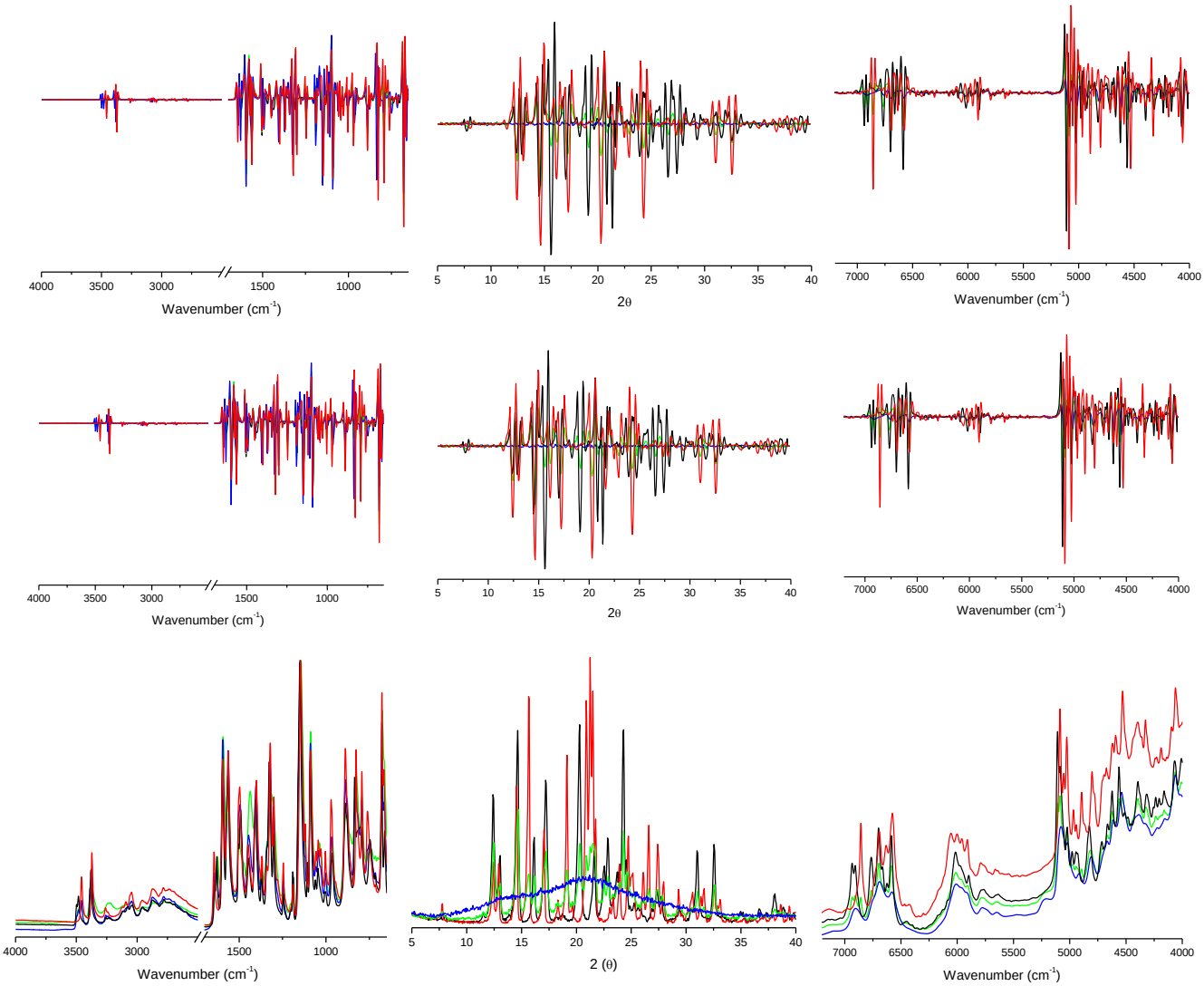

Fig. 1.24 The effects of Savitzky-Golay 1st (Top) and 2nd (Middle) transformation on raw data (Bottom)

Orthogonal signal correction (OSC)

OSC is a transformation which removes variation from the spectral or XRPD data that is mathematically uncorrelated to the response variable, i.e. it removes any spectral variation caused by other components, causing an increased linearity of the spectra to a single selected component. This is created by a similar method as the classical two block PLS system, where loading weights are computed, **w**, such that the score vector is orthogonal to **Y**.[35]

$$t = Xw \qquad \text{Eq. 17}$$

This makes the OSC algorithm very similar to the method used in PLS, only varying where **w** can be modified in OSC. The essential features of OSC are that that the signal correction is expressed as the subtraction of a bilinear expression TP^T (much like in PLS, equations 4 & 5), and that the OSC scores ($\mathbf{t_a}$) are calculated from other sample spectra $\mathbf{x_{new}}$, where;

$$t_{a,mod} = x_{new} + w_a \qquad \text{Eq. 18}$$

When regression models are created using OSC, great care should be taken in interpreting the data. Due to the nature of the data transformation, inaccurate data may be extrapolated to the point where it is incorrectly fitted as part of the calibration plot. It was found trough out this work that this creates a situation where some inaccurate data points seem to fit perfectly giving a good correlation, but when tested against the prediction set, the model fails to produce accurate results. OSC will make the model fit appear good, but may not improve on predictions from separate test sets, exemplifying the need for testing calibration models.

It is also worth noting that due to the nature of OSC only one component can be analysed at a time. This leads to the necessity to have multiple models composed of different OSC data, for each corresponding component. So that if there are multiple known responses

being measured, then there must be that many OSC models corresponding to each individual component, as seen in figure 1.25.

OSC data;

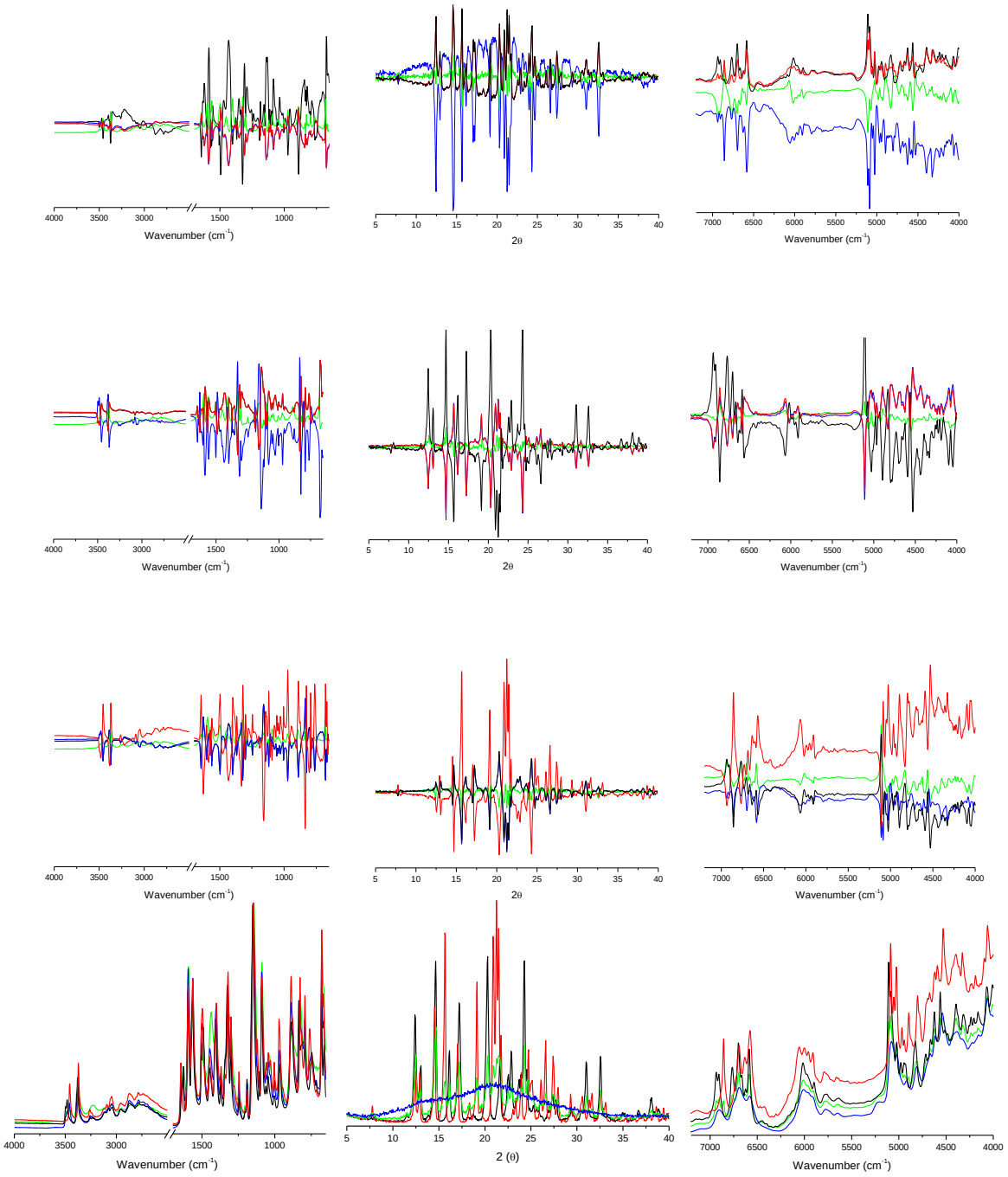

Fig. 1.25 The effects of OSC transformations using form I (Top), form II (2nd from top), and amorphous phase (3rd form top) as OSC components on raw data (Bottom),.

The solid phase properties of sulphonamides

Sulphonamide drugs (also known as sulfadrugs) are antimicrobial agents containing the sulphonamide functional group (Figure 1.26). These drugs are commonly synthesised from amine compounds, primarily from 4-aminobenozic acid (PABA), in which the sulfone functional group is attached to the amine. Sulphonamides work by acting as competitive inhibitors, binding to microbial enzymes, halting the production of dihydrofolic acid, which is crucial in the production of purine or pyrimidine, resulting in the inability to replicate DNA (Figure 1.27). This action has allowed sulfadrugs to be used as broad spectrum antibiotic, effective against Gram positive and negative bacteria, as well as Chlamydia, Rickets, and some protozoa. During the 1930s, '40s and '50s sulfadrugs were common place and became known as the first blockbuster drugs. Over the decades, the use of sulphonamides has declined to the point that their uses are primarily as veterinary antibiotics in animal feed, and specific medical cases, such as urethral infections. This decline is due to potential side effects and their ability to crystallise in the urethra. The most severe side effects are allergies, such as Stevens-Johnsons syndrome,[40] and their adverse effects on an unborn foetus due to interference in the production of folic acid. However, the greatest reasons for their decline is a growing microbial resistance towards sulphonamides, and being over shadowed by the advent of better drugs such as penicillin.

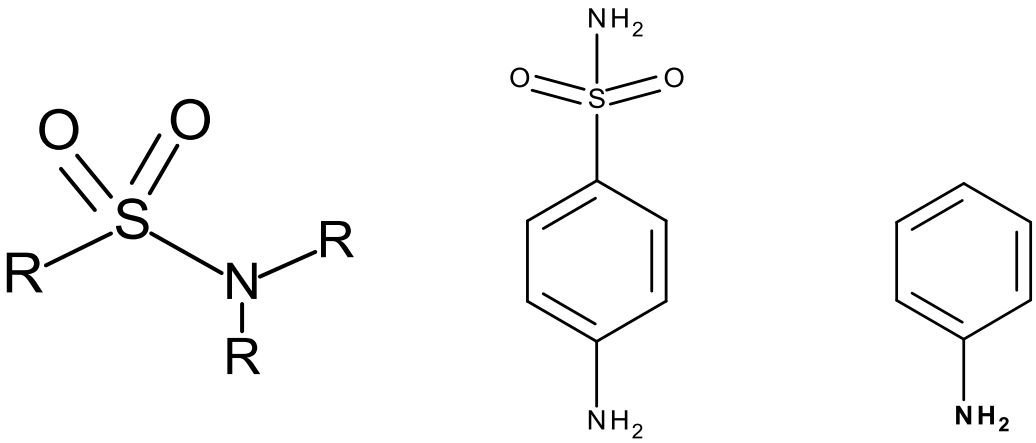

Fig. 1.26 The key functional groups (sulphonamide left and aniline right) whit an example of a sulfadrug (sulphanilamide) (centre).

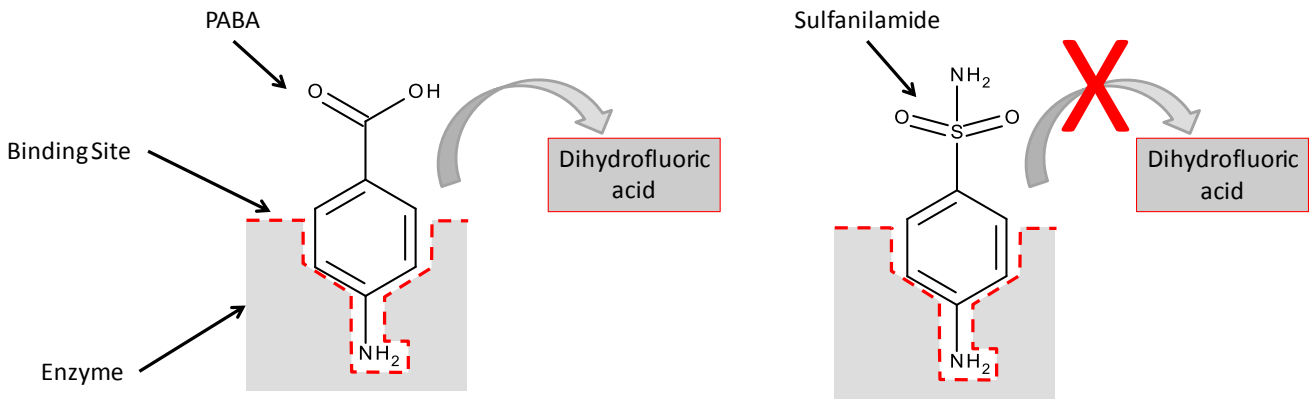

Fig. 1.27 The role of sulfadrugs in inhibiting the production of dihydrofluoric acid

The discovery of the antimicrobial properties of sulfadrugs began in 1930s. This is because in the 19th century it was hypothesised that since aniline was an established analgesic, other coal-tar type dyes could also have medical benefit. With this hypothesis a trial and error procedure was attempted on hundreds of dyes by Bayer AG. A striking success was achieved with Prontosil, a red dye compound synthesised by Josef Klarer in 1932. Prontosil was recognised as one of the first wide spectrum antimicrobial drugs that could effectively treat a range of bacterial infections in the human body.[41]

Even with its success it was seen as an oddity in combating infection in living organisms. Few if any 'test tube' experiments showed the degree of success Prontosil had as an antimicrobial agent, when compared to its efficiency when used on living organism. Later, in 1935 it was found by Bovet, Nitti and T. Tréfouël that Prontosil in fact breaks into two components when metabolised,[41] releasing the inactive dye component and generating sulphanilamide, a compound that was first synthesised in 1906, and at the time without a patent. This started a trend in the manufacturing of sulfa-medicines, flooding the market with cheap 'home remedies' eventually leading to the 'elixir sulphanilamide disaster', where sulphanilamide medicines were improperly prepared, killing over one hundred people and poisoning thousands. This in turn had a hand in the decision to form the FDA.

Thesis Proposal

As mentioned above the solid state of pharmaceuticals is an outstanding, but sometimes neglected property of an API. Though discriminative analysis is successful means of analysis this work takes a quantitative approach, allowing the quantitative analysis of any solid state transformations of an API. The aim of this work was to investigate the polymorphism of two model compounds (Sulfathiazole and sulfamerazine), and to try to prepare their known polymorphs and their amorphous phase via cryo-milling (which had not yet been reported). Different polymorphs of each model compound were cryo-milled for different lengths of time and were monitored to determine the means to prepare their most stable amorphous phase. The amorphous phases of sulfathiazole and sulfamerazine were then monitored at different temperatures, giving a novel insight in the effects of temperature on their stability.

Once the means to prepare stable samples of the amorphous phase is available, calibration models can be created using all achievable solid state. These calibration models give a novel means of analysis, where an exact account of the solid state transformations occurring to any polymorph or the amorphous phase of each model compound is possible. This allowed a new insight of the solid stated transformations occurring to the polymorphs of sulfathiazole and sulfamerazine during room temperature milling and cryo-milling, and monitoring of the stability of their amorphous phases.

Chapter Two

Materials

&

Methods

Instruments

Differential scanning calorimetry

DSC measurements were used to confirm the identity and purity of the sulfathiazole and sulfamerazine polymorphs and were carried out on a STA625 thermal analyser from Rheometric Scientific (Piscataway, NJ, USA) in open aluminium crucibles at a heating rate of 10°C min^{-1}. The temperature range was between 25°C and 250°C. Nitrogen was used as the purge gas. An indium standard was used for DSC calibration.

X-ray powder diffractometry

X-ray powder diffraction data was collected on a Siemens D500 powder diffractometer (Munich, Germany) which was fitted with a diffracted beam monochromator. Diffraction patterns were recorded between 5° and 40° (2θ) using Cu Kα radiation (ℓ = 1.54 Å) with steps of 0.05° and a 2s counting time per step. Simulated powder patterns were obtained from CDCC data, using the Olscail software.[42] These were used to identify and differentiate between different polymorphs.

Near infrared spectroscopy

NIR spectra were recorded in glass vials (15 mm × 45 mm) on a PerkinElmer Spectrum One spectrometer (Waltham, MA, USA) fitted with an NIR reflectance attachment. Spectra were collected over the 10,000 cm^{-1}–4000 cm^{-1} range with a resolution of 8 cm^{-1}, using 32 co-added scans. All samples were re-sampled three times and the mean spectrum was used.

Attenuated total reflectance-infrared spectroscopy

ATR-IR spectra were recorded from 4000 to 650cm^{-1} using a PerkinElmer Spectrum 400 (FT-IR/FT-NIR Spectrometer) with 32 accumulations at a resolution of 4cm^{-1}. This instrument was equipped with a DATR1 bounce Diamond Universal ATR sampling accessory. Every sample was measured in triplicate and for each of the three measurements a fresh aliquot of sample was used.

High pressure liquid chromatography (HPLC)

Hewlett Packard (HP) series 110 was used passing the solutions through a 150mm length Agilent coulomb (Eclipse XDB-C18) having a 5µm pore size at a rate of 5ml/min.

For calibration models, samples of sulfathiazole were prepared in a 70:30 (v/v) mixture of acetonitrile and methanol having the concentrations of 0.25, 0.1, 0.05, 0.025, 0.001 M. The HPLC peak areas of these solutions were plotted against their concentrations giving a calibration plot. Samples of the amorphous phase prepared by cryo-milling and the melt quench method were prepared in a 70:30 mixture of acetonitrile and methanol having the concentrations of 0.05M, these were plotted on the calibration plot to determine possible degradation from using the melt quench method.

Materials

Preparation of sulfamerazine crystal phases

Sulfamerazine form I was purchased from Sigma Aldrich (St. Louis, Missouri) with a purity of ≥99.0% and was used as received. The polymorphic form of the commercial sample was confirmed by comparing predicted XRPD patterns to those collected experimentally. Sulfamerazine form II was prepared according to the literature by crystallisation of commercial SMZ from an aqueous acetonitrile solution (800 mL, H_2O:acetonitrile 20:80) containing 5 g of sulfamerazine.[43] The solution was heated to 60°C for 2.5 hours to ensure complete dissolution. Seeds of FII were prepared by milling FI at 25Hz for 60 minutes and added and the solution was stirred overnight at 300 rpm using a magnetic stirrer. The FII seeds were confirmed to Form II by comparing the experimental powder pattern to the theoretical pattern. The solvent was decanted leaving a slurry which was left to dry under vacuum.

Preparation of amorphous sulfamerazine

An oscillatory ball mill (Mixer Mill MM400; Retsch GmbH & Company, Germany) was used for all milling experiments. 1 g of SMZ FI or FII was milled at 25 Hz in a 25 ml stainless steel jar containing one 15 mm stainless steel ball. For cryo-milling, the milling jars were sealed and immersed in liquid nitrogen for 3 minutes before milling for up to 180 minutes. Every 7.5 minutes the milling jars were recooled with liquid nitrogen for 2 minutes. The average sample temperature measured at 7.5 minute intervals was -10±2°C. Samples of sulfamerazine form I (FI) and form II (FII) cryomilled for 5, 7.5, 10, 15, 20, 22.5, 30, 45, 60, 90, 120, and 180 minutes were used to evaluate the degree of amorphisation of the two polymorphs.

The melt quench method was also used to prepare small quantities of amorphous sulfamerazine by cooling melted samples in liquid nitrogen.

Preparation of sulfathiazole crystal phases

Sulfathiazole form III was purchased from Sigma–Aldrich with a purity of 98% and was used as received. Forms I and V were prepared according to literature procedures.[44-46] The identity and purity of the polymorphs was confirmed by XRPD. The crystal structures of the polymorphs were verified by comparing the experimental XRPD patterns with the theoretical powder patterns calculated from atomic coordinates obtained from the Cambridge Crystallographic Data Centre (CCDC) using Mercury and Oscail Software.[42, 47, 48] Structures with reference codes suthaz01, suthaz02, and suthaz05 were used to generate the theoretical diffraction patterns of forms I, III and V. The bulk samples of the polymorphs were monitored by NIR spectroscopy and XRPD to confirm that each polymorph was physically stable over the course of the study. To minimise particle size effects, the bulk samples of each form were milled under the same conditions using a planetary micro-mill (Pulverisette 7, Fritsch GmbH, Idar-Oberstein, Germany). XRPD and NIR measurements demonstrated that all forms were stable towards grinding and neither amorphisation nor polymorph changes were observed.

Preparation of sulfathiazole amorphous phases

The oscillatory mill was used to prepare amorphous sulfathiazole by cryo milling form I for 60 minutes, recooling after 7.5 minute intervals.

The melt quench method was also used to prepare small quantities of amorphous sulfathiazole by cooling melted samples in liquid nitrogen.

Chemometrics

Preparation of binary mixtures of sulfathiazole forms I, III, and V

Six sets of binary polymorphic mixtures of forms I / III, I / V and III / V containing 0%, 1%, 2%, 3%, 4%, 5%, 6%, 7%, 8%, 9%, 10%, 11%, 13% and 15% (w/w) of the respective minor component were prepared (600 mg total for each mixture) (Figure 2.1). Prior to analysis, the physical mixtures were agitated repeatedly using a vortex mixer. All mixtures were sealed with Teflon-lined caps and kept in a desiccator at ambient temperature. In order to avoid possible systematic changes caused by instrumental and/ or environmental fluctuations, samples were analysed in a random order immediately after preparation.

Preparation of ternary mixtures of sulfathiazole forms I and III, and the amorphous phase

Two ternary model sets were prepared of sulfathiazole forms I, III, and the amorphous phase. The first ternary model set, focusing on whole content analysis was prepared in triplicate with the following mass ratios are of FI/FIII/FA; (100:0:0), (0:100:0), (0:0:100), (50:50:0), (50:0:50), (0:50:50) (70:0:30), (0:70:30), (70:30:0), (0:30:70), (30:0:70), (30:70:0), (33:33:33), (66:12:12), (12:66:12), and (12:12:66) (w/w/w) (Figure 2.2).

The other model set was focused on low content analysis of the solid phases, and was prepared in the ratios of (52:24:24), (68:16:16), (84:08:08), (88:06:06), (96:02:02), (97:01.5:01.5), (98:01:01), (100:0:0)(32:36:32), (16:68:16), (12:76:12), (06:88:06), (04:92:04), (02:96:02), (01:98:01), (00.5:99:00.5), (32:32:36), (24:24:52), (12:12:76), (08:08:84), (04:04:96), (02:02:96), (1.5:1.5:97), (0.5:0.5:98), (0:0:100), (36:32:32), (24:52:24), (16:16:64), (76:12:12), (08:84:08), (06:06:88), (92:04:04), (01.5:97:01.5), (01:01:98), (99:00.5:00.5), (0:100:0) (FI/FII/FA) (Figure 2.3). Due to the number of samples in this ternary set only a single sample set is use for the calibration model, cross-validation, and prediction set.

Preparation of binary and ternary mixtures of sulfamerazine forms I, II, and the amorphous phase

For the whole content binary analysis of sulfamerazine, three sets of binary mixtures were prepared, FI/II, FI/FA, and FII/FA, using the following mass ratios; (0:100), (10:90), (20:80), (30:70), (40:60), (50:50), (60:40), (70:30), (80:20), (90:10), and (100:0) (w/w) (Figure 2.4 middle). For the low and high content analysis a range of 0-10% having the mass rations; (0:100), (01:99), (02:98), (03:97), (04:96), (05:95), (06:94), (07:93), (08:92), (09:91), (10:90) (w/w) was used (Figure 2.4 top).

The preparation of the ternary polymorphic mixtures followed a previously described procedure.[49, 50] The mass ratios are of FI/FII/FA; (100:0:0), (0:100:0), (0:0:100), (50:50:0), (50:0:50), (0:50:50) (70:0:30), (0:70:30), (70:30:0), (0:30:70), (30:0:70), (30:70:0), (33:33:33), (66:12:12), (12:66:12), and (12:12:66) (w/w/w) (Figure 2.5). These sample sets were repeated in triplicate. The amorphous sulfamerazine used in these mixtures was obtained by cryo-milling FI for 60 minutes.

Physical mixtures (300 mg total for each mixture) were prepared and mixed uniformly for 3 minutes using a vortex mixer (Thermal Type 37600). To ensure the stability of the amorphous phase, a separate sample of each batch was set aside and checked for any crystallisation before the analysis a mixture using NIR spectroscopy. Mixtures were prepared and analyzed in triplicate. In order to avoid possible systematic changes caused by instrumental and/or environmental fluctuations, samples were prepared in a random manner and immediately analyzed.

Data analysis

Multivariate data analysis was carried out using the multivariate data analysis software The Unscrambler v.9.8 for sulfathiazole, and v.10.0 for sulfamerazine (Camo, Norway). Pre-treatment methods included multiplicative scatter correction (MSC), standard normal variate (SNV) transformation, first derivative calculations, and first derivative calculations combined with SNV for the NIR data and Savitzky–Golay smoothing and first derivatisation for the XRPD data. For univariate analysis a linear baseline correction and second derivative calculations were applied as pre-treatment methods. Savitzky-Golay, 1st and 2nd derivative calculations and smoothing were performed with a window size of 7 (XRPD patterns) and 11 points (NIR spectra) and a 2nd order polynomial. The gap and segment sizes used for second derivative

calculations were; Norris Gap (gap size 7) and Gap-segment (gap size 7, segment size 3). The gap and segment sizes were chosen by a trial and error method, comparing the calibration models produced different gap/segment sizes. The loading plots were used to identify suitable spectral and 2θ regions for building the calibration models. Different wavenumber and 2θ ranges were evaluated and the best-performing model was selected by comparing its Root Squared Error Calibration (RMSEC), Cross Validation (RMSECV) and Prediction (RMSEP), the standard deviation against blanks, and it's Limit of Detection (LOD). The spectroscopic data were mean-centred before applying partial least-squares (PLS) regression.

Sulfathiazole data sets

For analysis of sulfathiazole binary mixtures, every set of measurements was split into a calibration set (0%, 1%, 2%, 3%, 5%, 7%, 8%, 10%, 11% and 15%) and a prediction set (4%, 6%, 9% and 13%) (Figure 2.1).

For the whole content, ternary analysis of sulfathiazole three data sets (each containing 13 samples) were split into a calibration set and prediction set. Two sample sets (26 samples) were used for calibration, the other 13 samples used for predictions (Figure 2.2).

For the low content analysis, the 36 samples were split in two data sets. Two thirds of the data set with ratios of (52:24:24), (68:16:16), (84:08:08), (88:06:06), (96:02:02), (97:01.5:01.5), (98:01:01), (100:0:0)(32:36:32), (16:68:16), (12:76:12), (06:88:06), (04:92:04), (02:96:02), (01:98:01), (00.5:99:00.5), (32:32:36), (24:24:52), (12:12:76), (08:08:84), (04:04:96), (02:02:96), (1.5:1.5:97), (0.5:0.5:99), (0:0:100) (FI/FII/FA) (w/w/w) was used for calibration, the remaining third of the data points (36:32:32), (24:52:24), (16:16:64), (76:12:12), (08:84:08), (06:06:88), (92:04:04), (01.5:97:01.5), (01:01:98), (99:00.5:00.5), (0:100:0) were used for predictions (Figure 2.3).

The optimal PLS factor was determining by the local minimum of residual variances.[51] For comparing the different pre-processing methods, the root-mean-square errors of calibration (RMSEC), cross-validation (RMSECV), RMSEP, standard deviation, and limit of detection (LOD) were used in ternary analysis, and RMSEC, RMSECV, and RMSEP for binary analysis

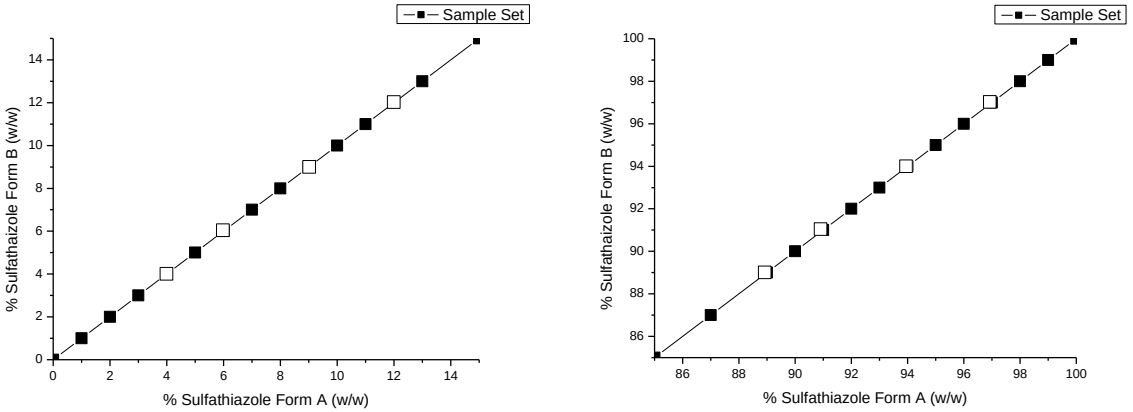

Fig. 2.1 Sample sets used for low content (Left) and high content (Right) binary analysis of the different solid states of sulfathiazole. ■ Samples were used for calibration and cross-validation models, samples as □ were used as prediction samples

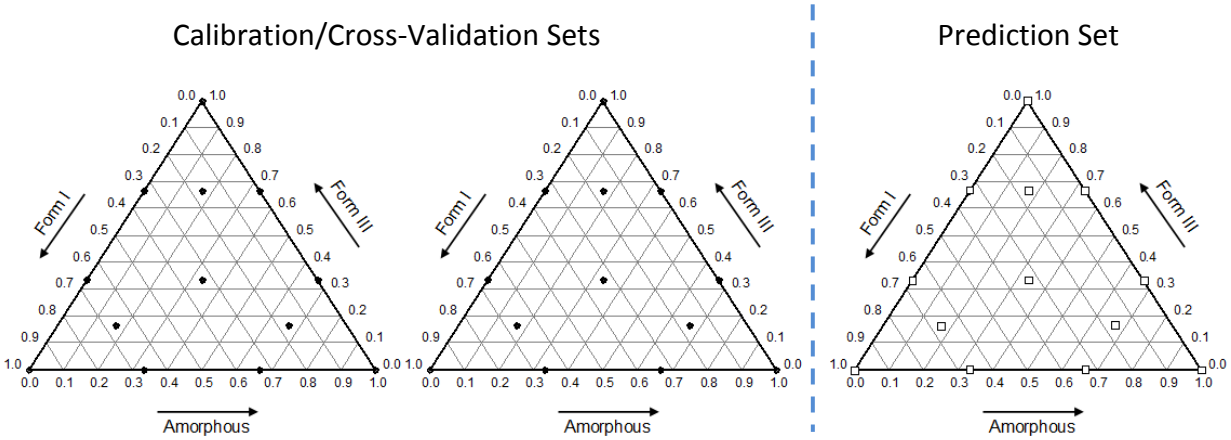

Fig. 2.2 Sample sets used for whole content ternary analysis of form I, form III and the amorphous phase of sulfathiazole. The 2 sets (Left and middle) shown as ● were used for calibration and cross-validation models, and one set (Right) shown as □ were used as a prediction set

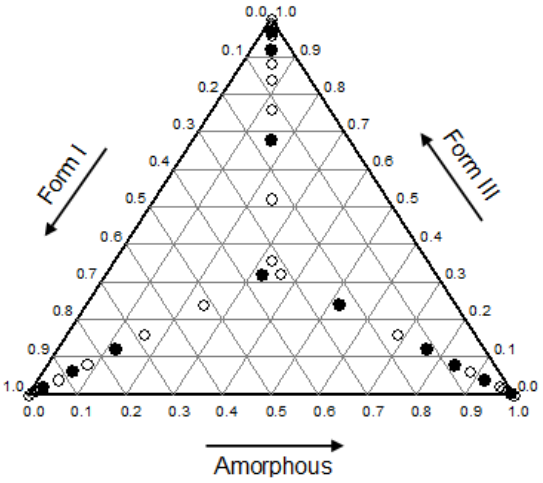

Fig. 2.3 Sample sets used for low content ternary analysis of form I, form III and the amorphous phase of sulfathiazole. One sample set needed for cross validated calibration model and prediction samples, ● samples were used in the calibration and cross validation model, and ○ samples were used as prediction samples

Sulfamerazine data sets

For the binary analysis of sulfamerazine the three data sets were split into three sets. Two were used for calibration and validation, the other used for predictions (Figure XY). This was also used in the ternary analysis. This allowed the collection of data during different days, creating a more robust model. The optimal number of PLS factors was determined using a "leave-one-out" cross-validation procedure or by finding the minimum root mean square error of prediction (RMSEP).[51] This method was repeated for the ternary analysis. For comparing the different pre-processing methods, the root-mean-square errors of calibration (RMSEC), cross-validation (RMSECV), RMSEP, standard deviation, and limit of detection (LOD) were used in binary and ternary analysis.

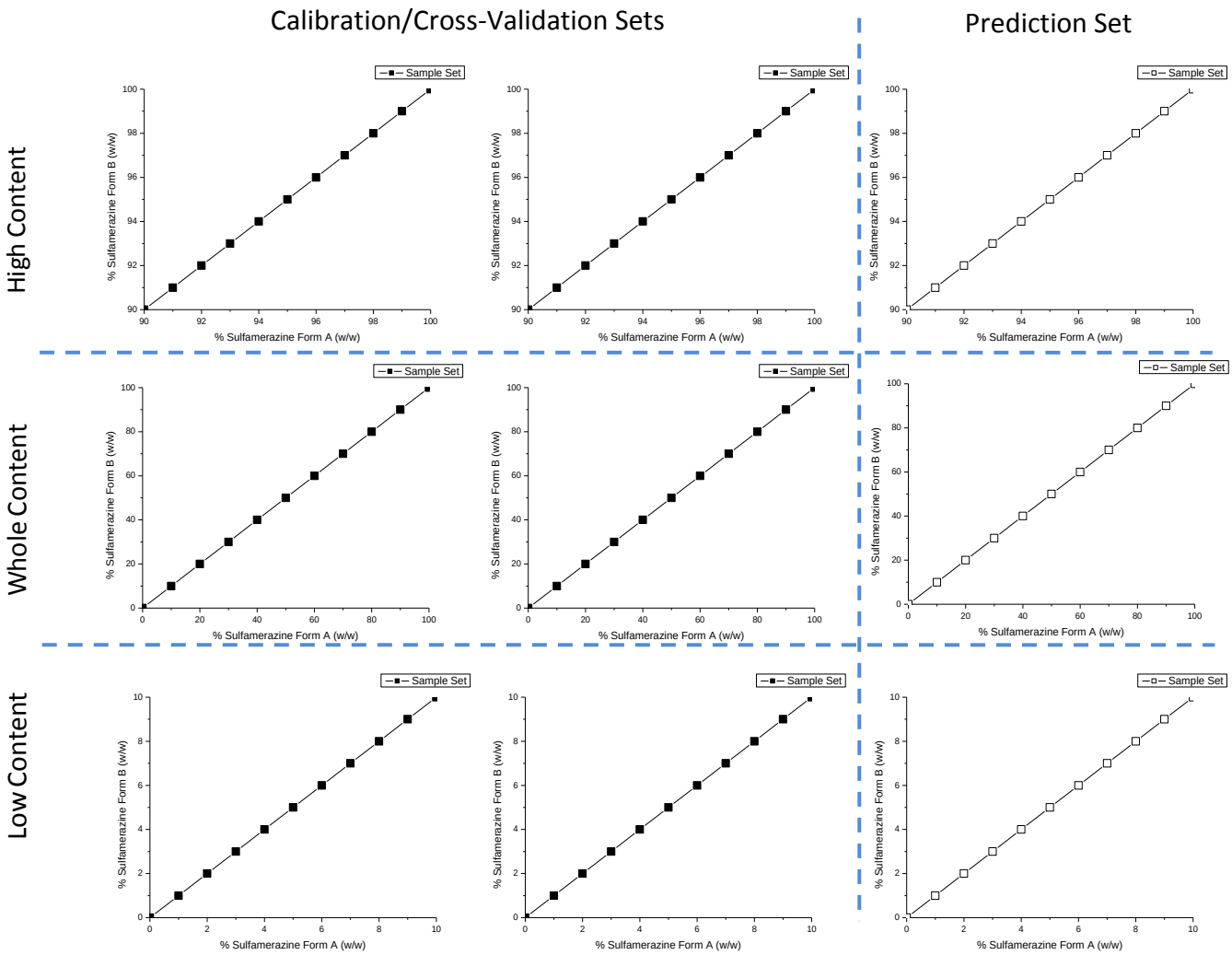

Fig. 2.4 Sample sets used for high content (Top), whole content (middle), and low content (bottom) binary analysis of the different solid states of sulfamerazine. The 2 sets (Left and middle) shown as ■ were used for calibration and cross-validation models, and one set (Right) shown as □ were used as a prediction set

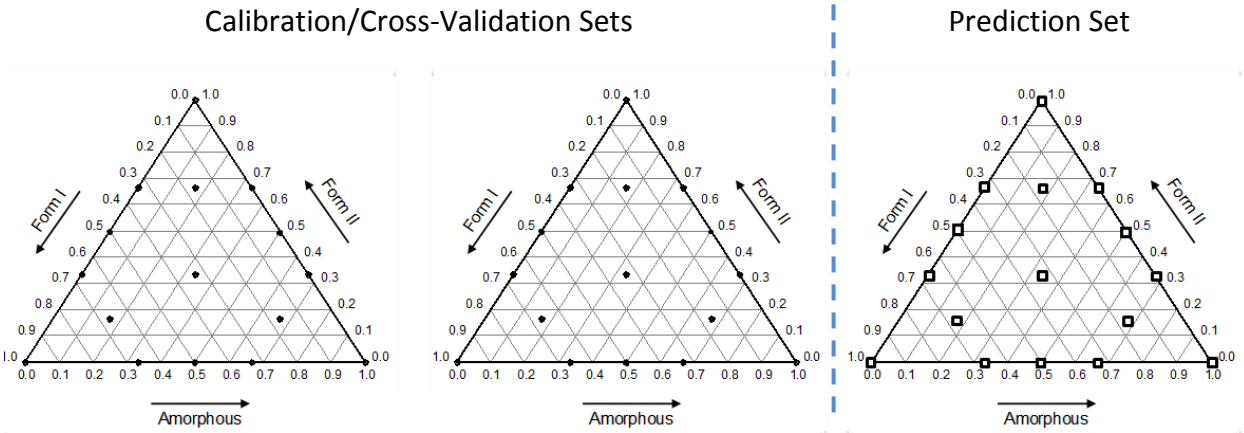

Fig. 2.5 Sample sets used for whole content ternary analysis of form I, form II and the amorphous phase of sulfamerazine. The 2 sets (Left and middle) shown as ● were used for calibration and cross-validation models, and one set (Right) shown as □ were used as a prediction set

Chapter Three

Solid state analysis of sulfamerazine

Introduction

Since the 1940s the pharmaceutical properties of sulfamerazine have been thoroughly investigated, where it has shown great promise in acting as an antimicrobial agent. Literature has documented its success when it was first administered to poultry,[52] and later in clinical trials when administered to children.[53] As common with many sulfadrugs, sulfamerazine was found to combat infections over a wide range of diseases acting as a broad spectrum antibiotic. Sulfamerazine has shown great promise in combating a range of prevailing diseases, particularly when combined with other drugs. This allowed the tailoring of medication against specific diseases and infections by combining specific drugs with an array of broad spectrum antibiotics to further treat disease. An example of this is that penicillin shows much greater therapeutic properties against meningitis when combined with sulfamerazine.[54, 55]

As with many sulfadrugs, the administration of sulfamerazine decreased through the following decades during the mid 20th century. This was due to a growing number of infections becoming resistant against sulfadrugs, and during the same period a superior array of antibiotics was being produced. These newer generations of pharmaceuticals were found to have greater success against a broader range of diseases and infection, with less severe side effects on humans. Currently sulfamerazine is administered as a veterinary drug in feed stocks to pigs and cattle. The structure of sulfamerazine is typical of most sulfadrugs, having a sulphonamide backbone, and an amine functional group (Figure 3.1). This allows the docking to enzymes, and in turn inhibits PABA binding to produce dihydrofolic acid, hindering the generation of bacterial DNA (Figure 1.26).

As with many sulfadrugs, the sulphonamide backbone and amine functional group in sulfamerazine give rise to multiple crystal structures. Reasons for this include having the sulphonamide backbone creating a polar environment and multiple H bonding sites allowing the existence of multiple polymorphs. To date there are three known polymorphs of sulfamerazine.[56-58] The first attempt to solve the crystal structure of sulfamerazine was performed by Deo et al. where (1980) form I (FI) was recrystallised from water, and was designated in the CCDC as SLFNMA and was reported to have the space group $Pca2_1$.[59] Acharya et al (1982) found this to be incorrect, discovering FI crystallises in the space group *Pbca* and

reported this in the CCDC as SLFMA01. Caira et al (1992) recrystallised form II (FII) by recrystallising FI in an acetonitrile/water mixture, where it was found to have the space group Pna_1 (SLFMA02) confirming it as a unique polymorph.[58] Hossain et al. (2006) are the most recent to discover a new polymorph form III (FIII), which was reported in the CCDC as SLFMA03. FIII was recrystallised from dimethylformamide (DMF), and again its uniqueness as a polymorph is evident from its space group $P2_1/c$.[56] FI and FII are enantiotropically related with slow interconversion kinetics making FII more stable at room temperature, whereas FI is more stable at higher temperatures.[4, 60] Solvent-mediated transformations of SMZ polymorphs in solution have been extensively studied.[43, 60-64] It can be seen from the arrangement of FI, FII, and FIII that H bonding and van der Waals forces are the predominant influence on the crystal structure of sulfamerazine. The effects of H bonding can be noted by the layering arrangement over the benzene ring, and the zigzag arrangement of the H bonding. It can be clearly seen that both FI and FIII posses slip planes, whereas the layers of FII are interlocked (Figure 3.2). The effect of compression and milling on powder samples has also been reported, where FI was found to be susceptible to transformation due to its structural slip planes.[3, 60, 65] To date little has been reported on FIII.

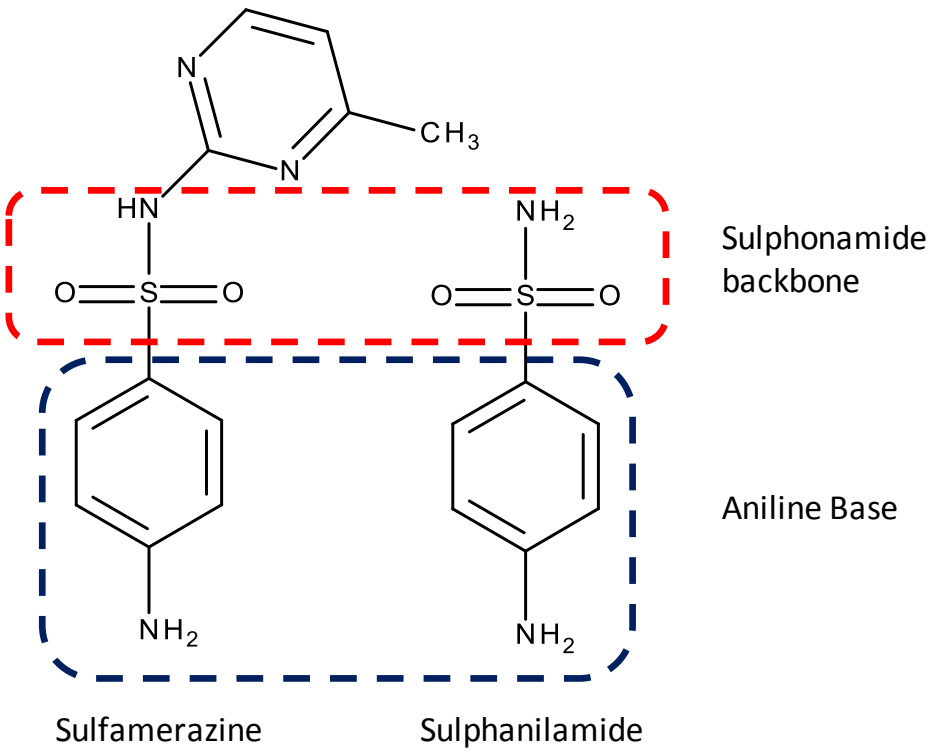

Fig. 3.1 Structural similarities between sulfamerazine and sulphanilamide

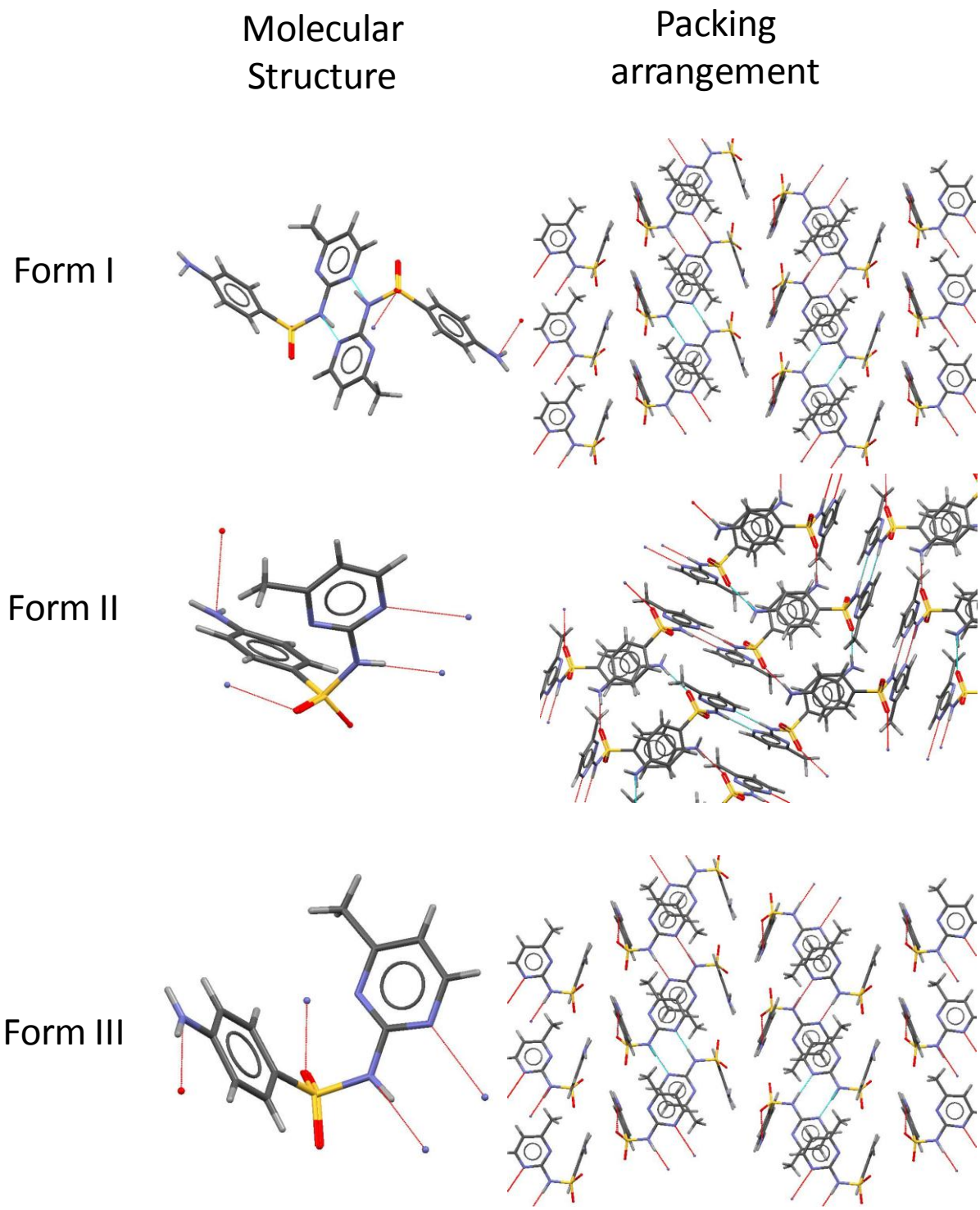

Fig. 3.2 Molecular structure of sulfamerazine forms I, II, and III (left), and their packing arrangement (right)

Chattoraj et al. (2012) observed partial amorphisation of FI during cryo-milling.[3] Samples of FI were cryo-milled at 10Hz for 120 minutes, and it was estimated that 79.3% had converted to the amorphous phase (FA). This study also determined the glass transition temperature (T_g) as 67°C. While amorphisation has been observed in the cryo-milling of FI, it has been shown that room temperature milling leads to a FI $\rightarrow$ FII transition.[4] It was hypothesised that the FI $\rightarrow$ FII transformation during milling takes place via a transient amorphous phase. Due to the structural slip planes of FI, transformation occurs more readily during milling. From this it can clearly be seen that polymorphic change can readily occur between FI and FII resulting from physical or mechanical stress, and it should be possible for a complete transformation to the amorphous phase of sulfamerazine.

Much work has been done in the analysis of both FI and FII, but little if any has been conducted on FIII. This is most likely due to the difficulty in obtaining bulk quantities of FIII to be used for analysis. Studies of FI and FII primarily focus on the transformations between both forms, and creating methods of analysis that produce characteristic information that can be used to quantify and distinguish both forms. In the last 10 years the focus has moved from investigating the structure of sulfamerazine to the quantification of the two polymorphs and properties the different polymorphs may possess.

The ability to identify and quantify different polymorphs has always been a challenge, and sulfamerazine has been a model compound to test different techniques, including NIR,[64] Raman, XRPD, DSC,[24] IR, and solid state NMR.[66] Qualitative analysis of sulfamerazine polymorphism was able to identify unique polymorphs to as low as 10mg using ssNMR, and the different morphology of FI and FII were differentiated to the µm scale, using atomic force microscopy (AFM).[67] Where rods of FI can be identified with width of 1µm and were distinguishable from FII plates, observed as 5µm plates. In quantitative analysis, different indications to measure the accuracy of calibration models have been used throughout many studies. These include RMSEC, RMSECV RMSEP, SEC, SEV, SEP, R^2, etc. This makes the comparison of different analytical methods difficult. Binary calibration models having R^2 of 0.9979 using NIR, with XRPD and DSC having a standard deviation of 1.89 % and 3.53 % respectively have been reported.[64] Raman microscopy has given a RMSEC of 5.98 % and RMSEP of 6.75 % and XRPD gave a RMSEC of 1.28% and a RMSEP of 1.65% using a PLS factor of 4.[24] All these studies have focused on forms I & II, which are the only forms that can be prepared in bulk, whereas FIII has only been prepared in small quantities in range of a few crystals. Also due

to FA only being partially generated, only binary models of FI and II could have been applied to the quantification of sulfamerazine polymorphs.

For this work the full transformation to the amorphous phase of sulfamerazine from forms I and II were achieved for the first time. This allowed the generation of binary and ternary calibration models that were successfully used to give a new insight into the transformations that occur to polymorphs form I and II during room temperature milling and cryo-milling, the stability of amorphous phase, and the effects further cryo-milling times has on the crystallisation of the amorphous phase.

Characterisation of commercial sulfamerazine

It was determined that the sulfamerazine obtained commercially was FI. This was confirmed by comparing the commercial sample with crystals of FI obtained by re-crystallising the commercially obtained sulfamerazine in H_2O. Both were analysed using NIR and IR spectroscopy, and was compared and matched to the commercial samples (Figures 3.3 and 3.4). In addition the theoretical XRPD patterns, generated from Oscail using single crystal data were used to confirm the recrystallised and commercially samples were sulfamerazine FI (Figures 3.5 and 3.6). This was confirmed by comparing the XRPD patterns of the commercially obtained and re-crystallised sulfamerazine to the theoretical XRPD patterns. The spectroscopic and XRPD data confirms the commercially available sulfamerazine is FI.

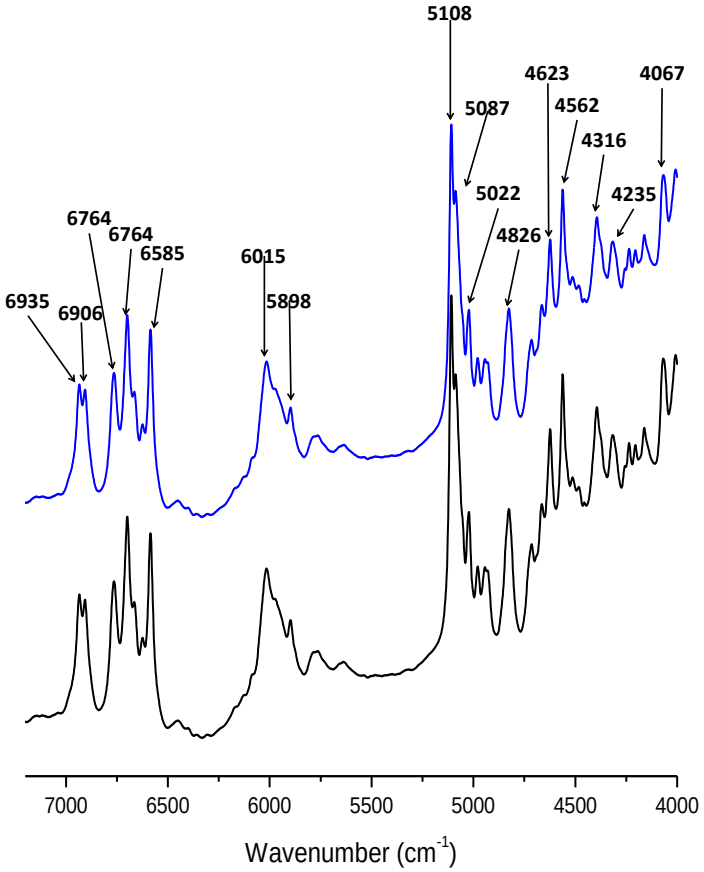

Fig. 3.3 Comparison showing the similarities of NIR spectra of recrystallised (bottom) and commercial (top) sulfamerazine

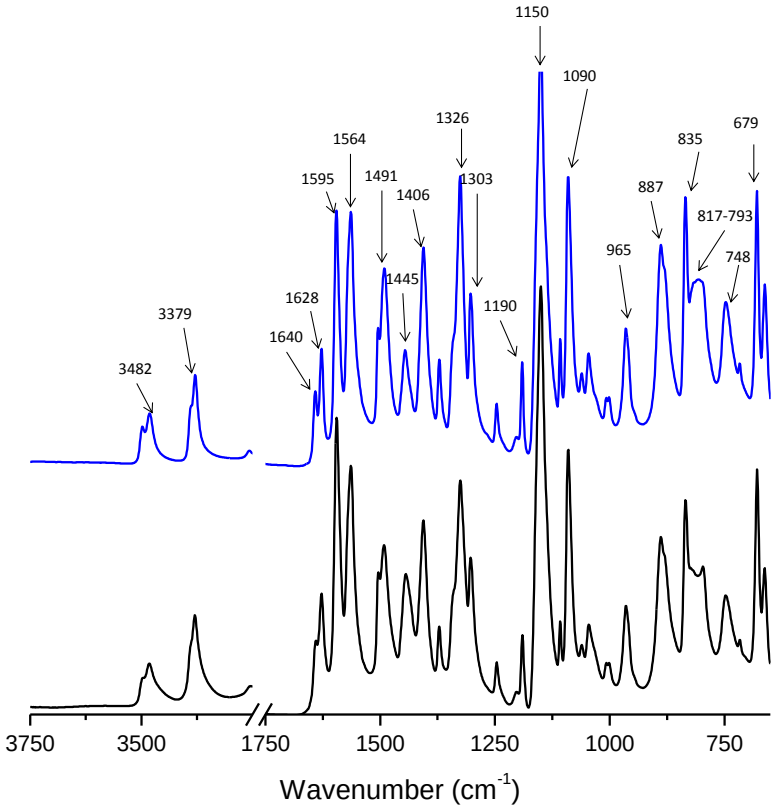

Fig. 3.4 Comparison showing the similarities of IR spectra of recrystallised (bottom) and commercial (top) sulfamerazine

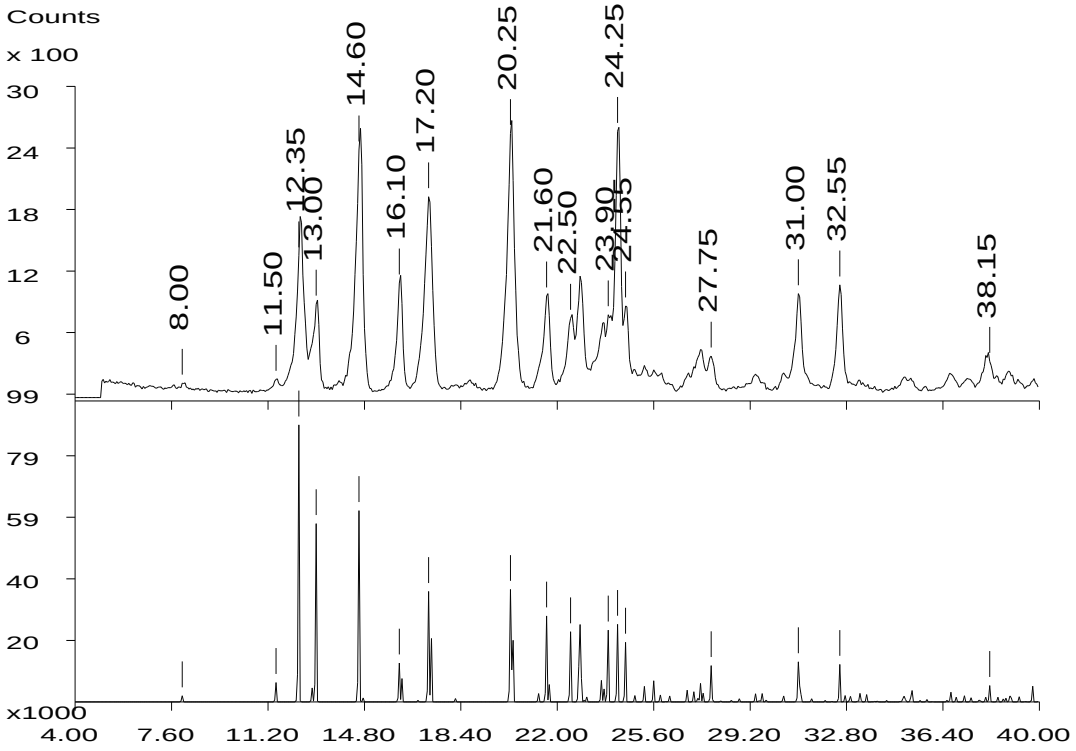

Fig. 3.5 Comparison of theoretical (bottom) and experimental (top) XRPD patterns of recrystallised sulfamerazine FI

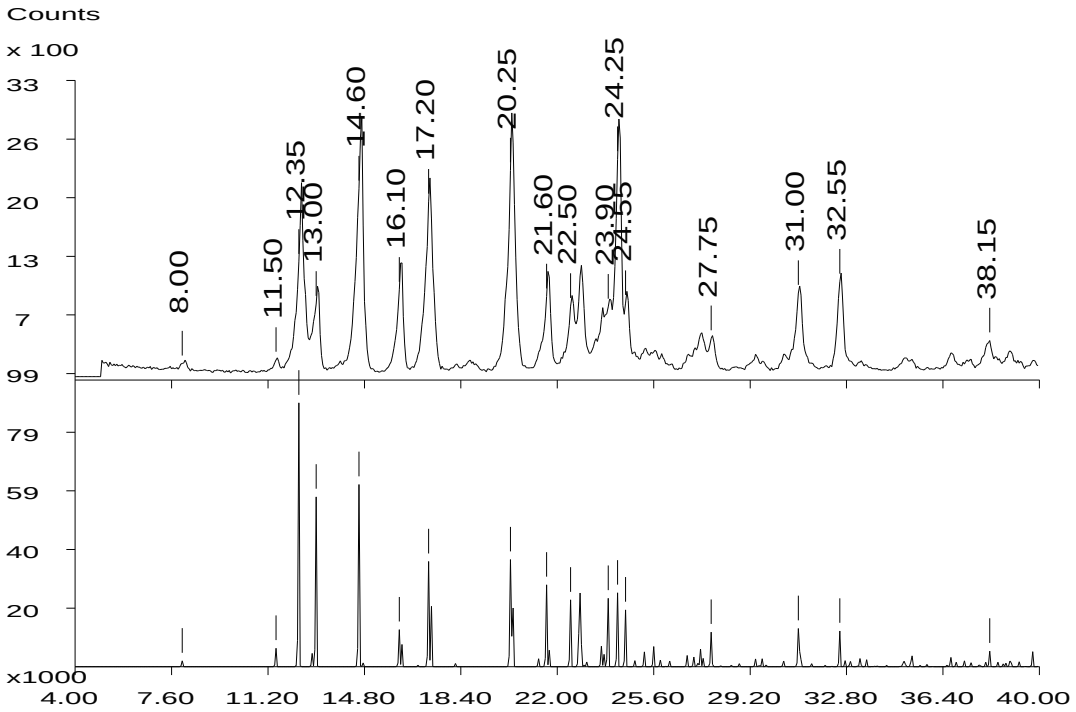

Fig. 3.6 Comparison of theoretical (bottom) and experimental (top) XRPD patterns of commercial sulfamerazine

Preparation and characterisation of sulfamerazine form II

Many methods in the preparation of FII were reviewed to determine the optimal method for bulk production. The goal of selecting an optimal method was to be able to crystallise bulk amounts of FII (3-7g), having complete crystalline transformation within 2 days. Several methods mentioned in previous literature were attempted,[4, 43, 58, 62, 67]. The material prepared using some of these methods showed signs of impurity with only partial transformation to FII (Table 3.1). [43, 58, 62, 67] Without a pure sample of FII spectroscopy was not able to be used in identification. Instead a theoretical powder pattern was derived from the single crystal data using the Oscail software, and used to detect and confirm the presence of FII. Milling small amounts of FI at 25Hz and waiting a day showed a transformation to FII,[4] and was confirmed to be pure FII by comparing its XRPD to the theoretical powder pattern (Figure 3.7). Though the method of milling FI to produce FII was successful it was deemed inefficient for the bulk production of FII (Figure 3.9 and 3.10), as the maximum sample size of the milling jars is less than 1 gram. Even though this method was found to be inefficient, it did produce a pure sample of FII. This allowed the collection of experimental spectroscopic and XRPD data, and a method to produce seeds for future crystallisations.

Methods use	Days aged	Polymorphic content	Colour	Time taken (Days)
Seeding a 1g/100ml 70:30 solution of acetonitrile and water. [43]	3	Mixture of FI/FII	White	4
Evaporation from acetonitrile [58]	1	Mixture of FI/FII	Yellow	6
Evaporation a 1g/100ml 70:30 solution of acetonitrile and water	2	Mixture of FI/FII	Yellow	5
Evaporation a 1g/100ml 70:30 solution of acetonitrile and water, held at 50°C [62-67]	1 & 3	Almost pure FII, some FI	White	3
Seeding a 1g/100ml 70:30 solution of acetonitrile and water, held at 60° for 24 Hr. [4]	1	Pure FII	White	2

Table 3.1 Methods studied the preparation of sulfamerazine form II

The crystallisation of FII was successfully achieved by seeding a saturated 4:1 acetonitrile and water solution of sulfamerazine with a small quantity of FII (prepared from milling FI). Temperature and aging time were varied to examine their effects on the crystallisation. The optimal method of crystallisation was found to involve letting the crystals age for 24 hours at room temperature, then decanting the mother liquor, and removing the remaining solvent under vacuum at room temperature.

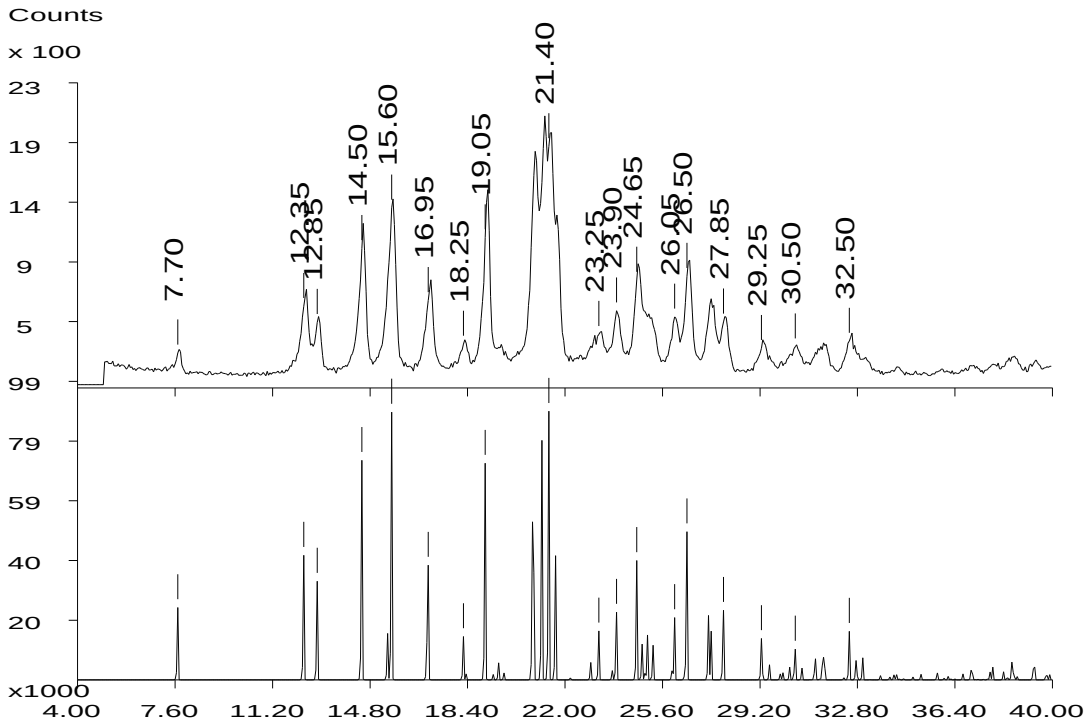

Fig. 3.7 XRPD pattern comparison of theoretical (bottom) and experimental XRPD patterns of sulfamerazine FII prepared from milling FI (top)

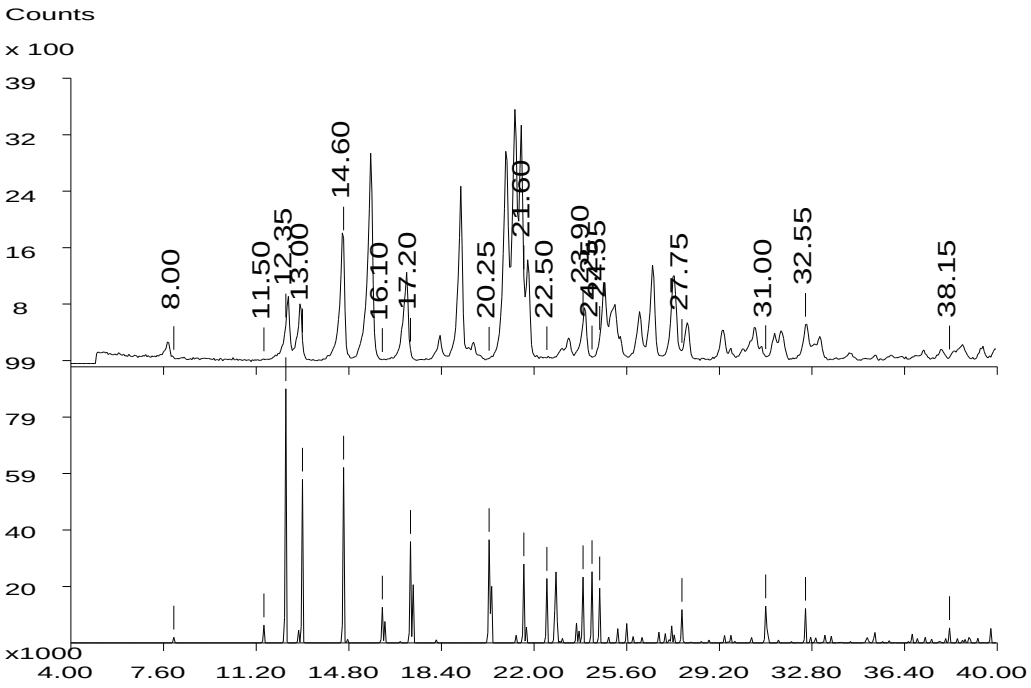

Fig. 3.8 XRPD pattern comparison of recrystallised sulfamerazine FII (top) and theoretical FI (bottom)

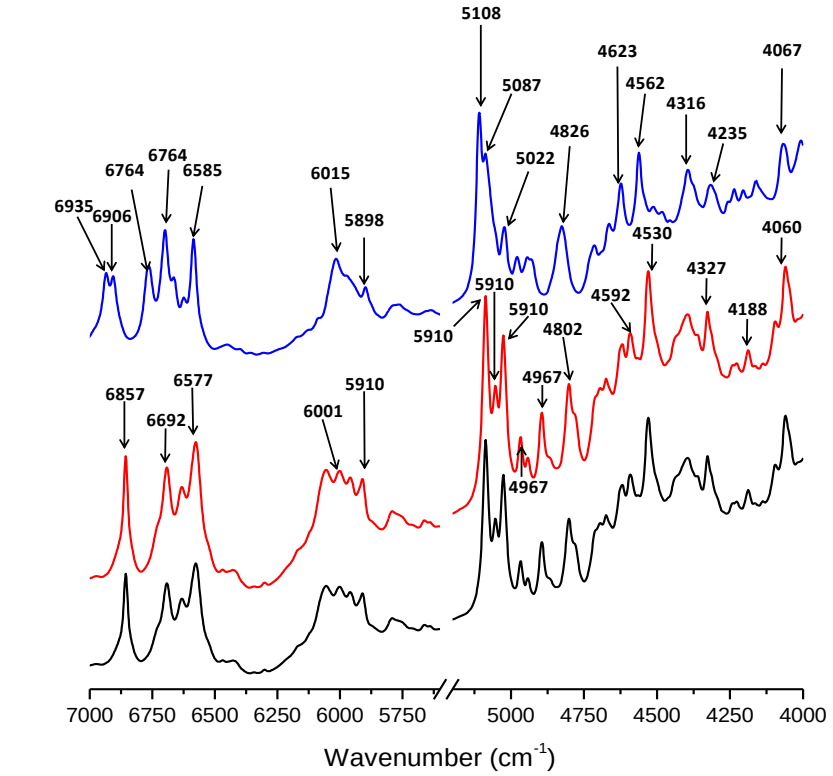

Fig. 3.9 Comparison of the NIR spectra of FII via milled FI (black), recrystallised FII (red), and FI (blue)

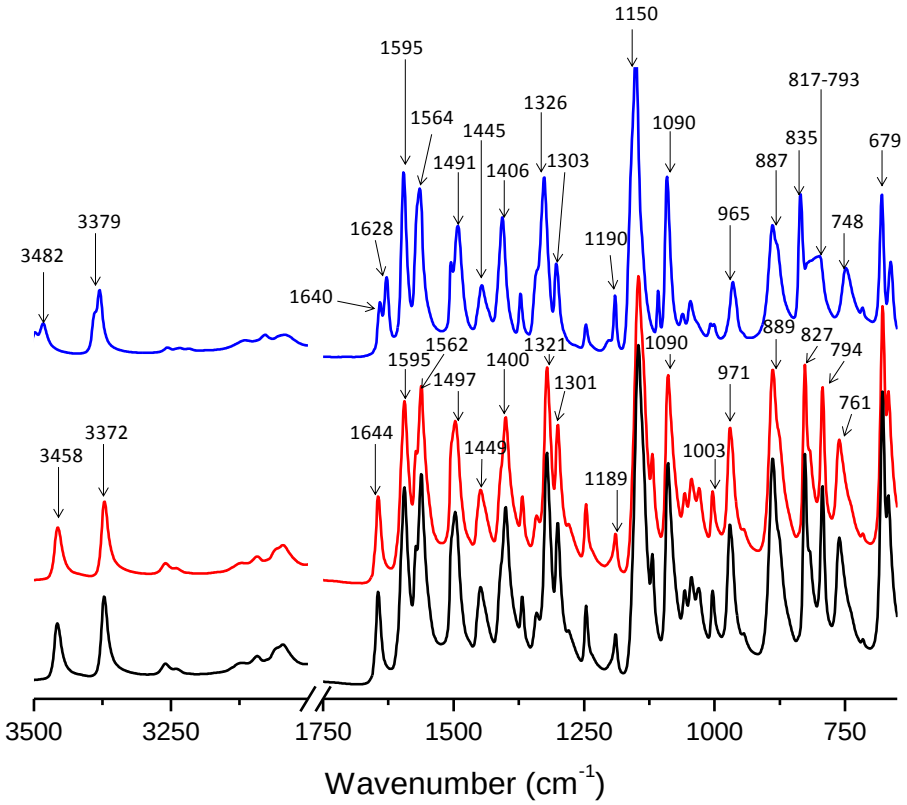

Fig. 3.10 Comparison of the IR spectra of FII via milled FI (black), recrystallised FII (red), and FI (blue)

Characterisation of amorphous sulfamerazine (FA)

FA was produced by cryo-milling both FI and FII, and shows unique NIR and IR spectra (Figures 3.11 and 3.12). Though many peaks seem to overlap those of FI and FII, it is clear that the spectra are unique to FA.

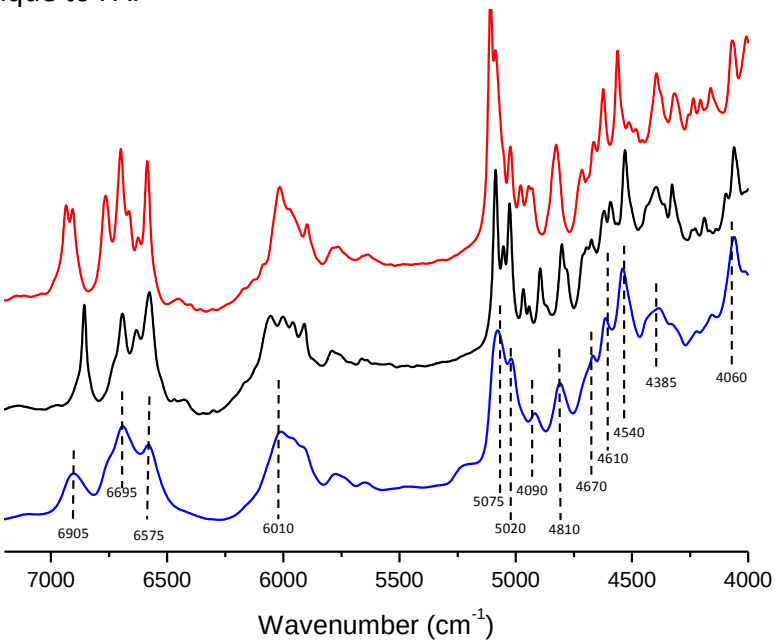

Fig. 3.11 Comparison of the NIR spectra of FA (blue) FII (black), and FI (red)

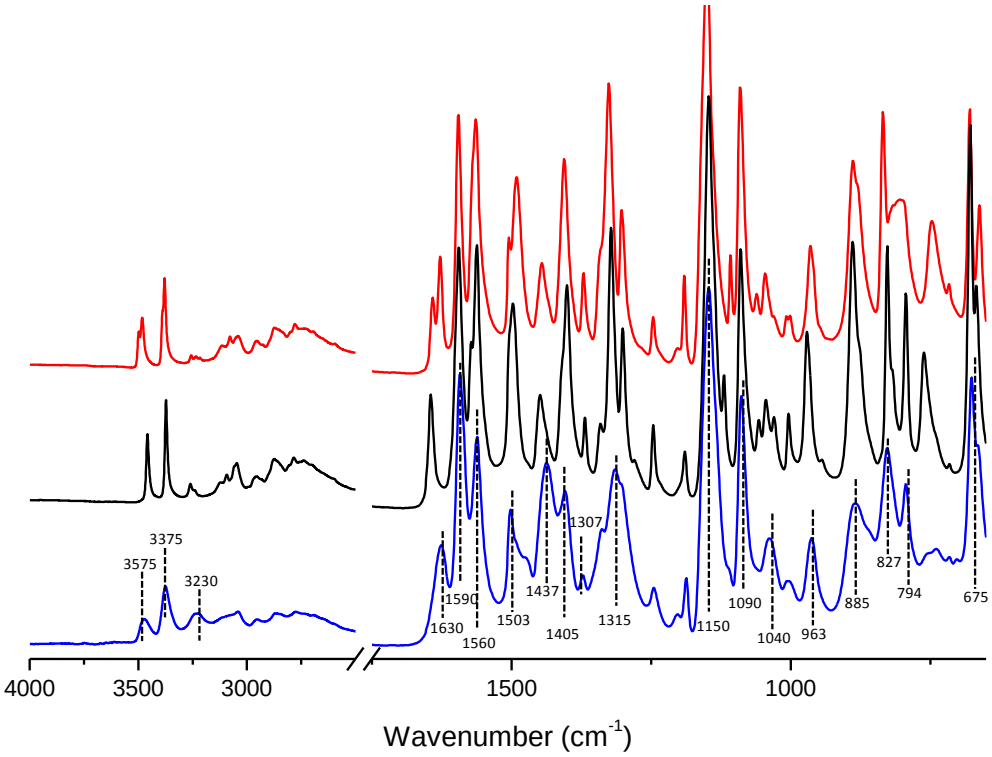

Fig. 3.12 Comparison of the IR spectra of FA (blue) FII (black), and FI (red)

Room temperature milling of sulfamerazine form I

Within minutes of milling sulfamerazine FI at room temperature a decrease in peak intensity can be observed in the XRPD patterns, showing the effect milling has on the solid state chemistry of sulfamerazine. The emergence of an amorphous hump is detected by an increased baseline within minutes of milling, coinciding with the broadening of crystalline peak (Figure 3.13). In the XRPD patterns, this decrease of FI peak intensity and increase of the amorphous hump are observed to continue for 45 minutes. At this point peaks characteristic to FII are observed at 19.10^{o} (2θ) (Figure 3.14). This peak and others unique to FII increase rapidly with further milling, as peaks characteristic to FI decrease into the amorphous hump. Within 55 minutes FI is no longer detected in the XRPD data. A gradual increase of FII peaks continues until 90 minutes of milling, after which no further changes can be detected. This indicates that equilibrium of FII and the amorphous phase (FA) has been reached. Due to the powerful milling the amorphous phase crystallises to FII, and FII is then being transformed back to FA, hindering complete transformation to either FII or FA. The XRPD data shows that FI is being converted to FA, acting as a transient phase, which is then transformed to FII. This transformation was analysed with further accuracy using NIR, and IR spectroscopy.

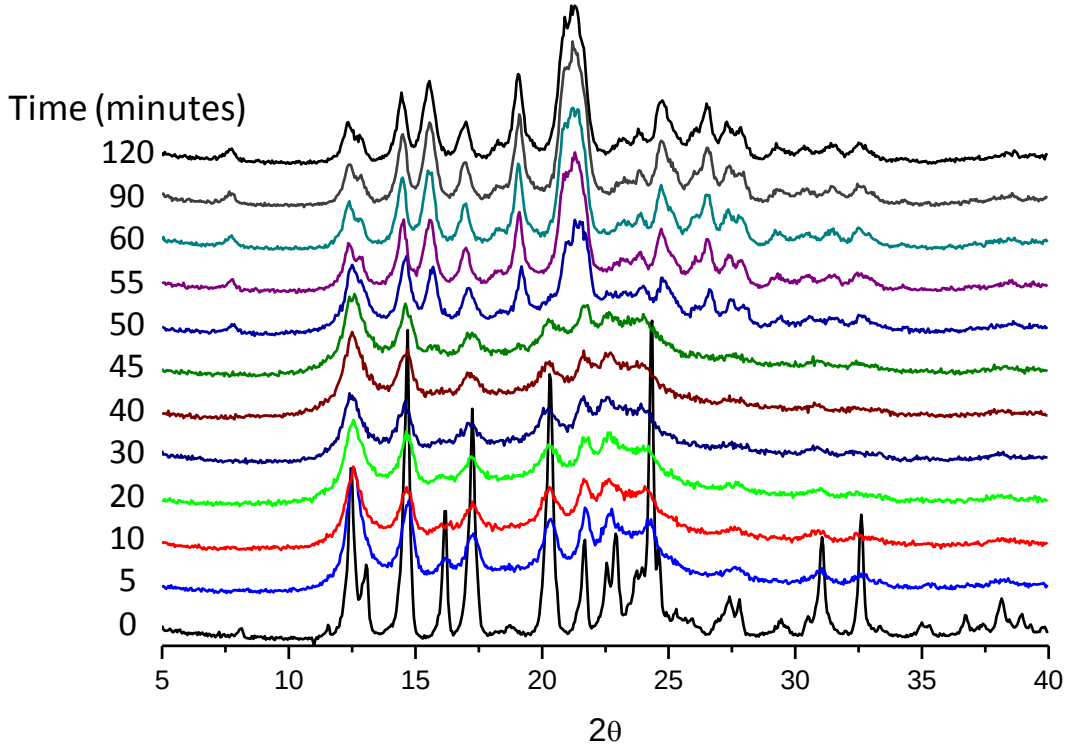

Fig. 3.13 XRPD pattern showing the transformations of FI during milling

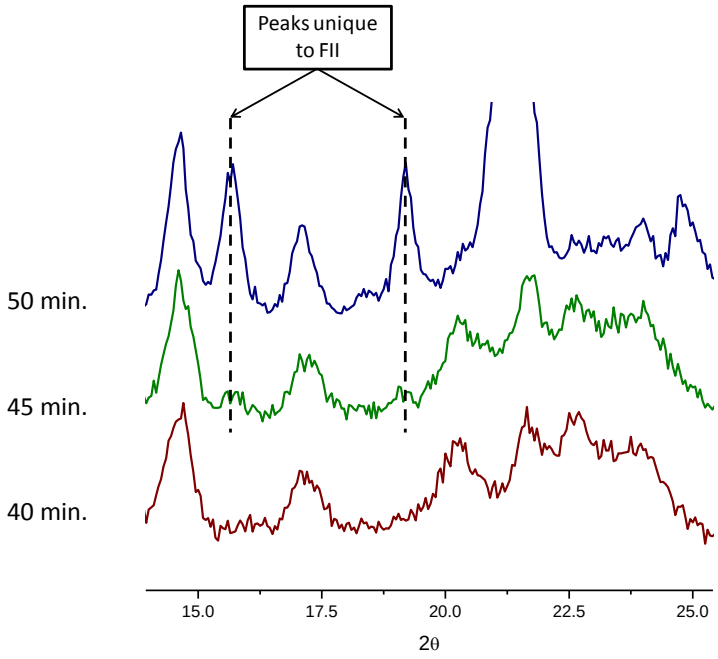

Fig. 3.14 The presence of FII in XRPD detected from 45 minutes of milling onwards

NIR analyses of samples taken at different intervals of milling FI were able to confirm the observations made using XRPD data (Figure 3.15). The characteristic dual peaks of FI at 6935 cm^{-1} and 6905 cm^{-1} recede as a single peak at a higher wavenumber appears. Even though this could be misconstrued as a particle size effect resulting from the milling, when the XRPD data was taken into consideration it was ruled out as possibility. As with the observation from the XRPD data the depletion of FI coincides with the generation of the amorphous content. The peak at 6855cm^{-1} characteristic of FII can be detected at 40 minutes. This shows an increase in sensitivity over XRPD, which detects FII formation at 45 minutes.

IR analysis of the samples taken at different intervals confirms the transformations occur by FA acting as a transient phase (Figure 3.16). Peaks characteristic to FI (1645cm^{-1} & 1450cm^{-1}) shift to peaks related to FA at 1625cm^{-1} and 1435cm^{-1} for the first 20 minutes of milling. The IR data confirms that a new component is being produced (this was confirmed to be FA when pure samples became available). As with the XRPD and NIR data, peaks characteristic of FII can be observed at 45 minutes, at which point peaks characteristic of FI cannot be detected. At this point peaks only characteristic of FII can be detected, though these are broadened suggesting the presence of FA. The amorphous content in these samples was

found to readily crystallise, where the amorphous phase would completely crystallise to FII within hours.

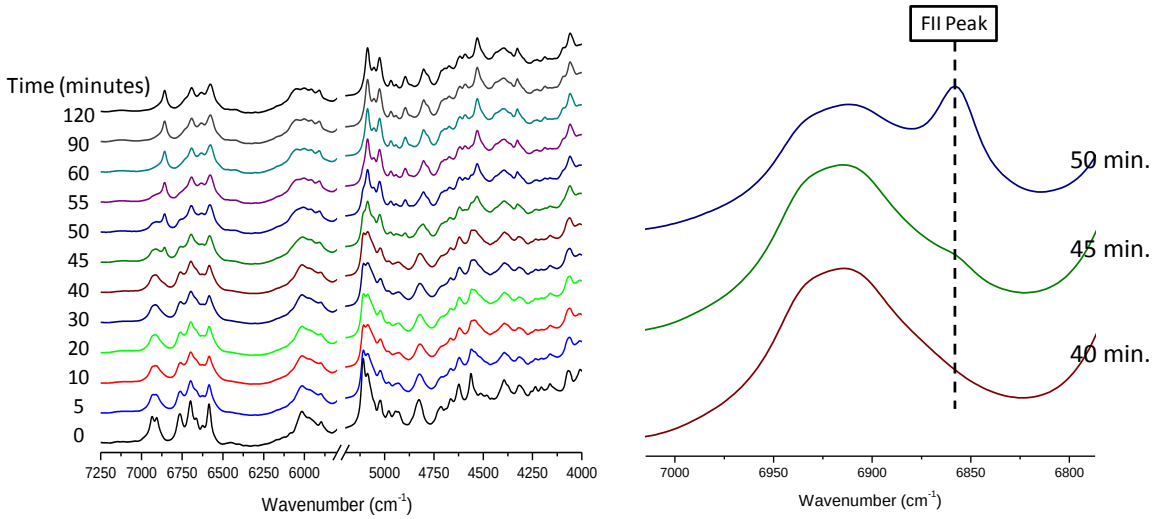

Fig. 3.15 NIR spectra showing the transformation of FI during milling (left). The presence of FII becomes apparent within 40 minutes (right)

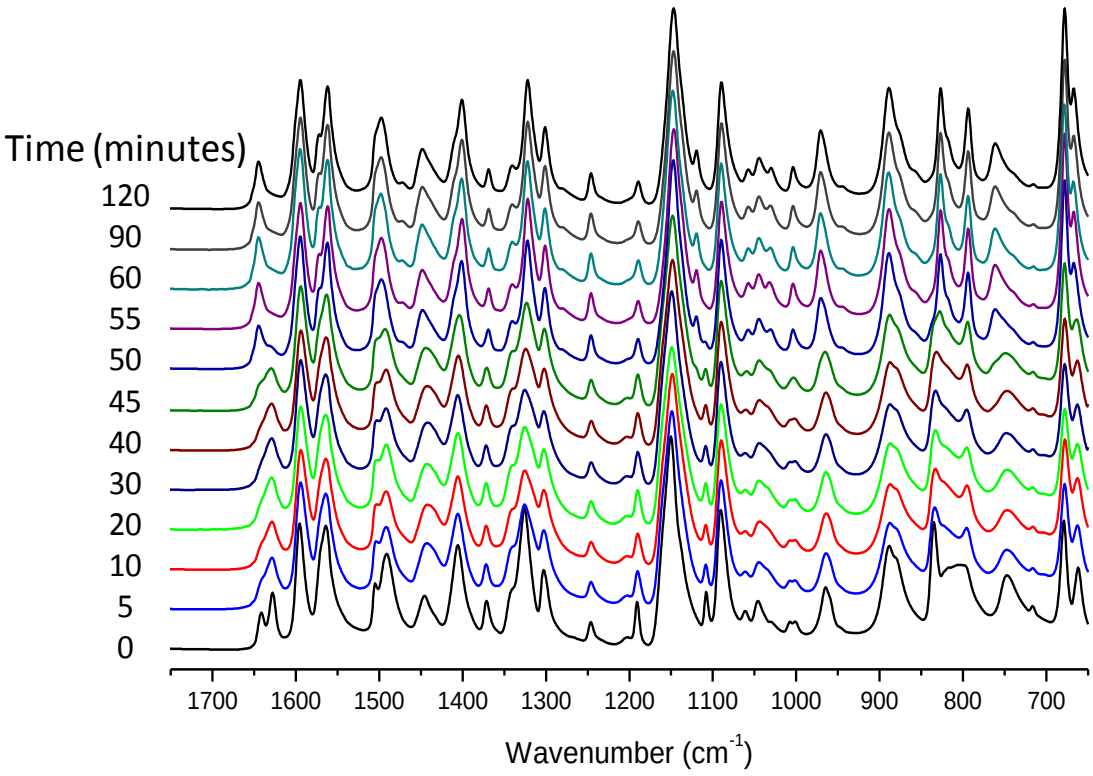

Fig. 3.16 IR spectra showing the transformation of FI during milling.

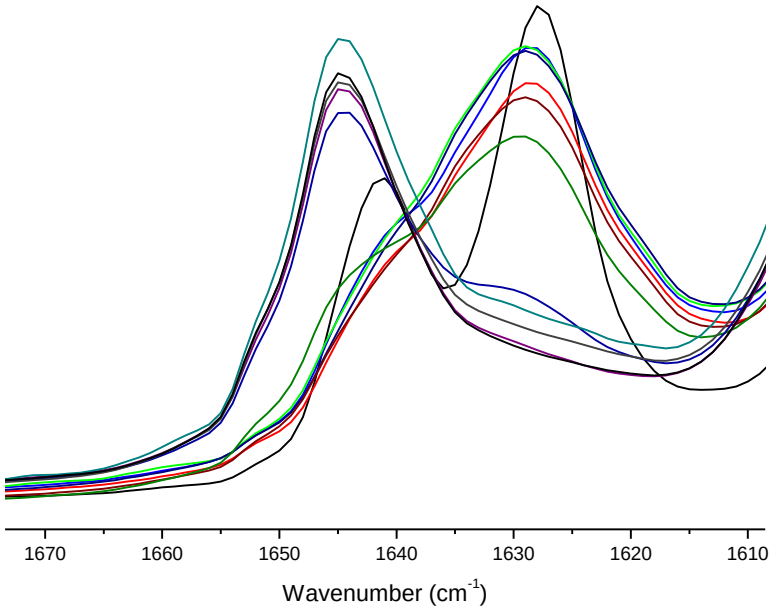

Fig. 3.17 Overlaid IR spectra showing the transformation of FI during milling, using the same colour coded labelling system as in figures 3.15 and 3.16

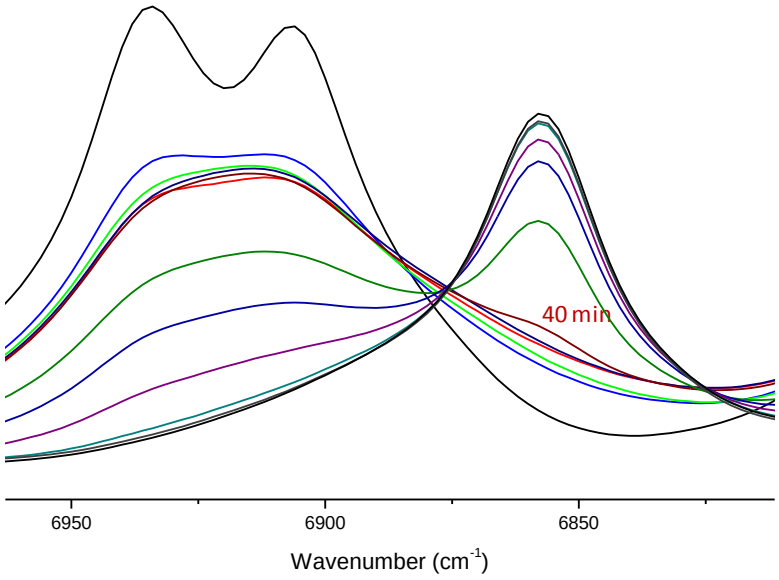

Fig. 3.18 Overlaid NIR spectra showing the transformation of FI during milling, using the same colour coded labelling system as in figures 3.15 and 3.16

Due to the similarities in the spectra of FI and FA, the presence of the FA was difficult to monitor, particularly when present at low content. This is in part due to background noise in the XRPD patterns masking low amorphous hump as a baseline. In the IR and NIR spectra the majority of peaks characteristic of FA were found to lie between peaks characteristic to FI and FII, making peaks distinct to FA difficult to detect in low content. A method to assess the transformations accurately and independently was needed. Because of this chemometric models were created to further understand the transformations occurring, being able to associate small spectral changes to different components and not mass scattering effects.

Room temperature milling of sulfamerazine form II

During the room temperature milling of FII, little change was observed when analysed using XRPD, NIR or IR spectroscopy. Some peak reduction and peak broadening was observed in the NIR and IR spectra and XRPD patterns (Figure 3.19). Even though it was initially thought FA could be formed at the time, it was not conclusive that the peak broadening in the spectroscopic and X-ray diffraction data was due to amorphous content seeing that a mass scattering effect resulting from a reduced particle size could cause similar peak broadening.

Similarities between samples of form II and form I milled over an hour can be observed. Both showed an increased baseline, and a decrease in peak intensity. This indicates the possible transformation from FII to FA. This was also seen in the IR and NIR spectra, where the base of many peaks can be seen to broaden, though unique peaks to FA are not observed (Figure 3.20 and 3.21).

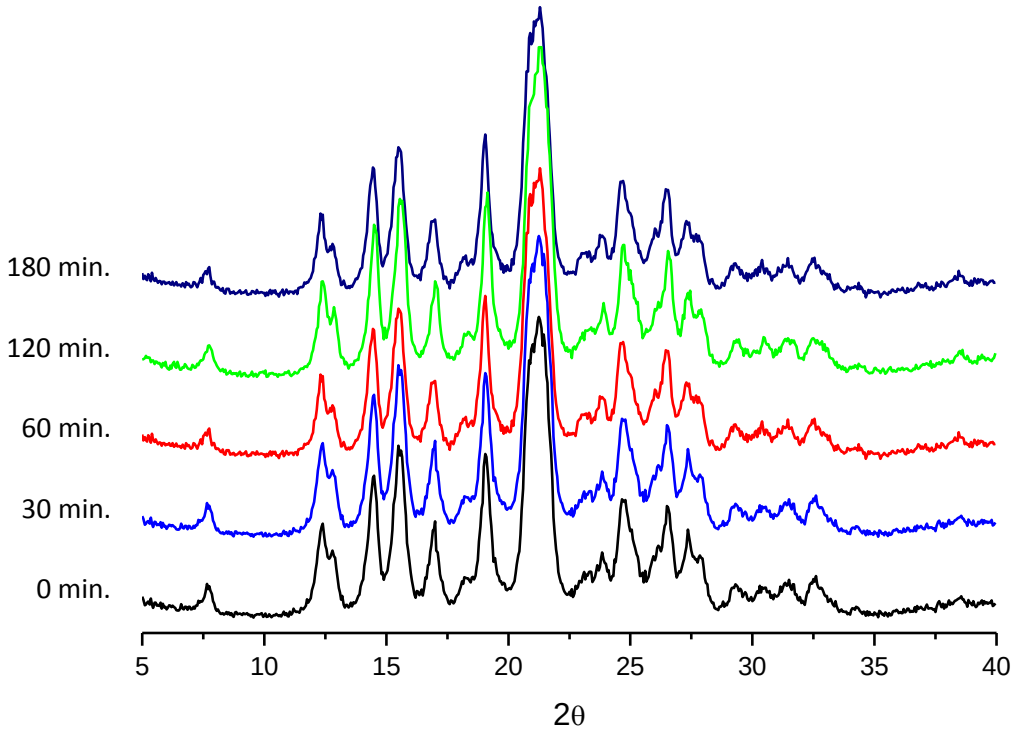

Fig. 3.19 XRPD patterns of FII being milled at room temperature

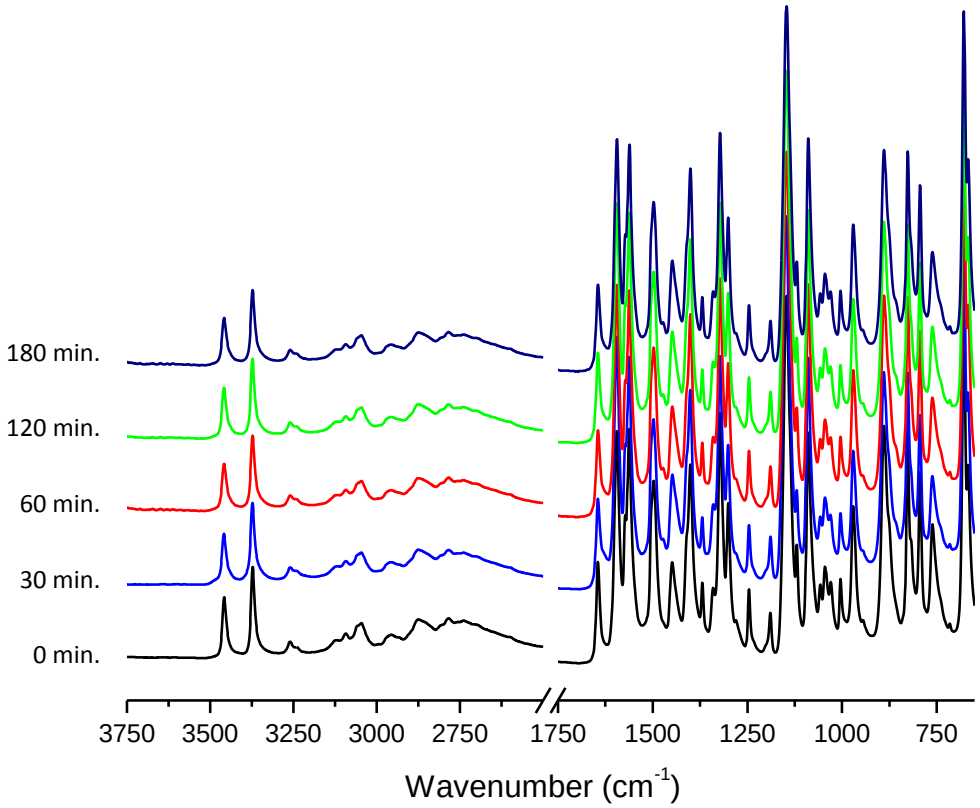

Fig. 3.20 IR spectra of FII being milled

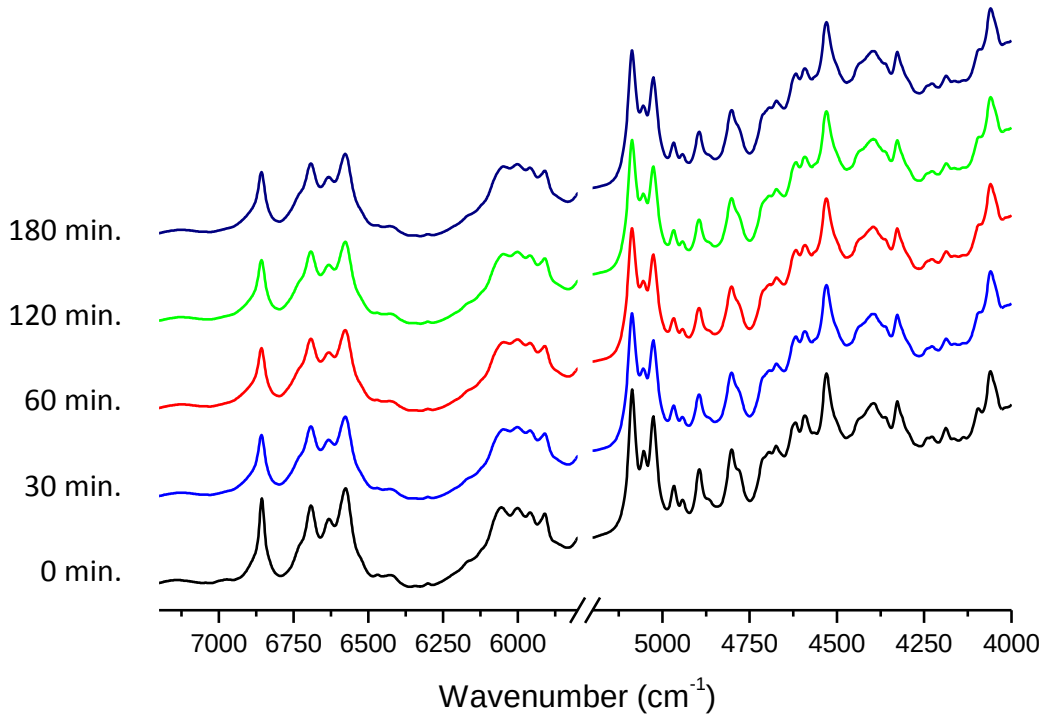

Fig. 3.21 NIR spectra of FII being milled

Cryo-milling of sulfamerazine form I

The cryo-milling of FI readily generated the amorphous phase. Within 10 minutes of cryo-milling FA was detected by XRPD, NIR and IR spectroscopy, and complete transformation to FA occured within 22.5 minutes (Figure 3.22). The reduced peak intensity and increase of the amorphous hump in the XRPD patterns shows an increasing presence of FA throughout the cryo-milling of FI. Peak shift in the NIR and IR spectra also show a steady increase of FA.

Spectroscopic data in the NIR region confirmed the generation of FA showing a single peak at 5075cm^{-1}, instead of a dual peak characteristic of FI at 6935cm^{-1} and 6905cm^{-1}. Other peaks at 6900cm^{-1}, and 4810cm^{-1} being the most prominent peaks also indicate the presence of FA (Figure 3.23). The rate of transformation from FI to FA agreed with observations made from the XRPD data. Within 22.5 minutes peaks characteristic to FI are absent, and peak changes were no longer detected with further cryo-milling times. This indicates that during cryo-milling FI is completely transformed to the amorphous phase. The NIR data also shows some moisture being absorbed during the cryo-milling process, with peaks characteristic to water at 5200cm^{-1} and 7400cm^{-1} increasing over time. This moisture was found to be absorbed from the environment during cryo-milling.

IR spectroscopy was also used to monitor the transformation of FI to FA, showing the appearance of peaks at 1625cm^{-1} found to be unique to FA, and broadening of the peak at 1436cm^{-1} (Figure 3.24). This coincides with the decrease of peaks unique to FI (5108cm^{-1}, 4979cm^{-1}, 4825cm^{-1}, 4715cm^{-1}, 4316cm^{-1}). The transformation from FI to FA continued for 22.5 minutes at which point the presence of FI cannot be detected, confirming the complete transformation to FA.

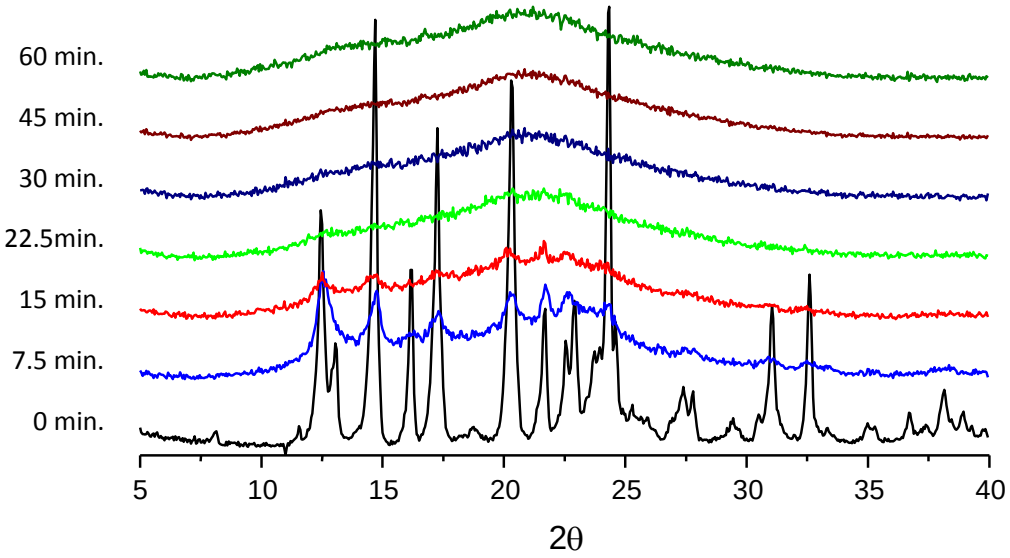

Fig. 3.22 XRPD patterns of the amorphisation of FI via cryo-milling

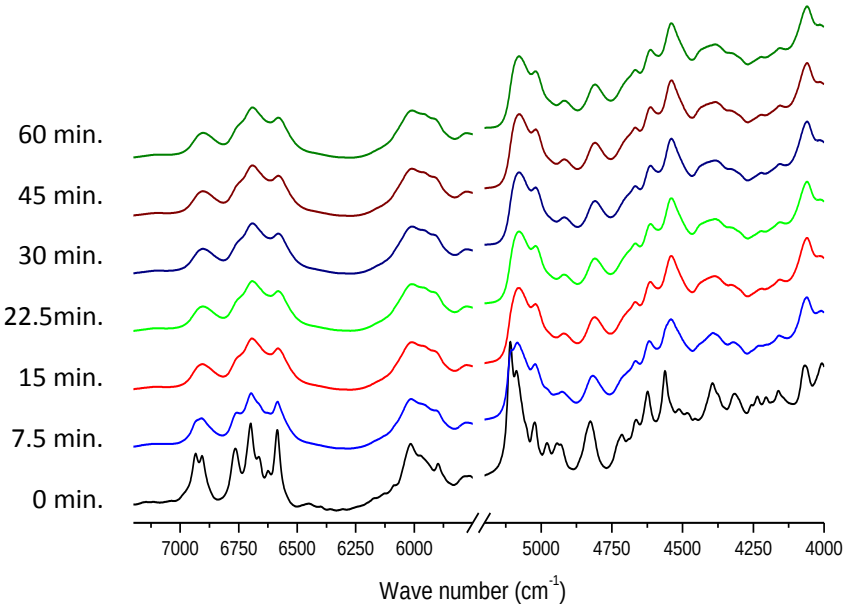

Fig. 3.23 NIR spectra of the amorphisation of FI via cryo-milling

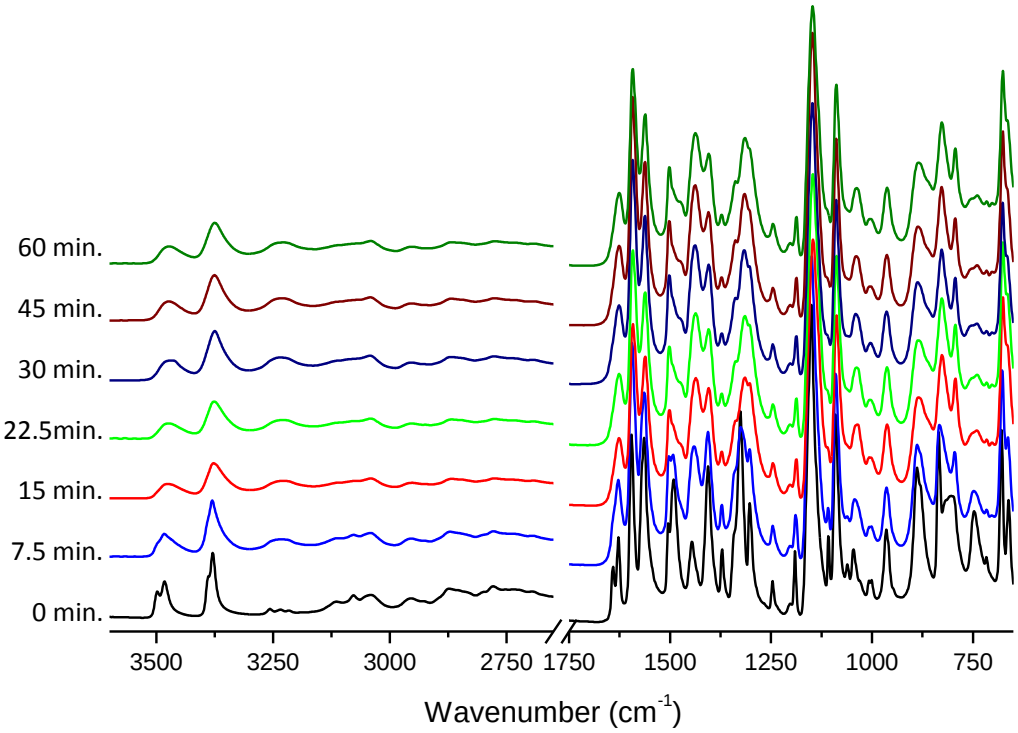

Fig. 3.24 IR spectra of the amorphisation of FI via cryo-milling

Cryo-milling of sulfamerazine form II

The cryo-milling of FII was found to generate FA, but at a much slower rate than the cryo-milling of FI. This is expected from FII being the more stable polymorph. As with the cryo-milling of FI, the generation of FA was followed using XRPD, and was confirmed using NIR and IR spectroscopy. Even though XRPD is an ideal candidate for the detection of changes in crystallinity, it is a questionable method in the quantitative analysis in the cryo-milling of FII. This was due to the time taken to analyse a sample (≈22 minutes), the amorphous content of these samples were found to crystallise at a faster rate than samples prepared by cryo-milling of FI, showing signs of the amorphous phase crystallising to FII. This is likely because of longer cryo-milling times needed to generate FA from FII, reducing the particle size distribution, and increasing the deformation to the particle surface area. This gave a narrow window to analyse the cryo-milled samples of FII causing uncertainty in the quantification of FA during the cryo-milling process. Even with this uncertainty a pattern in the gradual decrease of crystallinity is observed over the course of 2 hours. At this point only the amorphous hump remains, indicating complete transformation to the amorphous phase (Figure 3.26). Because of uncertainty using XRPD, NIR and IR spectroscopy were used in the primary analysis of any changes in the solid state.

Form II **Form II; 90 min. Cryo-milled**

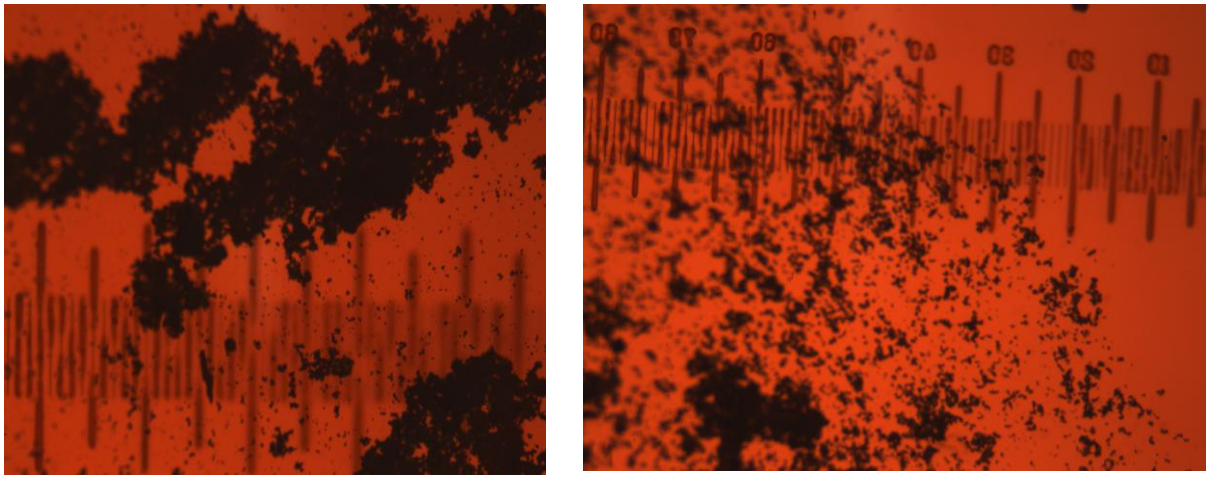

Fig. 3.25 Particle size reduction and distribution of FII after 90 minutes of cryo-milling using a confocal microscope

Even though there is some uncertainty with the accuracy of the XRPD analysis (due to noise and the possibility of mass scattering effect masking change in peak intensity), crystallisation of FA could be detected during XRPD analysis, allowing the amorphisation of FII to be monitored. This crystallisation was detected by a distortion in peak intensity during the step scan process. Any samples showing crystallisation during analysis were discarded. Samples that were stored in a desiccator under vacuum show an increase in stability, lasting up to 45 minutes without signs of crystallisation. Another factor thought to play a role in the crystallisation of FA is the increased number of fissures on the particle surface, acting as possible nucleation sites for crystal growth. With longer milling times more fissures occur, increasing the number of nucleation sites.

The most prominent and characteristic peak of FII in the NIR region at 6855 cm^{-1} shows a gradual decrease in peak height and broadening at its base during the course of cryo-milling (Figure 3.27). The gradual decrease in intensity of peaks characteristic to FII continued for 2 hours of cryo-milling and coincided with the appearance of peaks characteristic of FA. No further changes in the NIR spectra were observed with continued cryo-milling of up to 3 hours. Due to its quicker time to analyse samples NIR spectroscopy is regarded as a method to monitor the amorphisation of FII with greater accuracy than the XRPD.

Due to the instability of FA produced by cryo-milling FII, it was decided FI would be used as the starting material to produce FA for chemometric studies. FI requires shorter cryo-milling times to undergo complete amorphisation than FII. This can be rationalised by the different packing arrangements in the crystal lattices of FI and FII.[68] In both polymorphs, the basic building blocks are z-shaped H bonded dimers that form infinite H bonded chains.[69] These chains give rise to rigid layers parallel to the ac plane with only weak van der Waals forces existing between layers, which act as a slip plane. The layers in FI are flat and neighbouring layers can easily slide over each other. By contrast, the layers in FII are zigzag-shaped and interlock. The presence of slip planes in the crystal structure of FI results in high plasticity and facilitates amorphisation,[65] while the layers in FII do not easily slide over each other.

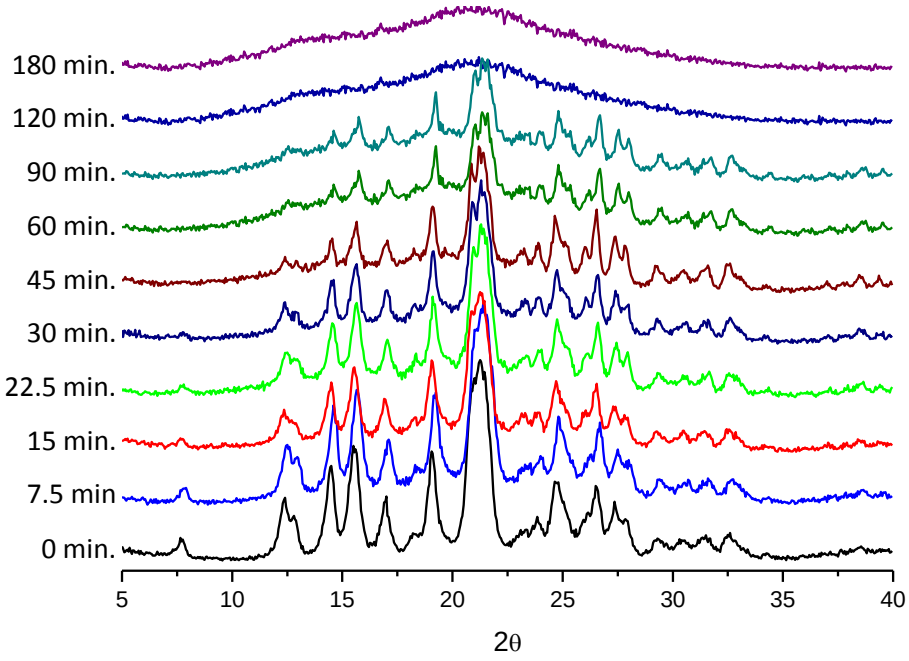

Fig. 3.26 XRPD patterns of the amorphisation of FII during cryo-milling

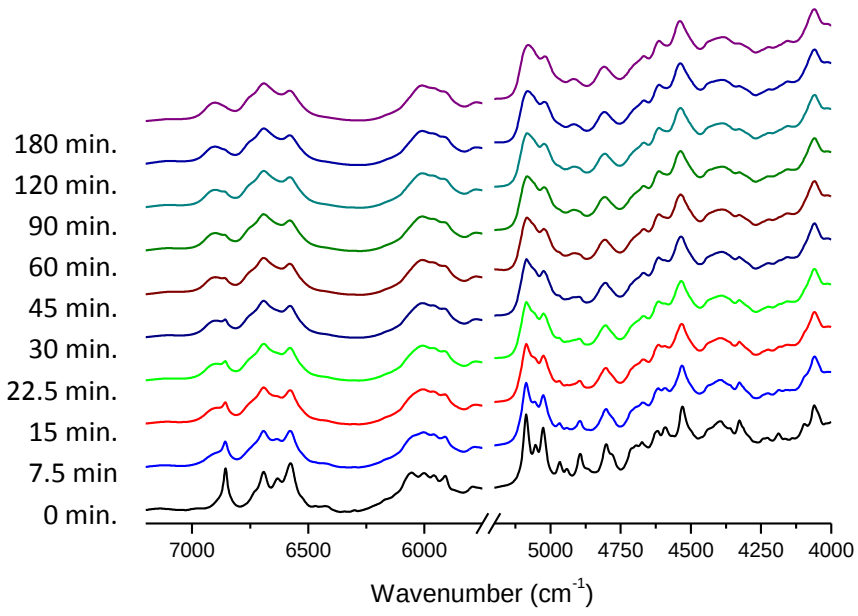

Fig. 3.27 NIR spectra of the amorphisation of FII cryo-milling

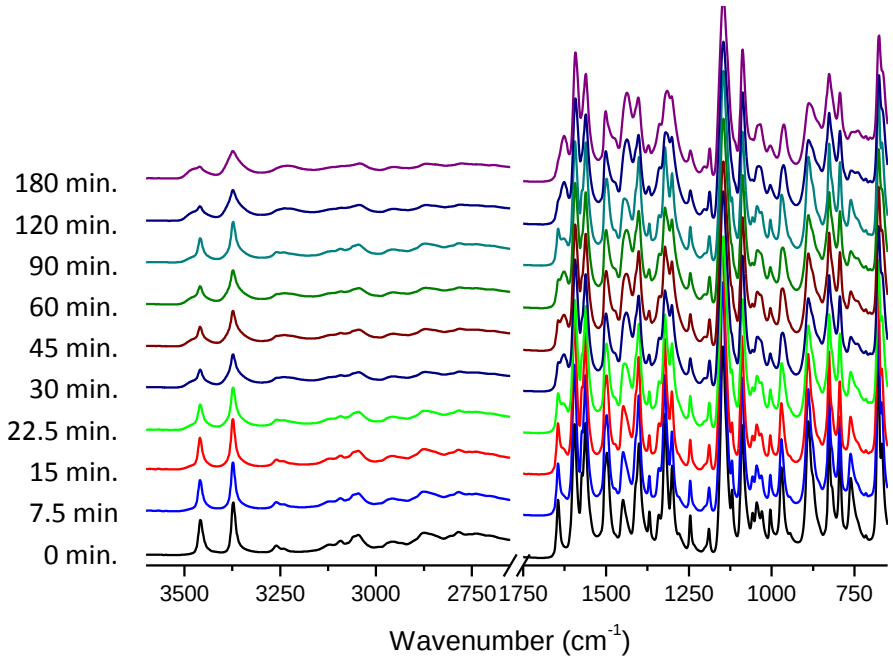

Fig. 3.28 IR spectra of the amorphisation of FII during cryo-milling

Stability of amorphous sulfamerazine

This study was to investigate if further cryo-milling after the complete transformation to FA at 22.5 minutes would have any effect on the stability of FA, and how effective cold storage was in enhancing its shelf life. This was done by monitoring of samples of FA prepared by cryo-milling over periods of time, at different temperatures. Due to the instability of the amorphous sulfamerazine generated from FII, it was decided that all preparation of FA would be produced via the cryo-milling of FI. Samples of FA were prepared by cryo-milling FI for 30 minutes, 45 minutes, 60 minutes, 75 minutes, and 90 minutes and were stored under vacuum at room temperature and 4^{o}C. Samples of 30 minutes of cryo-milling or above were chosen to ensure full transformation to FA had occurred.

Because of the problems presented in analysing the amorphisation of FII during cryo-milling XRPD was immediately ruled out as means of analysing the stability of FA, and IR spectroscopy was found to produce spectral variations due to force applied using the ATR sample plate, which would alter the nature of the sample. Also samples exposure to the environment during XRPD and IR analysis was problematic. NIR spectroscopy was chosen to monitor the stability of FA due to its high degree of sensitivity in detecting the solid phases of sulfamerazine and its quick time in running an analysis.[64] NIR also has the ability to be sampled 'in bottle', minimising samples exposure to the environment. This was a great benefit because atmospheric moisture acts as a catalyst and induces solid phase changes.[4]

All samples were stored in a desiccator under vacuum either at room temperature or at 4^{o}C. Peaks at 5200 cm^{-1} and 7400 cm^{-1} during the first sampling were taken as an indication of the amount of moisture in the samples before evacuation. Samples that showed low moisture content, as a shoulder instead of a peak at 5200 cm^{-1}. The samples were then evacuated for 40 minutes, reducing the moisture before being stored at 4^{o}C or at room temperature (20^{o} - 25^{o}C).

As expected storing samples at lower temperatures (at 4^{o}C) was found to reduce the rate of crystallisation, compared to those stored at room temperature. The shelf life of FA was extended to days when stored at 4^{o}C, instead of hours when stored at room temperature. Though an increase in shelf life can be seen in all samples by lowering the storage temperature

of sample, it had little if any observable effects on the crystallisation pathway of the samples (Figures 3.29-3.35).

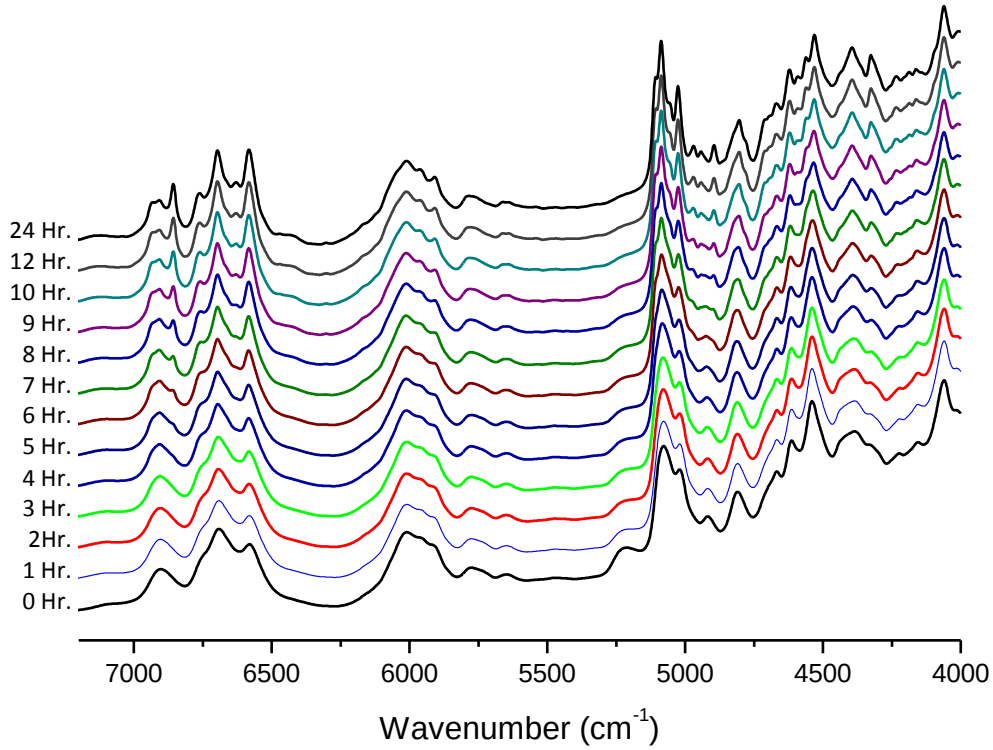

Fig. 3.29 NIR spectra following the crystallisation of FA prepared via cryo-milling FI for 30 minutes, stored under vacuum at room temperature

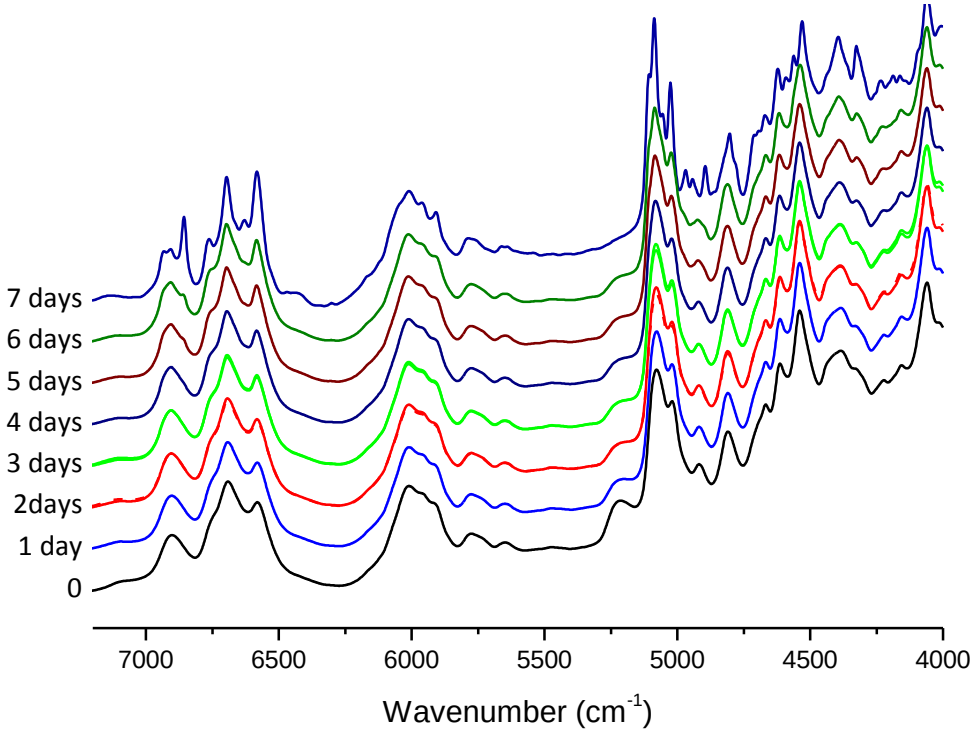

Fig. 3.30 NIR spectra following the crystallisation of FA prepared via cryo-milling FI for 30 minutes, stored under vacuum at 4° C

The samples of FI cryo-milled for 30 minutes and stored at room temperature were monitored hourly using NIR spectroscopy (Figure 3.29 & 3.90). Within 3 hours the presence of FII can be seen with the emergence of a peak at 6850 cm^{-1}. Also, within 4 hours the presence of the dual peaks unique to FI at 6935cm^{-1} and 6905cm^{-1}can be observed, complicating comparative NIR analysis. The simultaneous growth of two separate components and the decrease of another add an extra dimension of complexity creating a three component system. Also most peaks unique to FA lie between peaks characteristic of forms I and II, and peak broadening makes the detection of subtle changes difficult. Even with this, the gradual and simultaneous increase of FI and FII can be observed. Within 10 hours the presence of FA can no longer be detected. The sample was monitored for 7 days, showing no further changes afterwards. Though the crystallisation of the same polymorphic mixture of FI and FII was seen in samples stored at 4°C, the presence of FI and FII was undetected until day 3, and FA does not fully crystallise for a week. This pattern is observed throughout for the other samples, where storing samples at 4°C greatly increases the shelf life of FA, but does not affect the crystallisation of polymorphs from FA

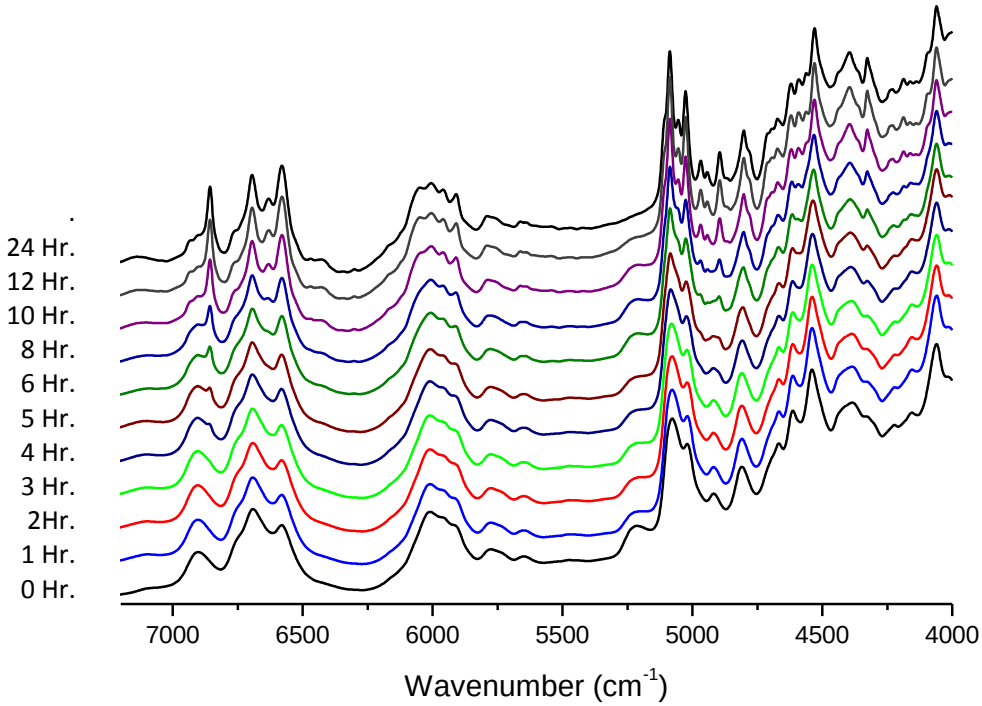

Fig. 3.31 NIR spectra following the crystallisation of FA prepared via cryo-milling FI for 45 minutes, stored under vacuum at room temperature

Samples cryomilled for 45 minutes (Figure 3.31 and 3.32) showed similar properties as samples of FI cryo-milled for 30 minutes. As expected samples stored at 4°C were more stable than samples stored at room temperature by a factor of days instead of hours. As with samples cryo-milled for 30 minutes, the temperature played a significant role in the shelf life of the sample, but not its crystallisation pathway. Here a lesser amount of FI was crystallised from FA, and FA showed an increase in stability. This indicates that FI seeds with no long range order are present throughout the sample, but at a lesser degree than in samples cryo-milled for 30minutes.

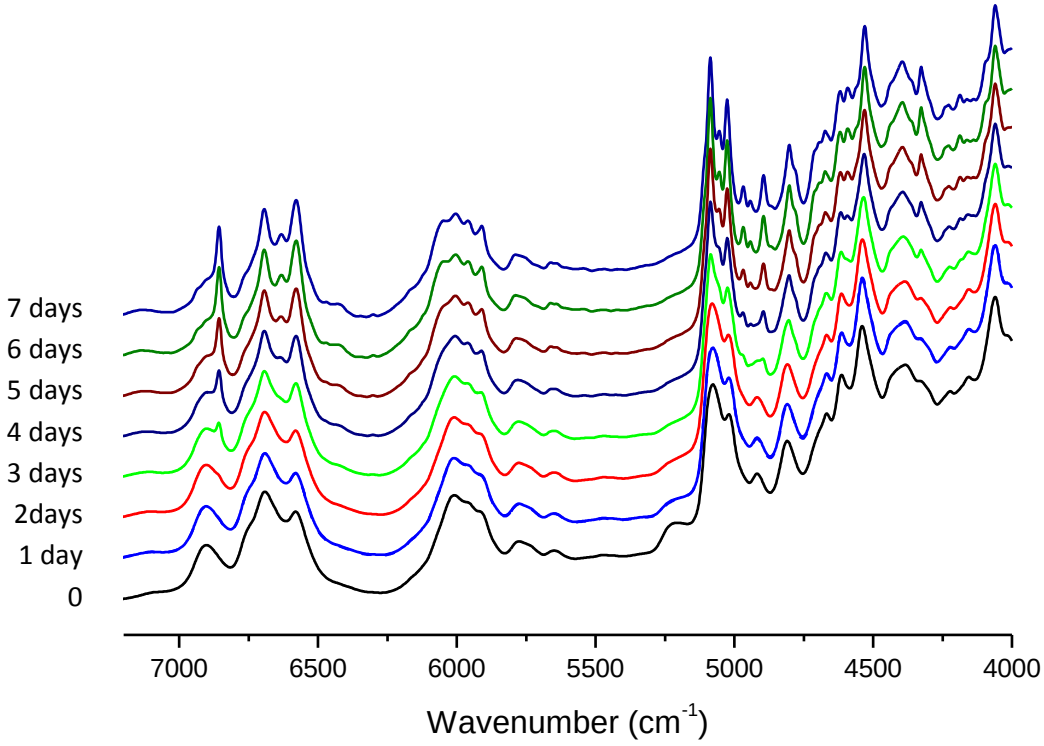

Fig. 3.32 NIR spectra following the crystallisation of FA prepared via cryo-milling FI for 45 minutes, stored under vacuum at room temperature

During the recrystallisation of samples cryo-milled for 60 minutes only FII can be detected (Figure 3.33). As the peak at 6855cm^{-1} decrease, only peaks unique to FII can be seen to emerge. Here the presence of FI cannot be detected during the crystallisation of FA. This was also seen in samples cryo-milled for longer times of 75 minutes and 90 minutes.

With cryo-milling time above 60 minutes, the stability of FA decreases, where samples cryo-milled for 60 minutes, stored at room temperature, showed the crystallisation of form II within 3 hours, whereas samples cryo-milled for 90 and 75minutes showed signs of

crystallisation within 1 and 2 hours respectively (Figure 3.34 and 3.35). An increased shelf life of the FA when cryo-milled for 60 minutes was also observed in samples stored at 4°C. In samples cryo-milled for 60 minutes crystallisation can be seen within 3 days, whereas samples cryo-milled for 90 and 75 minutes show crystallisation of FII within 2 days and 1 day respectively.

The instability of FA sample prepared by cryo-milling for longer than 60 minutes is likely to be caused by a number of factors. The most prominent factor is likely to be the absence FI seeds. Another factor was found to be moisture being introduced to the samples during cryo-milling catalysing the crystallisation to more stable polymorphs.[4] With longer cryo-milling times more moisture is introduced to the samples further catalysing crystallisation to FII.

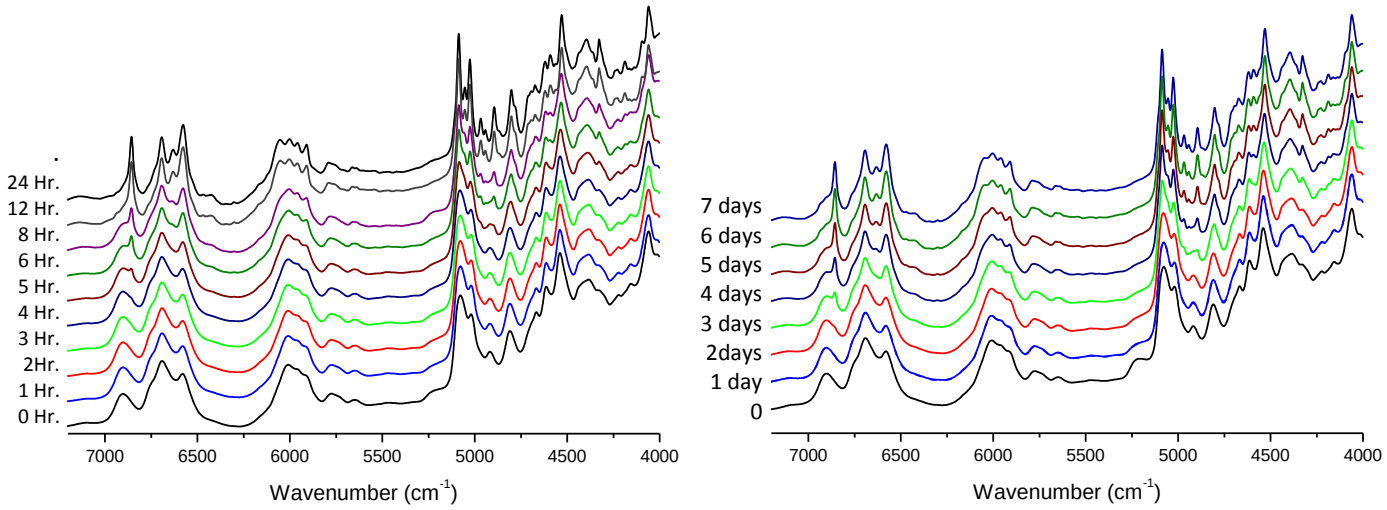

Fig. 3.33 NIR spectra following the crystallisation of FA prepared via cryo-milling FI for 60 minutes, stored under vacuum at room temperature (left) and 4°C (right)

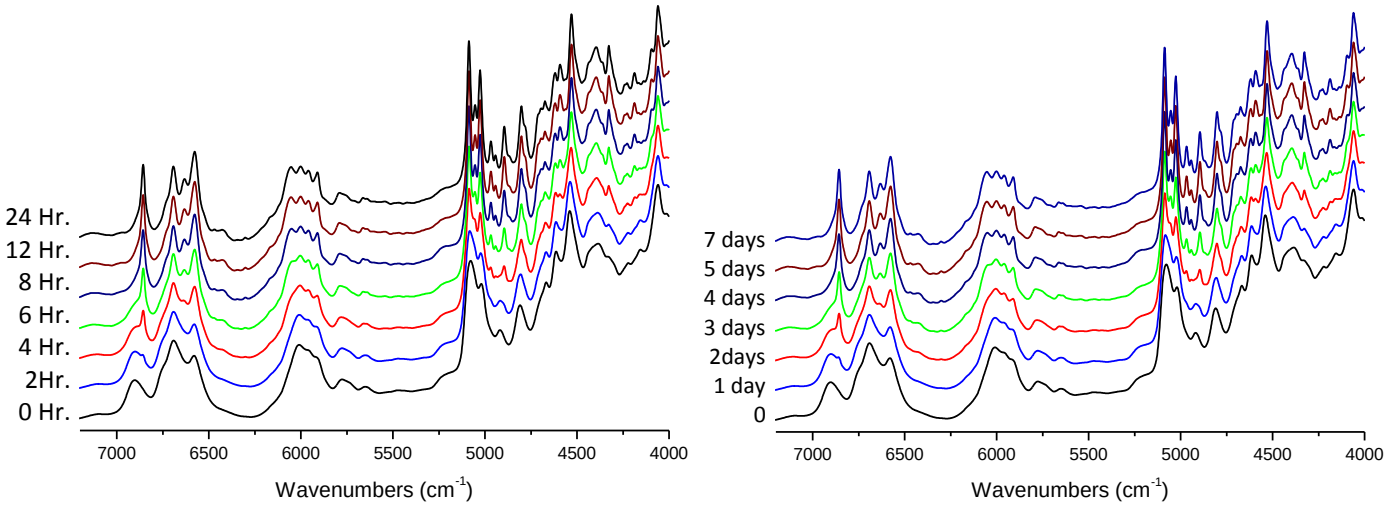

Fig. 3.34 NIR spectra following the crystallisation of FA prepared via cryo-milling FI for 75 minutes, stored under vacuum at room temperature (left) and 4°C (right)

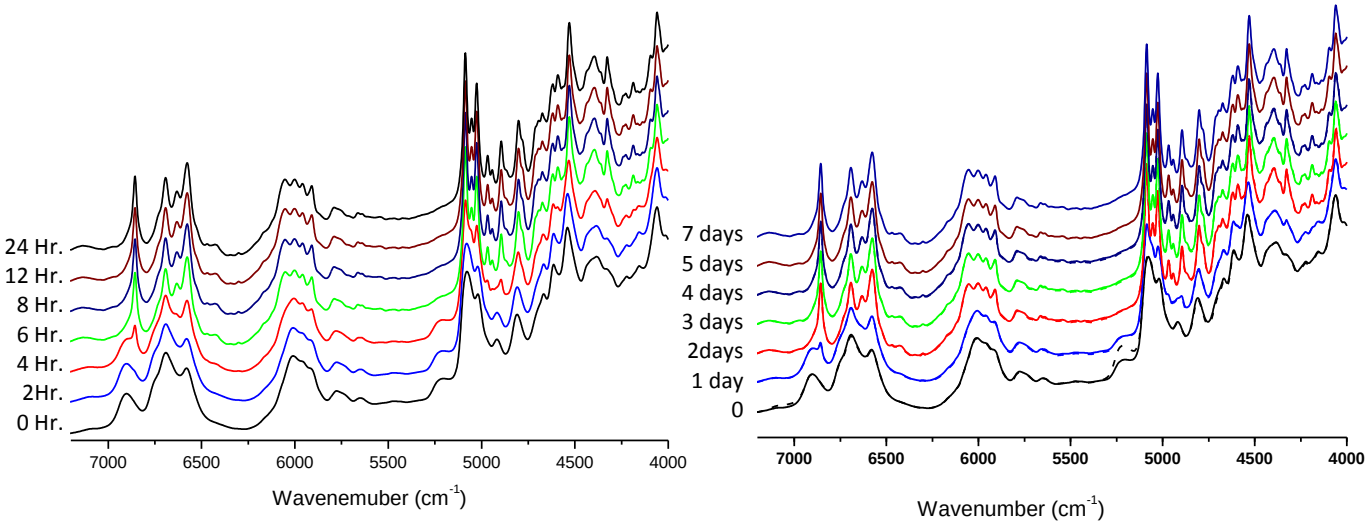

Fig. 3.35 NIR spectra following the crystallisation of FA prepared via cryo-milling FI for 90 minutes, stored under vacuum at room temperature (left) and 4^{o}C (right)

Due to the multicomponent crystallisation of FA samples prepared for less than 60 minutes, and the instability of FA samples cryo-milled for longer than 60 minutes, cryo-milling FI for 60 minutes was chosen as the optimal method to prepare FA.

Comparison of the amorphous sulfamerazine prepared via melt quenching and cryo-milling

The amorphous phase of sulfamerazine was also prepared using the melt quench method. This was done by melting samples of sulfamerazine then cooling in liquid nitrogen solidifying the melt into a solid material retaining the disordered arrangement of the melt. FI was initially chosen having the lower melting point of 215°C as the lesser stable polymorph. The sample of FI was heated to 220°C for 7.5 minutes under nitrogen and cooled in liquid nitrogen was found to produce a polymorphic mixture of FI and FII, with some degradation of the sample (seen as a blackening or browning of the sample). The polymorphic mixture of FI and FII was a result of the thermal transformation from FII to FI occurring above the temperature of crystallisation (T_c).

Other samples held at 220° for longer times produced FII or showed too much degradation, appearing as a burning throughout the sample, seen as a blackening of the once white sample. FII was then used with the temperature set above the melting point of FII (236°C). A glassy residue over the powder was formed for samples heated for 3 minutes. For samples heated for 5-10 minutes light yellow glassy material was present, but was still crystalline sulfamerazine. In heating samples for 15.5 minutes the glassy material turned brown. Though the NIR analysis of this glassy material showed some noise, it is clear that it is the amorphous phase (Figure 3.36). This noise is due to the degradation of sulfamerazine during melting.

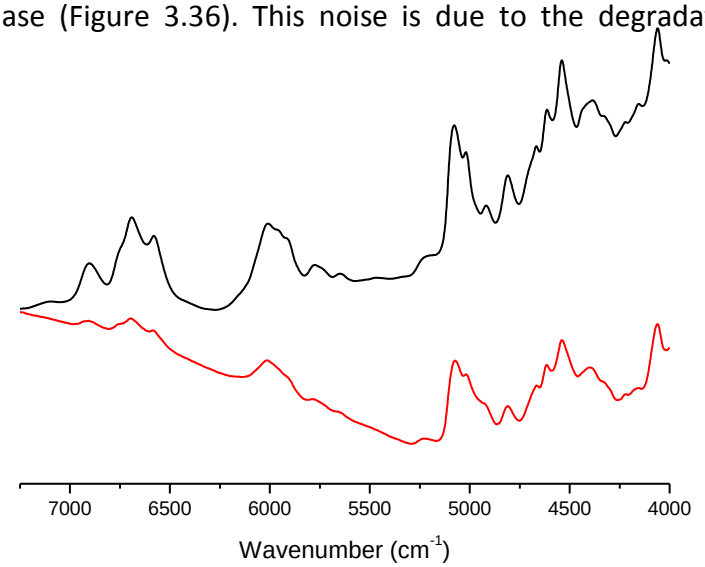

Fig. 3.36 NIR spectra comparing amorphous sulfamerazine prepared via cryo-milling (black) and melt quench (red) method

DSC Analysis of the amorphous phase of sulfamerazine

The glass transition temperature (T_g) kink in the DSC analysis of amorphous pharmaceutical is one of the most evident characteristic of amorphous pharmaceuticals. The T_g of sulfamerazine has already been reported, at 62°C using mDSC, by Chattoraj et al (2012). [3]

Samples of FA prepared via cryo-milling showing very little moisture in TGA, showing only a slight reduction of mass (< 1%, from calculating the area under the curve). This thermal event was taken to be the T_g of sulfamerazine (Figure 3.37). Thermo Gravimetric Analysis (TGA) shows little moisture in the samples (<0.01% w/w), minimising the effect of moisture on the T_g.

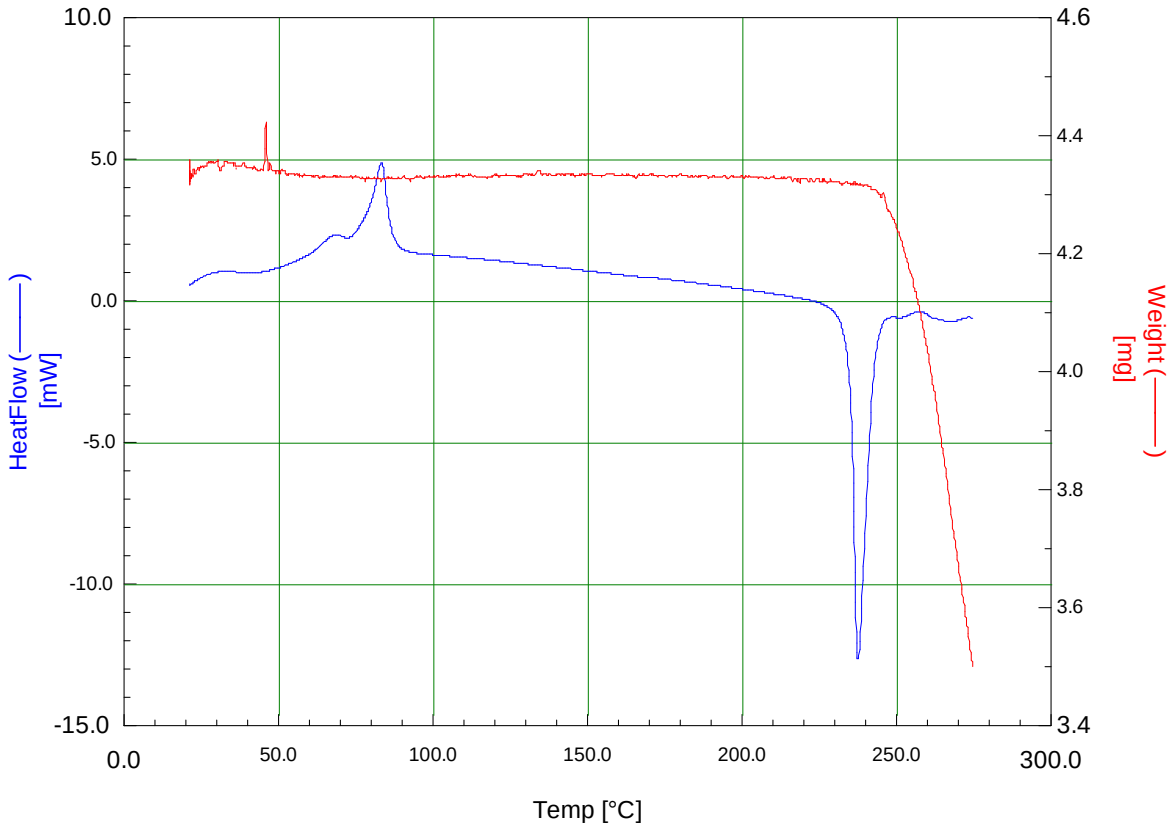

Fig. 3.37 DSC of amorphous sulfamerazine prepared via cryo-milling FI for 60 minutes

Quantification of binary and ternary mixtures of sulfamerazine forms I, II, and the amorphous phase

Multivariate calibration models were developed In order to quantify the solid state transformations during room and cryo temperature milling, and the stability of FA. As described above it is possible to differentiate FI, FII and FA by XRPD, NIR and IR spectroscopy. First, models were constructed for the quantification of FI, FII and FA in binary mixtures (FI/FA, FII/FA, FI/FII) using XRPD, NIR and IR spectroscopy and a partial least-squares (PLS) regression. PLS models were made for the calibration for the 0 - 100 % range. Different spectral pre-processing algorithms including multiplicative scatter correction (MSC), standard normal variate (SNV) transformation, 1^{st} and 2^{nd} derivative calculations and combinations of MSC or SNV with derivation were applied to the data. The results having the lowest average of RMSEC, RMSECV, and RMSEP, and the lowest standard deviation of blanks and LOD were regarded as the best performing models, and were obtained, when either SNV or a combination of SNV and 1st derivative was used. The performance characteristics of the best-performing models are summarised in table 3.2. The RMSEP values of the 0 - 100 % models are below 2 %. The results for the analysis of 0 - 100 % FI / FII binary mixtures by the multivariate spectroscopic method compare well with the XRPD method reported in the literature where RMSEC and RMSEP values of 1.28 and 1.65 % have been obtained.[24] However, the speed of analysis gives NIR spectroscopy a significant advantage. Plots of the predicted vs. actual content for the different binary mixtures all show excellent linear correlations. For the low content analysis, RMSEC, RMSECV and RMSEP values are $\leq$ 0.62 %.

The suitability of IR spectroscopy and XRPD combined with multivariate analysis for the quantification of binary mixtures was also explored. However, the calibration models obtained had significantly higher RMSE values than the NIR models. Even though XRPD is regarded as the gold standard in the analysis of crystalline material, it showed less accuracy in creating calibration models. IR spectroscopy data showed variations and distorted absorptions resulting from samples of FI being subjected to varying pressures from the ATR sample plate during sampling. This decreases the reliability of calibration models produced using IR spectroscopy.

It was also possible to derive a satisfactory calibration model for the simultaneous determination of the three solid-state forms in ternary mixtures having RMSEC, RMSECV and RMSEP values for the three components generally below 5.1 % (Table 3.3, Figure 3.38).

Mixture	Range	Pre-treatment	Loadings	RMSEC (%)	RMSECV (%)	RMSEP (%)	Standard dev. (%)	L.O.D. (%)
FI / FA	0 - 10 % FA	SNV & 1st derv	1	0.444	0.492	0.589	0.595	1.79
	0 - 100 % FA	SNV & 1st derv	2	1.799	2.64	1.536	0.691	2.07
	90 - 100 % FA	SNV & 1st derv	1	0.563	0.591	0.452	0.475	1.43
FII / FA	0 - 10 % FA	SNV	1	0.375	0.525	0.574	0.320	0.96
	0 - 100 % FA	SNV	1	2.287	2.675	1.812	1.070	3.21
	90 - 100 % FA	SNV & 1st derv	1	0.521	0.561	0.802	0.178	0.53
FI / FII	0 - 10 % FI	SNV & 1st derv	1	0.333	0.390	0.339	0.458	1.38
	0 - 100 % FI	SNV & 1st derv	1	1.414	1.482	1.038	2.237	6.712
	90 - 100 % FI	SNV & 1st derv	2	0.480	0.615	0.336	0.243	0.72

Table 3.2 Selection of best results for each binary analysis (FI/ FA), (FII / FA), and (FI / FII), using the 6965-6475cm-1 and 5115-4000cm-1 regions of NIR spectrum.

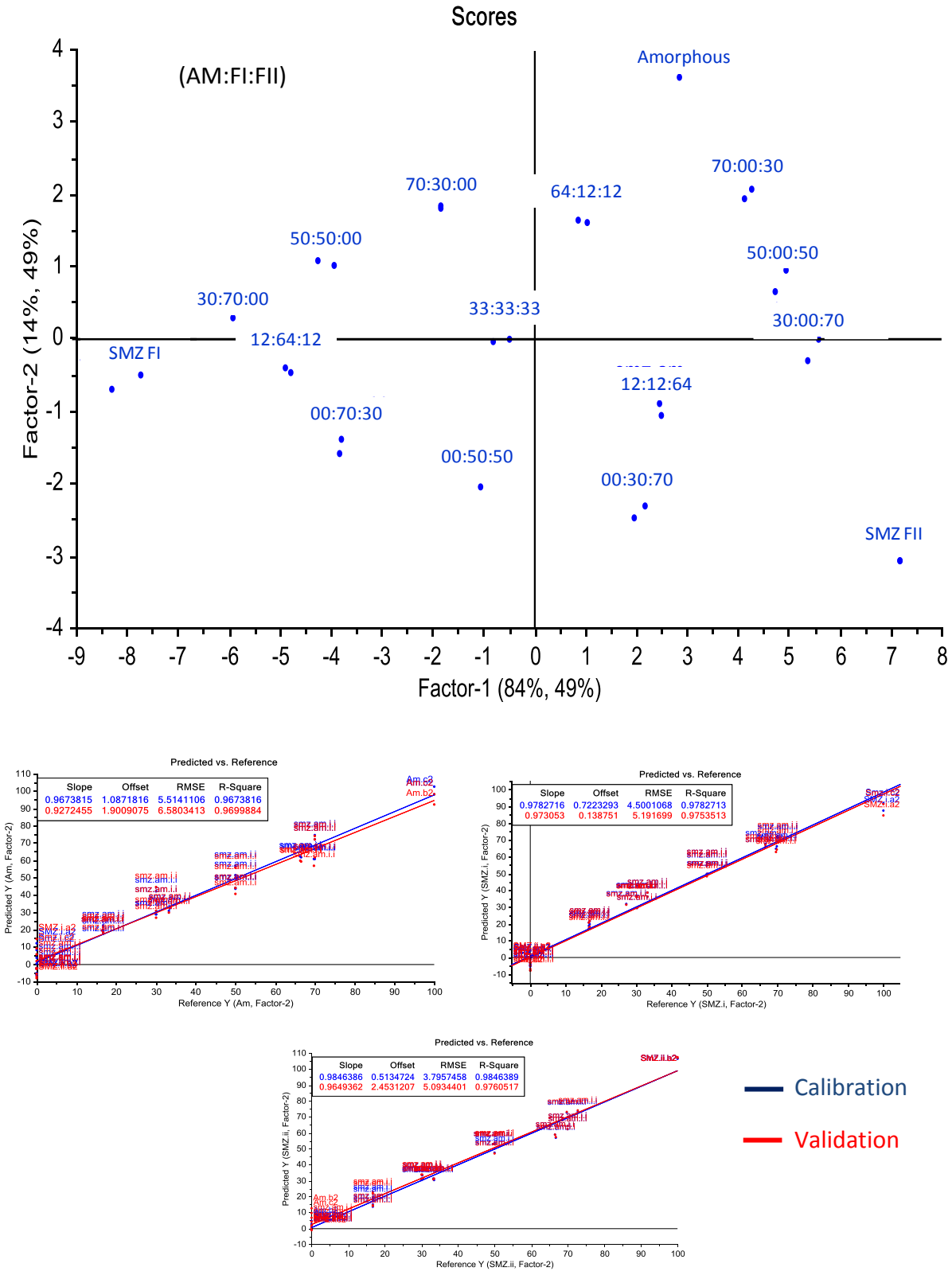

Fig. 3.38 Calibration results from ternary analysis of FI/FII/FA; (a) score plot, calibration plots of (b) FA, (c) FI, and (d) FII

Amorphous						
Pre-treatment	**Loadings**	**RMSEC (%)**	**RMSECV (%)**	**RMSEP (%)**	**Stand. Dev. (%)**	**LOD (%)**
Raw data	6	2.283	2.977	3.403	3.403	10.209
Raw, 1st derivative	4	4.192	5.612	3.694	3.024	9.072
Raw, 2nd derivative	5	1.829	4.813	1.657	3.670	11.010
SNV	2	5.514	6.580	5.137	2.051	6.152
SNV, 1st derivative	2	5.351	6.420	5.229	2.276	6.828
SNV, 2nd derivative	3	4.170	5.126	4.156	3.030	9.090
MSC	2	5.861	6.589	5.265	2.139	6.417
MSC, 1st derivative	2	5.241	6.330	5.104	2.513	7.539
MSC, 2nd derivative	3	4.255	5.567	3.893	3.787	11.361

Sulfamerazine Form I						
Pre-treatment	**Loadings**	**RMSEC (%)**	**RMSECV (%)**	**RMSEP (%)**	**Stand. Dev. (%)**	**LOD (%)**
Raw data	6	1.745	2.696	1.805	1.679	5.037
Raw, 1st derivative	4	2.859	4.031	2.102	3.121	9.363
Raw, 2nd derivative	5	2.610	4.909	1.951	2.978	8.934
SNV	2	4.500	5.192	3.997	1.873	5.618
SNV, 1st derivative	2	4.852	5.761	4.460	2.357	7.071
SNV, 2nd derivative	2	3.431	4.108	3.973	2.989	8.967
MSC	2	4.804	5.371	4.113	1.979	5.937
MSC, 1st derivative	2	4.726	5.801	4.323	2.461	7.383
MSC, 2nd derivative	3	3.355	4.059	3.526	2.784	8.352

Sulfamerazine Form II						
Pre-treatment	**Loadings**	**RMSEC (%)**	**RMSECV (%)**	**RMSEP (%)**	**Stand. Dev. (%)**	**LOD (%)**
Raw data	6	2.076	2.798	3.072	2.961	8.883
Raw, 1st derivative	4	3.065	3.685	3.045	4.293	12.879
Raw, 2nd derivative	5	2.173	3.983	1.768	1.895	5.685
SNV	2	3.796	4.459	3.348	0.277	0.831
SNV, 1st derivative	2	3.822	4.220	3.391	1.109	3.327
SNV, 2nd derivative	2	4.146	4.691	4.731	1.723	5.169
MSC	2	3.823	4.395	3.374	0.537	1.611
MSC, 1st derivative	2	3.880	4.123	3.415	1.242	3.726
MSC, 2nd derivative	3	4.220	4.931	3.653	2.019	6.057

Table 3.3 Results for each ternary analysis, using SNV pre-treated data from the NIR regions 6965-6475 cm^{-1}, 5115-4000 cm^{-1}

Quantification of solid-state transformations during milling

The NIR models were applied to monitor the degree of crystallinity vs. time during cryo-milling. Plots for both polymorphs showing the decrease in crystallinity with cryo-milling time are displayed in figures 3.39 and 3.40. Likewise, the compositions of FI samples were analyzed during room temperature milling (Figures 3.41 and 3.40). As evident from the time profile of the room temperature milling of FI, FI rapidly converts into the amorphous form within the first 20 minutes of milling (Figure 3.41). After that time significant amounts of FII are detected as the percentage of FA decreases. After 60 minutes FI has disappeared and the final mixture contains 73.7 % FII and 25.9% FA. No further changes occur after longer milling times. The same FII / FA mixture (74 % / 26 %) results, when FII is milled at room temperature. This gives a much greater insight compared to simple spectral comparisons, where even the presence of amorphous content was debatable.

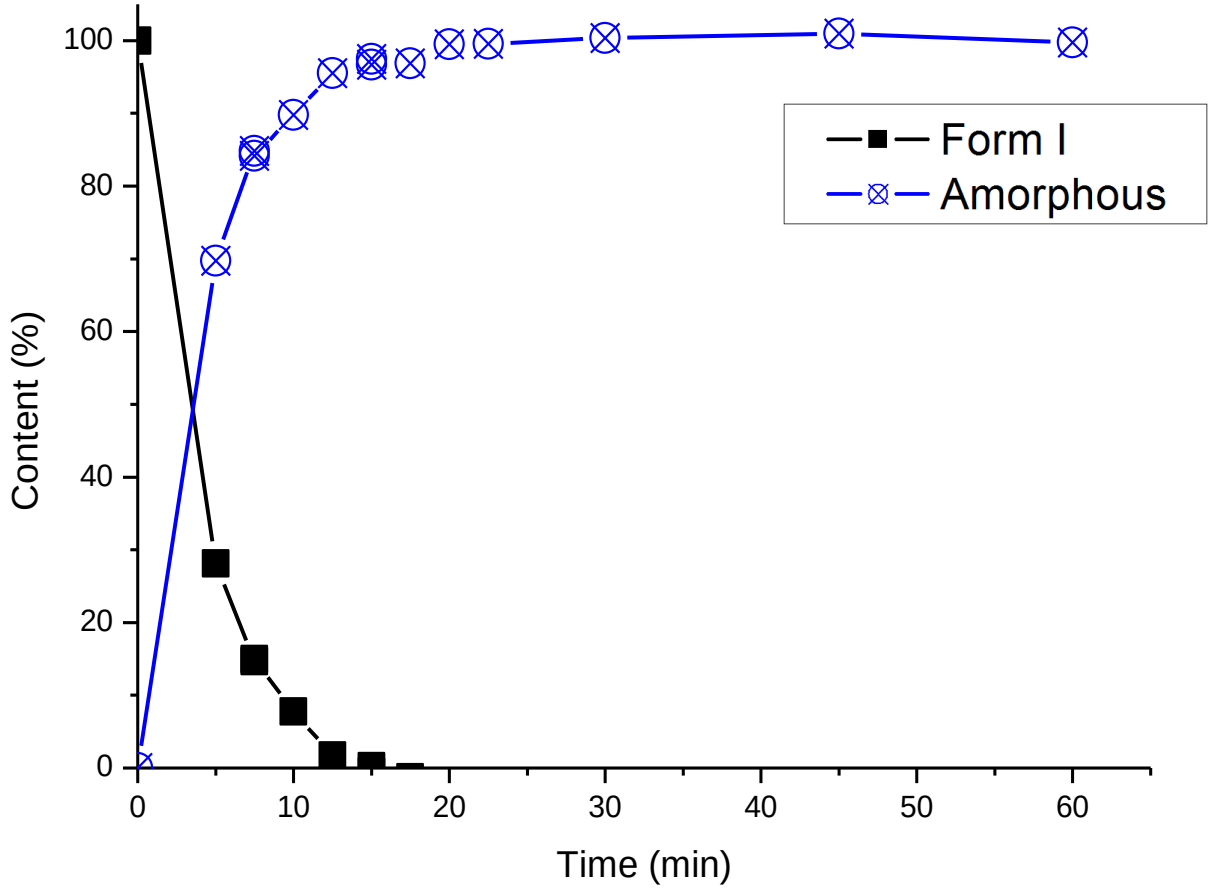

Fig. 3.39 The time profile of the polymorph composition of FI samples during cryo-milling

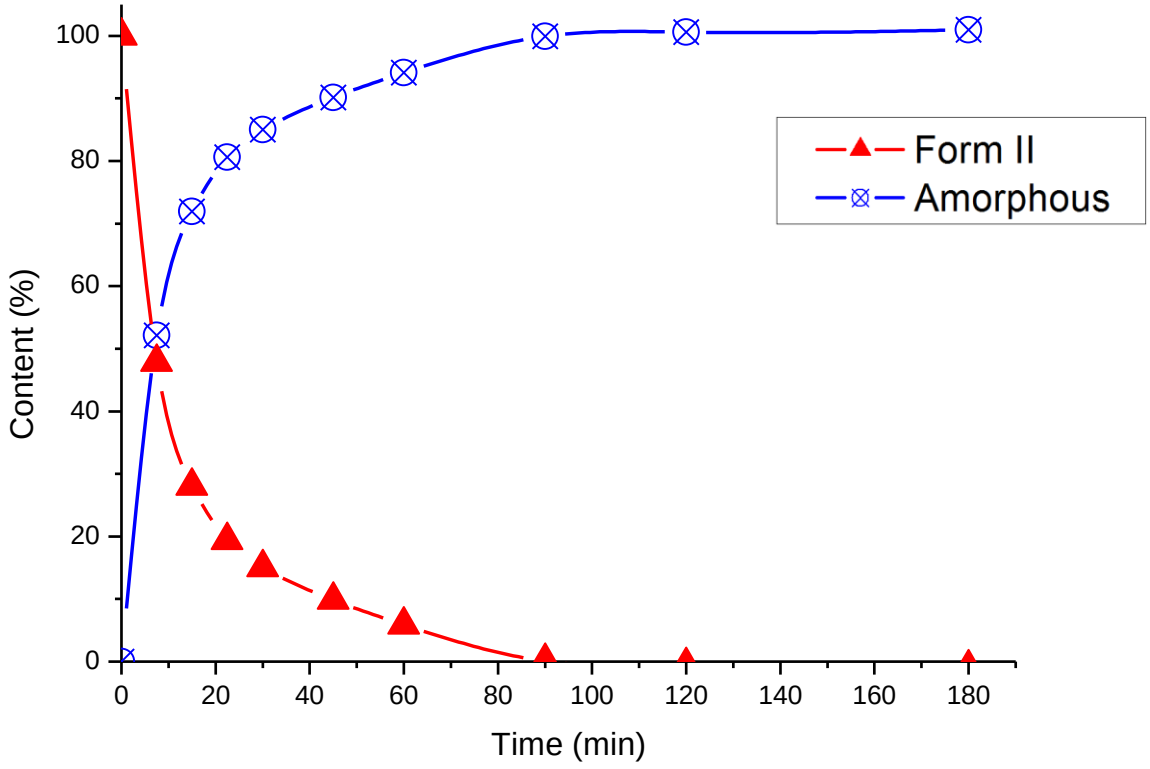

Fig. 3.40 The time profile of the polymorph composition of FII samples during cryo-milling

Zhang et al. (2002) used XRPD to observe the solid-state transitions of FI and FII during ball-milling at room temperature.[70, 71] They reported the complete conversion of FI into FII after 120 minutes. The multivariate NIR spectroscopic analysis gives further insight into the polymorphic transformation in that the sample composition-time profile for FI confirms the earlier hypothesis that the FI→FII conversion takes place via the amorphous state.[71] The mechanism of milling-induced polymorphic transformations has been discussed. Two possible scenarios include a direct crystal-crystal transformation and the transient amorphisation, or the transient formation of an unstable crystalline phase, followed by a rapid recrystallisation process. As pointed out in the literature, the detection of a transient amorphous phase is inherently difficult, as recrystallisation is generally faster than amorphisation, in particular when a crystalline component is present that can act as a crystallisation catalyst. By milling just above T_g where the recrystallisation kinetics are slow, De Guesseme et al. (2005) could show that in the case of fananserine grinding-induced polymorphic transitions occur via a transient amorphous state.[72] The FA fraction crystallizes towards FII and not back to the starting form. As this requires the nucleation and growth of the new form, the time-profile of the milling process

shows an induction period before the percentage of FII increases rapidly after 40 minutes, while FA accumulates at the start and reaches its maximum after 20 minutes. The observation that room temperature milling of FI and FII samples generates the same ≈75%/25% FII/FA mixture indicates that the milling-induced FA → FII transformation is reversible.

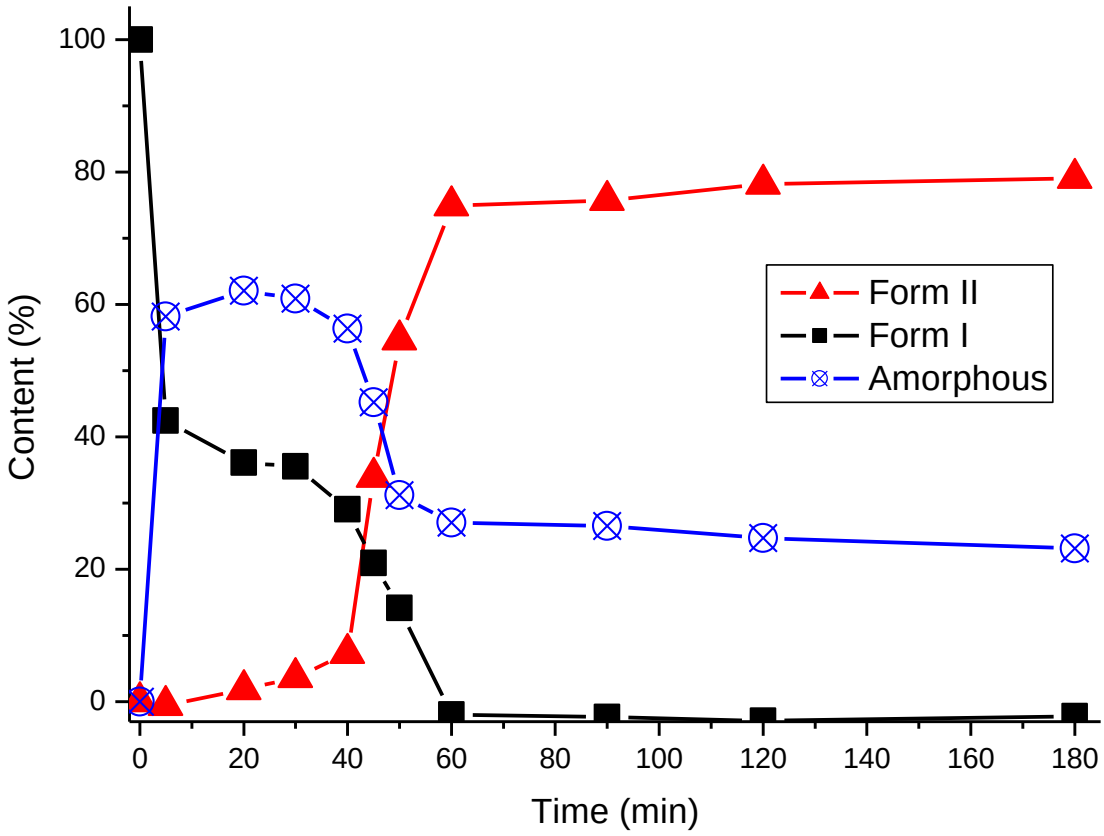

Fig. 3.41 The time profile of the polymorph composition of FI samples during room temperature milling using ternary regressional models

The stability of amorphous sulfamerazine obtained by cryo-milling FI for 30, 45, 60, 75, and 90 minutes was evaluated by NIR spectroscopy (Figures 3.29 - 3.35). Samples were kept under vacuum over silica gel at 4 °C and 22 °C. Plots of the sample composition vs. storage time are shown in figure 3.43 using ternary models pre-treated with SNV. In samples kept at 4 °C, 50% of the amorphous SMZ recrystallised within 2 to 5 days depending on the milling time. Longer milling times gave a less stable amorphous phase, as the reduction in particle size with milling duration gives rise to more sites of nucleation, thus enhancing the probability of crystallisation.

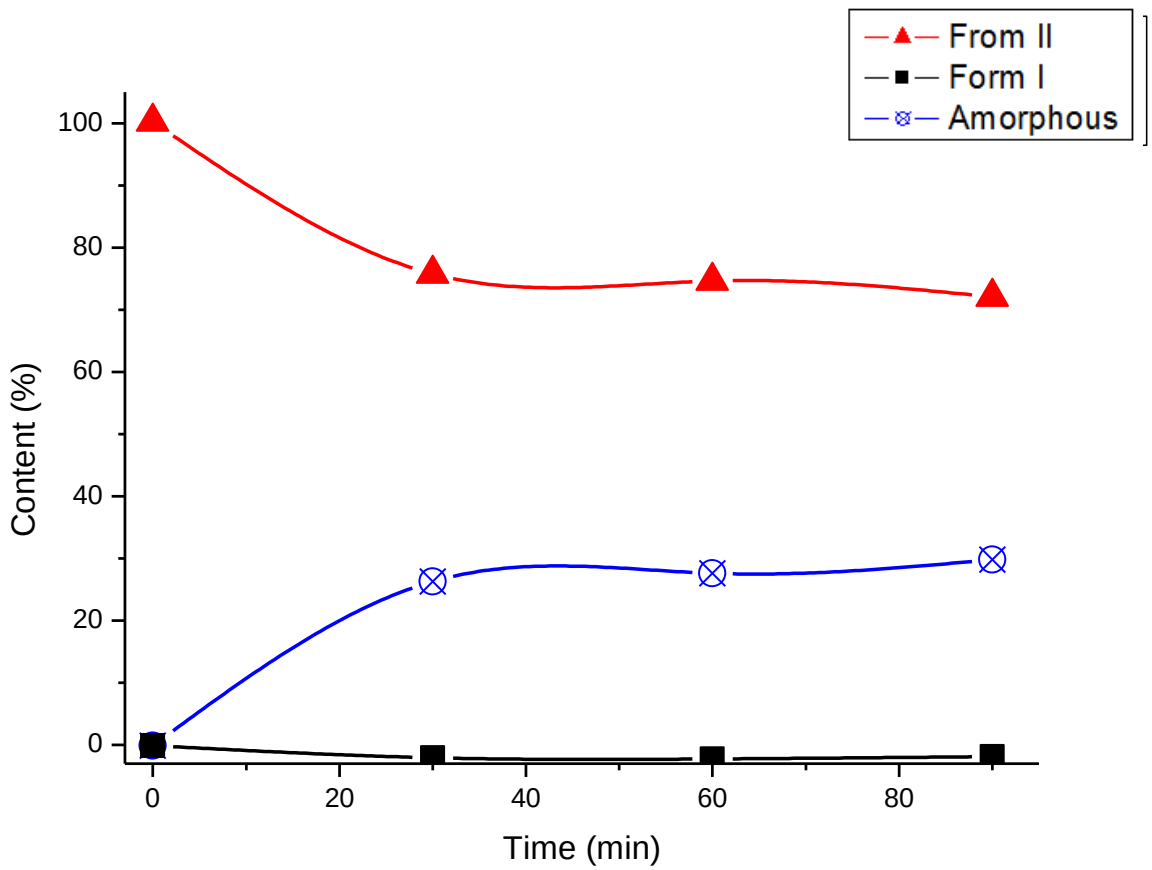

Fig. 3.42 The time profile of the polymorph composition of FII samples during room temperature milling

More importantly, the milling time affected the polymorphic forms observed. Samples milled for 30 and 40 minutes, recrystallised to mixtures of 67 % FII / 33 % FI and 76 % FII / 24 % FI respectively, while samples milled for 60 minutes or longer recrystallised to FII only. A similar behaviour was observed when samples were stored at room temperature. Samples milled for less than 60 minutes recrystallised to a mixture of FI and FII and samples milled for more than 60 minutes recrystallised to pure FII.

According to Ostwald's Rule of stages recrystallisation of the amorphous samples should occur toward the less stable polymorph FI which should then convert to FII as the most stable form at room temperature. Figures 3.33 – 3.35 and 3.43 (e - j) clearly shows that FA crystallises directly to the more stable polymorph in the absence of FI seeds. In the presence of FI seeds both polymorphs form concomitantly. There is no indication of polymorphic conversion on the timescale of the stability studies. The extreme slowness of the FI → FII

transformation due to a high kinetic barrier has been pointed out by Zhang et al.[71] The observation that the recrystallisation of the amorphised samples does not follow Ostwald's Rule when stored under vacuum by recrystallising either to a polymorphic mixture or directly to the most stable polymorph. This has also been made for sulfathiazole (Discussed in greater detail in Chapter 4).[2]

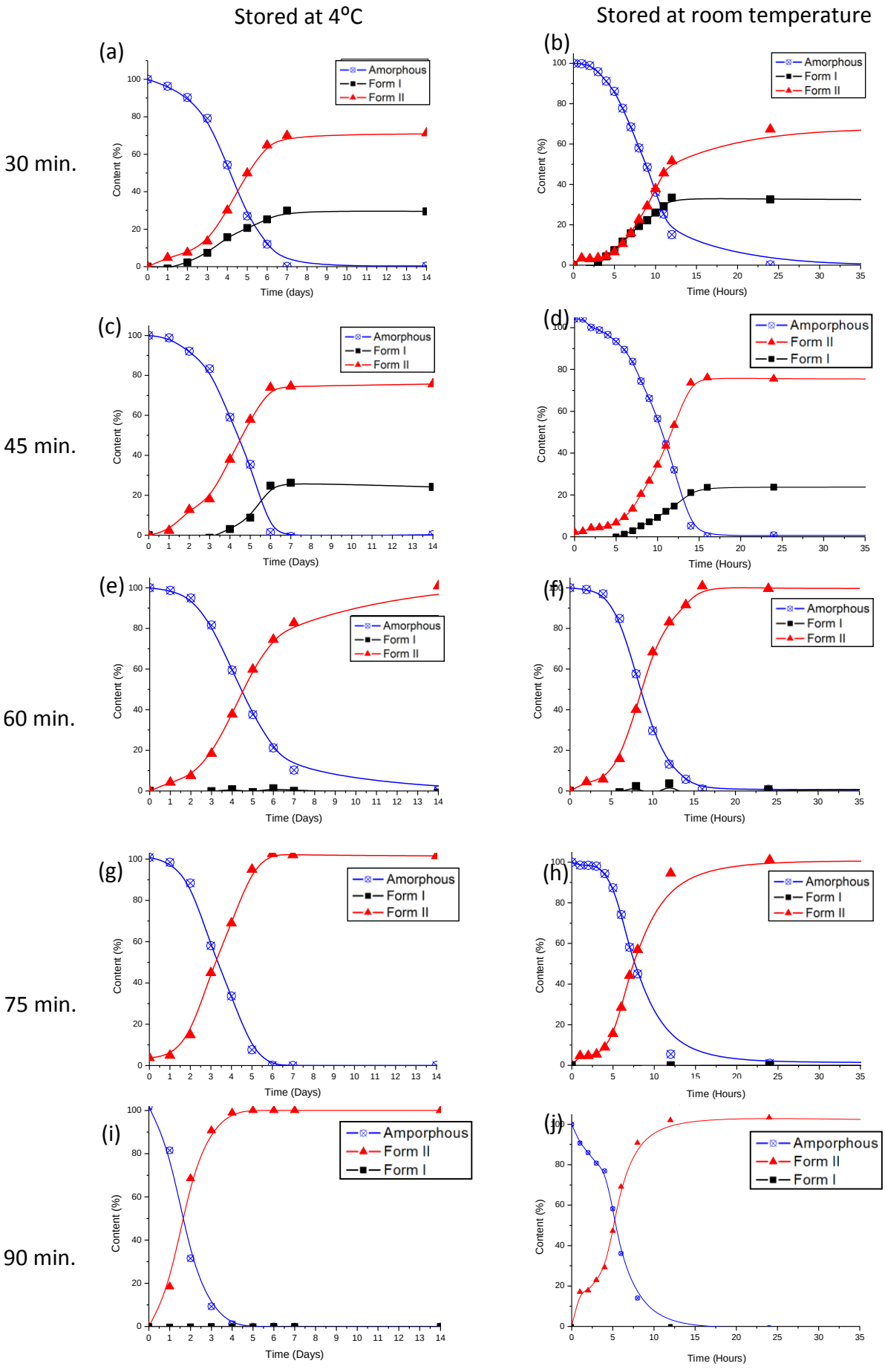

Fig. 3.43 Solid-state form composition of amorphous SMZ samples prepared by cryomilling FI *vs.* storage time

Discussion

Through this work on sulfamerazine it was found that cryo-milling is a successful means of generating the amorphous phase of sulfamerazine. For the first time full transformation to the amorphous phase of sulfamerazine was achieved, and its stability was found to dependent on the polymorph being cryo-milled, and the length of time it was cryo-milled. With the amorphous phase, chemometric models were prepared for binary and ternary analysis. This allowed the analysis, for the first time of the transformations of both polymorphs during room temperature milling and cryo-milling, and monitoring of the stability of the amorphous phase as a function of time.

Chapter Four

Solid state analysis of sulfathiazole

Introduction

The history of sulfathiazole as a pharmaceutical

Sulfathiazole (Figure 4.1) was first produced by Fosbinder & Walter in 1939,[73] and is regarded as one of the most famous sulfadrugs of its times. The development of sulfathiazole took place in the early 40s during a boom period in the production of sulfadrugs. Its popularity grew due to its greater effect in combating infectious disease,[74] while being less toxic and having fewer adverse side effects.[40] This allowed sulfathiazole to be administered at higher dosages than other sulfadrugs over longer times, amending its reputation of problematic side effects and was commonly mixed with other pharmaceuticals. This made sulfathiazole's popularity as a pharmaceutical escalate quickly. Sulfathiazole is regarded as the first sulphonamide to be discovered and fully developed in the USA, with Maltbie being the first to announce its promising results as a pharmaceutical in April 1939, with other firms such as Squibb and Winthrop publishing similar results shortly afterwards.[75] Due to vested interests from many firms, the development and patents of sulfathiazole were shared among 6 companies; Maltbie, Lederle, Winthrop, Merck, Squibb, and Calco. Because of its superior therapeutic index, sulfathiazole replaced many other sulfadrugs (such as sulfamerazine and sulfapyridine)[74] as the first choice in sulphonamides.[76] By the end of 1940s over 48 firms were marketing sulfathiazole.[77]

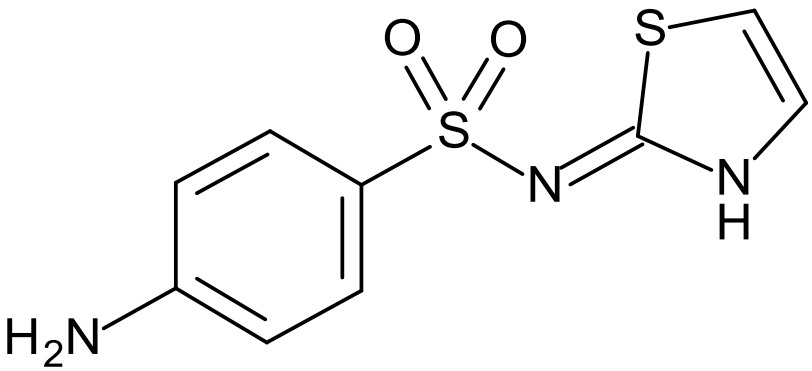

Fig. 4.1 Drawn structure of sulfathiazole

In 1941 a scandal involving Winthrop emerged regarding the production and distribution of sulfathiazole batch M29. The consequence of this is regarded as one of first major operation of the FDA following the passing of the federal food drugs and cosmetics act of 1938. During an FDA investigation of Winthrop's production of sulfathiazole, many sub-standard practices were found to cause a contamination from other products. This was worsened by Winthrop's failure to issue a prompt and efficient recall when the contamination became known. It was found that during the tabletting of sulfathiazole, Luminal (Winthrop's brand of Phenobarbital) cross-contaminated a batch of sulfathiazole (M29). At first the contamination was incorrectly designated as a disintegration problem, masking the actual threat of the Luminal contaminant. This prompted Winthrop to only recall the tainted product from primary distribution points (wholesalers, large hospitals, and certain pharmacies), disregarding the contaminated product that was already distributed to hospital wards, patients, and smaller pharmacies. This lead to between 120,000 – 160,000 tablets being unaccounted for, which Winthrop dismissed assuming that they were already consumed.[78] This was considered a systematic failure and lead to the deaths of 82, and injuring over 200 patients.[79] Even though the batch M29 was produced in December of 1940 and the first reported death in February 1941, it was not until April of that year that Winthrop took action to notify all pharmacists, physicians, wholesalers, hospitals and medical societies of the contamination. The other 47 firms were subsequently investigated by the FDA comparing their practices and the production of sulfathiazole.

An example of the popularity of sulfathiazole is depicted in literature by being mentioned in Kurt Vonnegut's Cat's Cradle. Mr. Crosby stating that sulfathiazole saved his life. This was part of the novel's central discussion of the expansion and encroachment of science on advancing technology and its possibility in bettering medicine and society.

Polymorphism of sulfathiazole

Sulfathiazole is a model polymorphic compound exhibiting at least five polymorphic forms, and over 100 solvates.[80] The manifestation of different morphology resulting from the different sulfathiazole polymorphs makes it a classic model compound in the study of polymorphism and

morphology (Figure 4.2).[81, 82] The main differences between the polymorphs of sulfathiazole lie in hydrogen bonding and the packing of the molecules in the crystal lattice (Figure 4.3).[83]

As expected over the decades the nomenclature used in the polymorphism of sulfathiazole has evolved. In this study the labelling system issued by Abu Bakar, et al. in their 2011 paper 'investigation of the riddle of sulfathiazole polymorphism' is used.[82] The first investigation to report polymorphism of sulfathiazole was by Grove et al. finding form I (FI) as rods, and form II (FII) as hexagonal plates.[84] These were confirmed as unique polymorphs by Miyazzaki et al. who also were the first to crystallise form III which they labelled as (α').[85, 86] Mesley et al. were the first to crystallise and characterise form IV, naming the new polymorph as IIB.[86] The most recent polymorph form V was produced by Hughes et al. in 1999, at this point a more uniformed nomenclature was in practice and was labelled form V.[87]

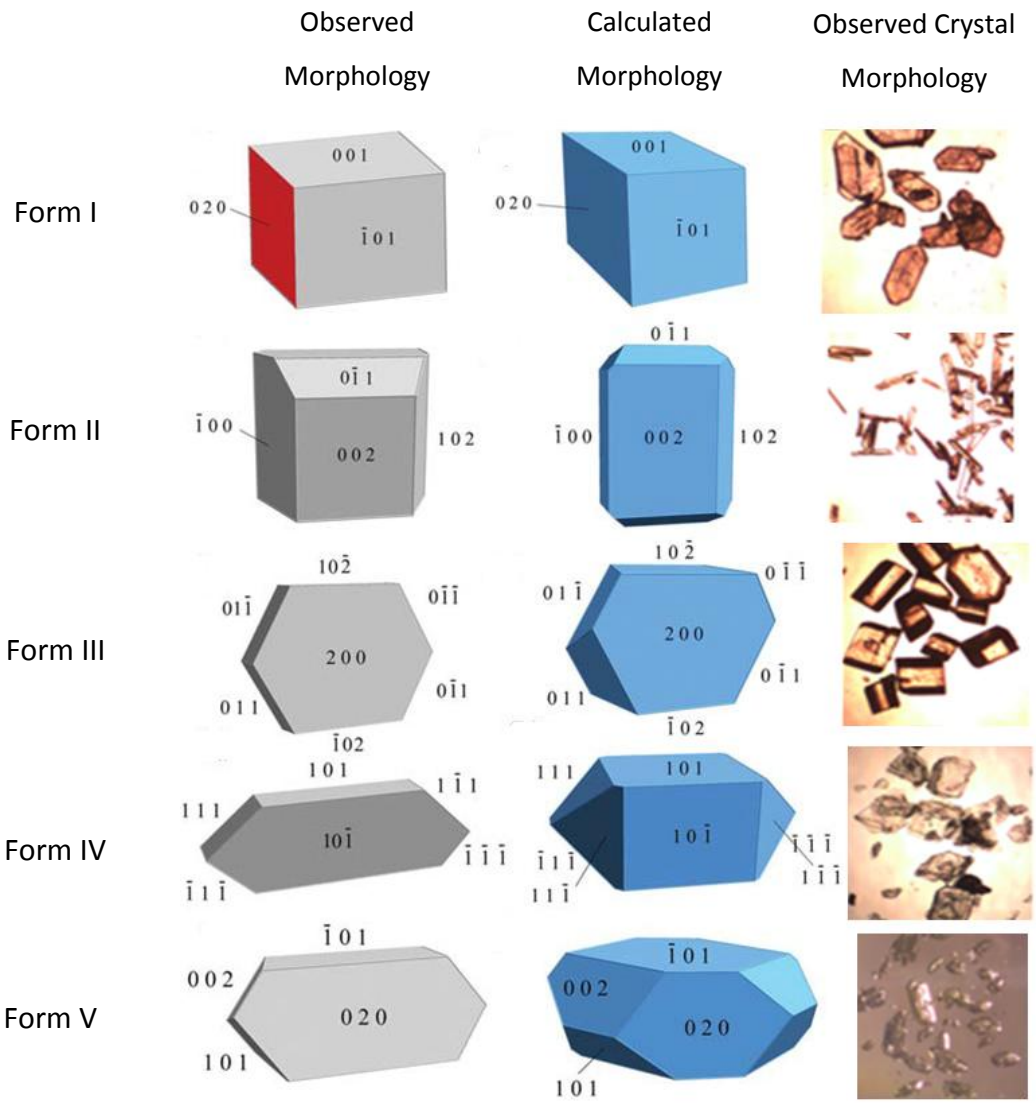

Fig. 4.2 Calculated and observed morphology of sulfathiazole forms I-V

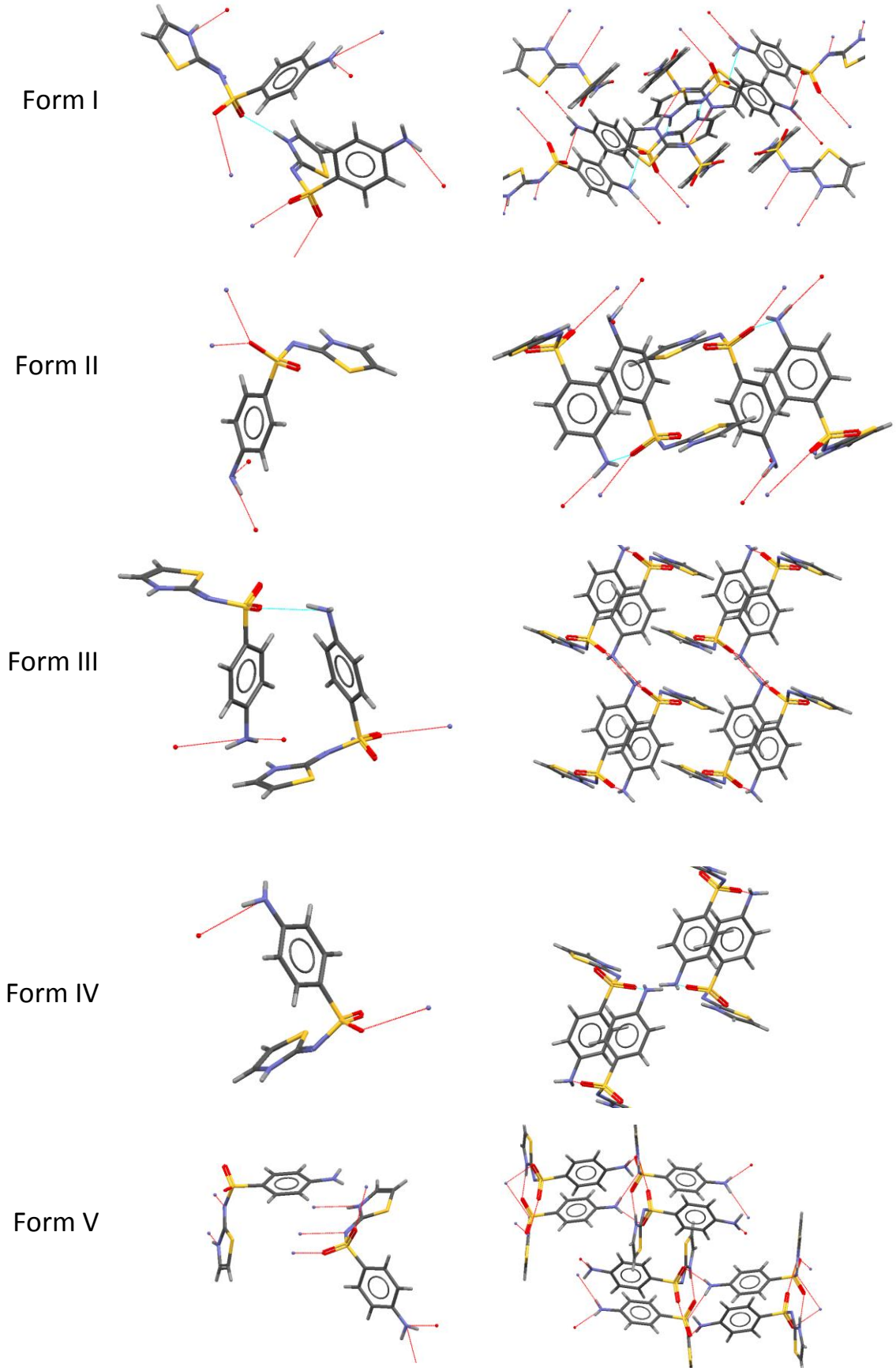

Fig. 4.3 Molecular structures of sulfathiazole polymorphs I-V (left),

and packing their packing arrangement (right)

The physicochemical properties of the five forms have been described in detail.[44-46, 88-90] Relative thermodynamic stabilities at 0K are generally accepted to follow the order of the densities of the structures, that is; III ≈ IV > II > I > V, with form I being metastable at room temperature.[45, 90] Shakhtshneider and Boldyrev reported the influence of mechanical treatment in a planetary ball mill on the polymorphic transformation of sulfathiazole, and sulfathiazole–polyvinylpyrrolidone.[91-93] They found that mechanical treatment of sulfathiazole led to the partial amorphisation. This amorphous content then crystallised to a polymorphic mixture of forms I and III. Aaltonen et al. have monitored the decrease in a decrease in crystallisation of amorphous content by milling samples at room temperature.[94] However, in contrast to Shakhtshneider and Boldyrev,[91, 92] they did not note any polymorphic transformatiosns in the XRPD patterns of samples subjected to mechanical treatment. Lagas and Lerk prepared amorphous sulfathiazole by melt-quenching,[88] and Kordikowski et al. obtained a mixture of form I and amorphous sulfathiazole from acetone using supercritical CO_2. Recently, the preparation of amorphous sulfathiazole by cryo-milling has been reported but no stability testing of the amorphous phase was described.[95, 96]

Polymorphic analysis

When the structures of forms II and III were initially reported by Kruger and Gafner the melting behaviour of these forms suggested a transition to form I.[97, 98] More recently, Zeitler and co-workers characterised the transformations of all five sulfathiazole polymorphs by terahertz pulsed spectroscopy and DSC and reported solid state transformations of forms II, III and IV to form I at varying temperatures.[89] The crystal lattices of forms II, III and IV are very similar, and analysis using the program XPac has shown that forms II and IV contain the same monolayers with the difference between them being that the monolayers are slipped in form IV relative to form II, and that form III is a combination of the bilayers of II and IV.[99] The epitaxial growth of form IV on form II crystals has also been observed in solution and the nucleation process has been associated with their structural similarities.[27] It is thus not surprising that it is difficult to crystallise pure samples of forms II, III and IV from solution.

Traditional univariate or bivariate methods based on the analysis of the absorbance at single characteristic wavelengths in the NIR spectrum have been successfully applied for the quantification of binary polymorphic mixtures of solid-state pharmaceuticals.[100] However,

more sophisticated multivariate methods such as partial least square(PLS) regression that utilise spectral information from the whole spectrum or selected spectral regions are used to show a high co-linearity varying spectra and change in content (or concentration). These have been found to more effective, especially when the spectral differences between polymorphs are small. Multivariate techniques often result in more reliable and robust calibration models and are generally considered superior to uni- or bi-variate approaches.[101-104]

Literature reports on the quantification of sulfathiazole polymorphs have previously focused on the quantification of forms I and III. Luner et al. used uni- and bi-variate approaches for the quantification of binary mixtures of forms I and III by NIR spectroscopy and XRPD and obtained accurate linear regression models with high correlation values (R^2) and low standard errors of calibration.[105] Patel and co-workers evaluated the ability of NIR spectroscopy combined with univariate, multiple linear regression and PLS methods to accurately determine low content (0%–5%) of form I in form III.[95] Pöllänen et al. have used Diffuse Reflectance Infrared Fourier Transform Infrared (DRIFT-IR) spectroscopy and developed PLS models to quantify forms I and III in polymorphic mixtures of form I, II, III and V.[106]

Objective

Low content analysis of forms I, III, and V were conducted using XRPD, IR and NIR spectroscopy. This was to determine the best and most accurate means of analysing the sulfathiazole polymorphs, and the limitations of the analytical techniques.

Previously ternary analysis was used on Forms I, III, and V.[19] Using NIR data pre-treated with SNV, the RMSEC and RMSEP were both found to be 3.2% or less for the detection of all polymorphs, and 2.0% in the detection of Form I. In this body of work multivariate analysis was expanded to ternary analysis focusing on low content analysis and throughout the whole content for the detection and quantification of the amorphous phase, and forms I and III. Because of this, two different sample designs which have shown success in previous literature were used and compared (Figure 4.4).[19, 49, 50] NIR was chosen as a means of analysis for the ternary system of sulfathiazole form I, III, and the amorphous phase because of the success of NIR spectroscopy in the ternary analysis of sulfathiazole's forms I, III, and V. NIR also showed its superiority in analysing binary mixtures of sulfathiazole forms I, III, and the amorphous phase,

and has shown great success in previous literature.[19, 100] This was then used to analyse the amorphisation of forms I and III via cryo-milling.

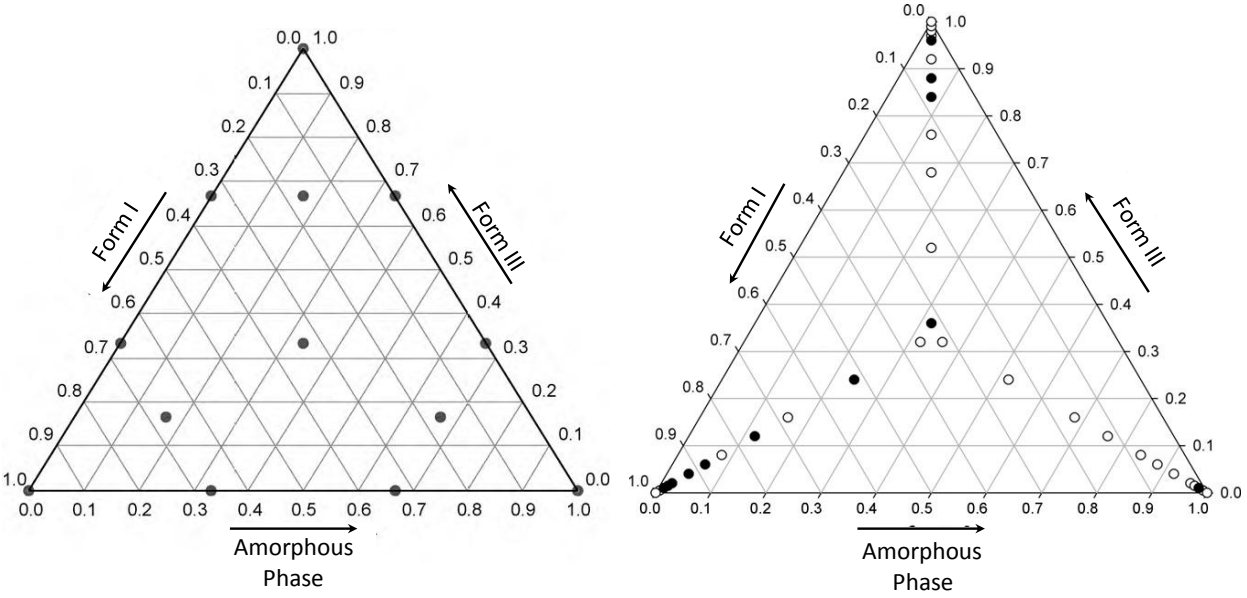

Fig. 4.4 Sample set designed for whole content ternary analysis (Left) and low content ternary analysis (Right), where ● are prediction samples and ○ are calibration

.

Characterisation of sulfathiazole forms I, III, V, and the amorphous phase

Forms I, III, and V were identified and confirmed by comparing their theoretical XRPD patterns to experimental patterns produced from recrystallised samples. Figure 4.5 a-c shows the peak alignment between the theoretical and experimental patterns, confirming the full transformation during recrystallisation. The amorphous phase is identified by the characteristic amorphous hump in the XRPD pattern (Figure 4.6 d). The amorphous phase of sulfathiazole was prepared via cryo-milling and using the melt quench method. The chemical purity of samples prepared by both methods was compared using a HPLC internal standard calibration method (Figure 4.7). Here it was found that samples prepared using the melt quench method could be up to 95.6% pure, whereas samples of amorphous sulfathiazole prepared via cryo-milling were up to 99.7% pure, i.e. no degradation took place during cryo-milling.

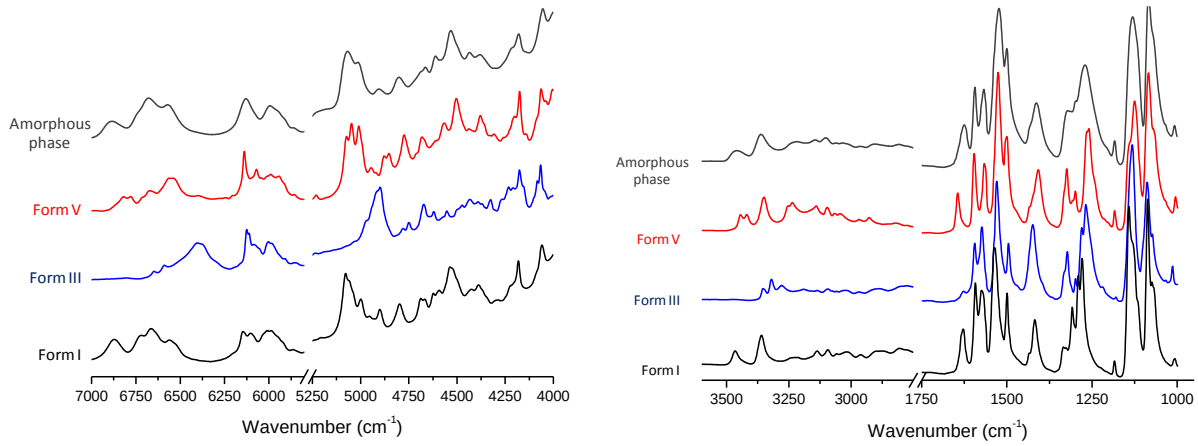

Fig. 4.5 NIR (Left) and IR (Right) spectra of sulfathiazole forms I (black), III (blue), V (red), and the amorphous phase (Grey)

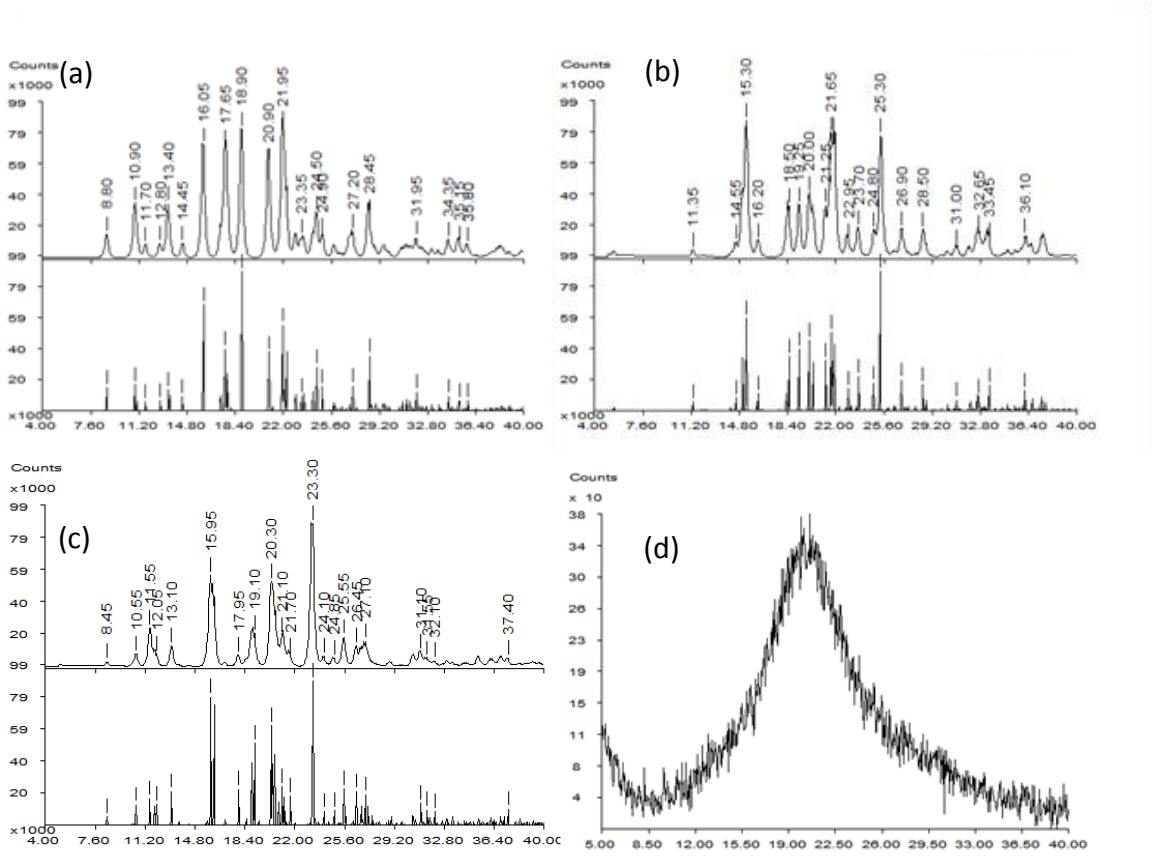

Fig. 4.6 Experimental (top) and theoretical (bottom) XRPD patterns of sulfathiazole forms I (a), III (b), V (c), and the amorphous phase (d)

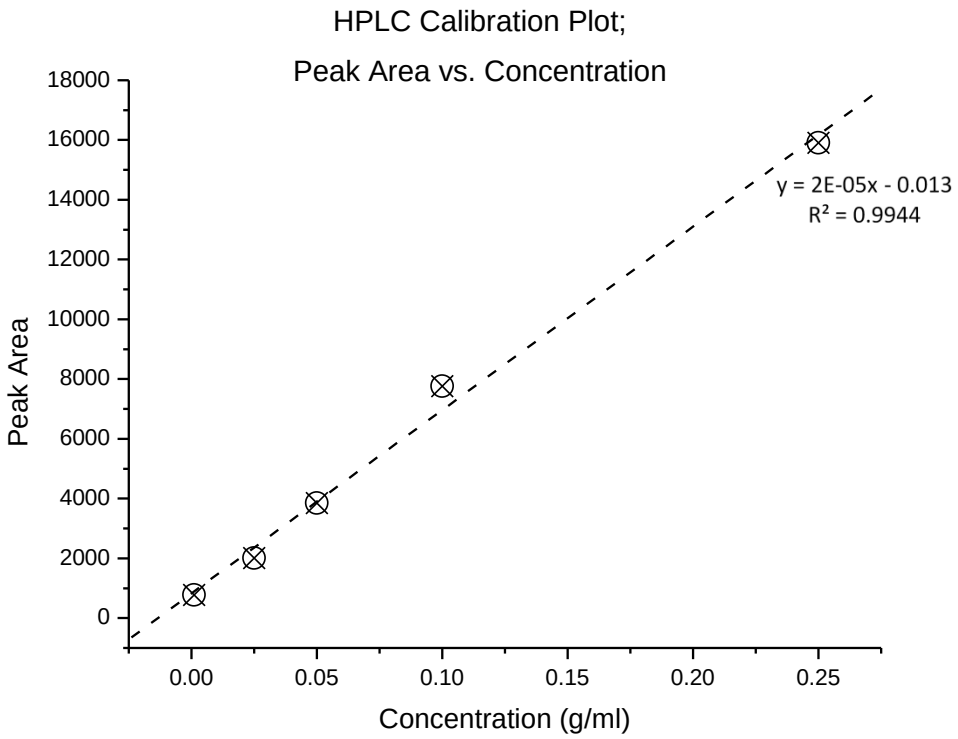

Fig. 4.7 HPLC calibration model used to predict the purity of amorphous sulfathiazole

Characteristic peaks in the IR and NIR spectra of sulfathiazole forms I, III, V, and the amorphous phase.

Form I

NIR spectrum; 6875 cm^{-1}, 6725 cm^{-1}, 6660 cm^{-1}, 6560 cm^{-1}, 6155 cm^{-1}, 6105 cm^{-1}, 6010 cm^{-1}, 5985 cm^{-1}, 5862 cm^{-1}, 5080 cm^{-1}, 4997 cm^{-1}, 4950 cm^{-1}, 4895 cm^{-1}, 4795 cm^{-1}, 4687 cm^{-1}, 4670 cm^{-1}, 4623 cm^{-1}, 4600 cm^{-1}, 4537 cm^{-1}, 4430 cm^{-1}, 4390 cm^{-1}, 4227 cm^{-1}, 4180 cm^{-1}, 4063 cm^{-1}

IR spectrum; 3465 cm^{-1}, 3360 cm^{-1}, 3140 cm^{-1}, 3090 cm^{-1}, 3013 cm^{-1}, 2960 cm^{-1}, 2800 cm^{-1}, 1630 cm^{-1}, 1592 cm^{-1}, 1575 cm^{-1}, 1535 cm^{-1}, 1500 cm^{-1}, 1420 cm^{-1}, 1335 cm^{-1}, 1310 cm^{-1}, 1290 cm^{-1}, 1278 cm^{-1}, 1185 cm^{-1}, 1140 cm^{-1}, 1087 cm^{-1}, 1070 cm^{-1}

Form III

NIR spectrum; 6650 cm^{-1}, 6590 cm^{-1}, 6405 cm^{-1}, 6380 cm^{-1}, 6127 cm^{-1}, 6120 cm^{-1}, 6085 cm^{-1}, 6003 cm^{-1}, 5985 cm^{-1}, 5908 cm^{-1}, 5853 cm^{-1}, 4899 cm^{-1}, 4782 cm^{-1}, 4750 cm^{-1}, 4672 cm^{-1}, 4623 cm^{-1}, 4555 cm^{-1}, 4480 cm^{-1}, 4435 cm^{-1}, 4392 cm^{-1}, 4370 cm^{-1}, 4320 cm^{-1}, 4270 cm^{-1}, 4232 cm^{-1}, 4210 cm^{-1}, 4175 cm^{-1}, 4083 cm^{-1}, 4065 cm^{-1}

IR spectrum; 3350 cm^{-1}, 3320 cm^{-1}, 3280 cm^{-1}, 3190 cm^{-1}, 3137 cm^{-1}, 3095 cm^{-1}, 3017 cm^{-1}, 2970 cm^{-1}, 2880 cm^{-1}, 2775 cm^{-1}, 1595 cm^{-1}, 1575 cm^{-1}, 1530 cm^{-1}, 1490 cm^{-1}, 1425 cm^{-1}, 1320 cm^{-1}, 1300 cm^{-1}, 1280 cm^{-1},1270 cm^{-1}, 1280 cm^{-1},1132 cm^{-1}, 1088 cm^{-1}, 1072 cm^{-1}, 1012 cm^{-1}

Form V

NIR spectrum; 6820 cm^{-1}, 6780 cm^{-1}, 6670 cm^{-1}, 6560 cm^{-1}, 6540 cm^{-1}, 6395 cm^{-1}, 6140 cm^{-1}, 6070 cm^{-1}, 5990 cm^{-1}, 5945 cm^{-1}, 5076 cm^{-1}, 5050 cm^{-1}, 5010 cm^{-1}, 4950 cm^{-1}, 4885 cm^{-1}, 4860 cm^{-1}, 4775 cm^{-1}, 4685 cm^{-1}, 4570 cm^{-1}, 4504 cm^{-1}, 4440 cm^{-1}, 4377 cm^{-1}, 4304 cm^{-1}, 4200 cm^{-1}, 4170 cm^{-1}, 4065 cm^{-1}

IR spectrum; 3445 cm^{-1}, 3420 cm^{-1}, 3350 cm^{-1}, 3250 cm^{-1}, 3235 cm^{-1}, 3140 cm^{-1}, 3100 cm^{-1}, 3065 cm^{-1}, 3032 cm^{-1}, 2968 cm^{-1}, 2930 cm^{-1}, 1640 cm^{-1}, 1600 cm^{-1}, 1566 cm^{-1}, 1525 cm^{-1}, 1500 cm^{-1}, 1407 cm^{-1}, 1323 cm^{-1}, 1298 cm^{-1}, 1260 cm^{-1}, 1185 cm^{-1}, 1125 cm^{-1}, 1085 cm^{-1},

Amorphous Phase

NIR Spectrum; 6890 cm^{-1}, 6680 cm^{-1}, 6570 cm^{-1}, 6127 cm^{-1}, 5995 cm^{-1}, 5857 cm^{-1}, 5070 cm^{-1}, 5010 cm^{-1}, 4900 cm^{-1}, 4797 cm^{-1}, 4665 cm^{-1}, 4610 cm^{-1}, 4530 cm^{-1}, 4440 cm^{-1}, 4378 cm^{-1}, 4220 cm^{-1}, 4180 cm^{-1}, 4060 cm^{-1}

IR spectrum; 3455 cm^{-1}, 3360 cm^{-1}, 3200 cm^{-1}, 3145 cm^{-1}, 3102 cm^{-1}, 2905 cm^{-1}, 1623 cm^{-1}, 1593 cm^{-1}, 1568 cm^{-1}, 1525 cm^{-1}, 1500 cm^{-1}, 1415 cm^{-1}, 1322 cm^{-1}, 1270 cm^{-1}, 1185 cm^{-1}, 1130 cm^{-1}, 1085 cm^{-1}

Low content analysis of sulfathiazole binary mixtures of forms I, III, and V

The initial attempt of this study was to include all five polymorphs of sulfathiazole in multivariate analysis. Though forms I, III, and V were readily obtained it was not possible to obtain polymorphically pure samples of forms II and IV. All attempts to crystallise form II from methanol or nitromethane following literature reports were unsuccessful.[68, 90] It was found that solvent-controlled crystallisation of sulfathiazole yielded polymorphic mixtures. Samples obtained from ethanol consisted mainly of form II, while crystallisation from water gave samples containing form IV as the main component. The observation that forms II, III and IV usually crystallise together has also been made in previous literature.[46] The reason for this is likely the close similarity of their crystal lattices, creating uncertainty in the purity in recrystallising either forms II or IV.

The NIR spectra of forms II and IV differ from the spectrum of form I in that II and IV give rise to a broad band at 6400 cm^{-1} that is not observed for form I. It has already been reported that forms II & IV can grow concurrently and form IV has been reported to grow on the surface of form I.[27] Any attempt to prepare bulk samples of forms II and IV would present contamination. Consequently, as pure samples of forms II and IV are not available, accurate binary model mixtures could only be prepared for forms I, III and V. The limits that this places on the comprehensiveness of the analysis are discussed below.

Due to differences in H bonding, forms I, III and V show distinct vibrational spectra which allow for screening and quantification by IR and NIR spectroscopy.[19, 94, 100, 106] The NIR spectra of polymorphs I, III and V differ most in the 7050 cm^{-1}–6200 cm^{-1} region which encompasses the region of the first overtones for the N–H stretching vibrations and in the region from 5150 cm^{-1} to 4800 cm^{-1} where the combination bands of N–H stretching and NH_2 bending vibrations appear.

For solid samples the systematic variation is due to, among others factors, light scattering and differences in path length, and may often constitute a major part in the variation of the sample spectra. Because of this, the pre-processing of data is needed. As with all multivariate systems, the component that produces the most varied spectrum will be the most distinguishable, and thus will be easier to quantify. This is observed throughout most results,

particular mixtures of form I and III, showing a lower RMSEC, RMSECV, and RMSEP. Pre-treatment of the data also shows an improvement in calibration models.

Calibration models were developed for each form in mixtures of forms I / III, I / V and III / V in the 0%–15% concentration range using a PLS regression model. PLS models with low root mean square error (RMSE) values were obtained when the following spectral ranges were selected (Figure 4.8): 6970–6540 cm^{-1} and 5120–5000 cm^{-1} for 0–15% form I in form III; 6504–6230 cm^{-1}, 6132–6060 cm^{-1} and 4964–4850 cm^{-1} for 0%–15% form III in form I; 6960–6830 cm^{-1}, 5084–5050 cm^{-1} and 4558–4516 cm^{-1} for 0%–15% form I in form V; 6750–6300 cm^{-1} and 6160–6046 cm^{-1} for 0–15% form V in form I; 6900–6520 cm^{-1} and 5100–4990 cm^{-1} for 0–15% form V in form III and 6485–6174 cm^{-1} and 4982–4862 cm^{-1} for 0–15% form III in form V. For form I in III, form III in I, form I in V and form V in III, the selected ranges encompass bands specific to the respective minor component. Low levels of form I in I / III mixtures are visible as weak bands at 6870 cm^{-1}, 6730 cm^{-1}, 5078 cm^{-1}, 5058 cm^{-1} and 5036 cm^{-1}, while low levels of form III can be identified by characteristic new bands at around 6400 cm^{-1}, 6126 cm^{-1} and 6110 cm^{-1} and clear changes around 4900 cm^{-1}. Similarly, low levels of form V in III / V mixtures give rise to weak new bands at 6800 cm^{-1}, 5076 cm^{-1}, 5048 cm^{-1} and 5010 cm^{-1}. Low levels of form I in I / V mixtures can be visually identified by a characteristic form I band which appears as a shoulder at around 6870 cm^{-1}. Low levels of form III in V result in clear changes around 6400 cm^{-1} and 4900 cm^{-1}. The spectral similarities of low content form V in form I have an effect on the accuracy of the calibration models. Form V gives small increases in the intensity of the band at 6140 cm^{-1} resulting in the increased RMSEC, RMSECV and RMSEP of 0.458%, 0.605%, and 0.485% respectively (Figure 4.8b). Whereas due to the emergence of the clearly defined form I peak at 6900 cm^{-1} in form V (Figure 4.8e).Low content analysis of form I in form V produces models with improved accuracy, having the RMSEC, RMSECV and RMSEP values of 0.664%, 0.808%, and 0.994% respectively.

The RMSEC, RMSECV and RMSEP values and the number of PLS factors for the calibration models developed for the NIR measurements using raw and pre-treated data are reported in Table 4.1. Pre-treatment of the raw data can enhance the model performances and reduced the number of PLS factors required. Using SNV or MSC as pre-treatment techniques gave the best results for calibration models developed for each form in mixtures of forms I / III, I / V and III / V in the 0%–15% concentration range using a PLS regression. In all cases, MSC and

SNV gave very similar results. This is often observed, as the equations for MSC and SNV have a similar formulation and are widely regarded as exchangeable.[38, 107] MSC and SNV remove offsets and slopes in the spectra caused by the light scattering intrinsic to solid state analysis. The advantage of SNV is that it is applied to an individual spectrum, whereas MSC uses a reference spectrum, because of this it can be argued that using SNV can give truer pre-treated data than that of MSC. The best models for the determination of 0–15% form V in form III and of 0–15% form III in form V were obtained, when first derivative calculations were applied or when SNV and first derivative were combined. Overall, the best-performing calibration model resulted for the low content determination of form III in I / III mixtures with RMSEC, RMSECV and RMSEP values of 0.201%, 0.340% and 0.298% and two PLS factors. Projection of the prediction sets onto the calibration models show an excellent linear correlation, where the predicted values stray very little form the calibration line (Figure 4.9).

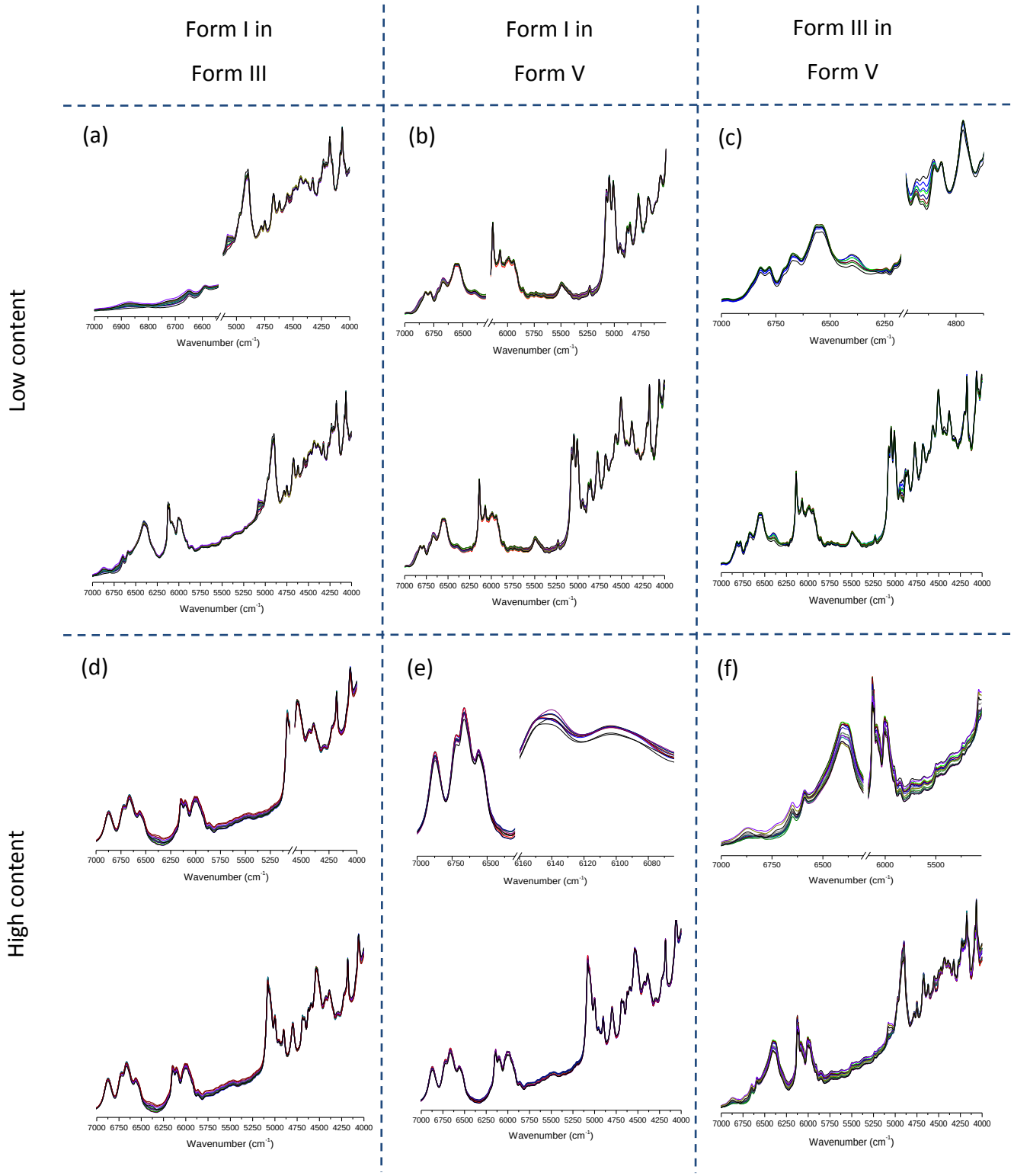

Fig 4.8 NIR regions used in low content binary analysis

Binary mixture	Pre-processing	PLS factor	RMSEC (%)	RMSECV (%)	RMSEP (%)	PLS factors	RMSEC (%)	RMSECV (%)	RMSEP (%)
			Range (0-15%)				Range (85-100%)		
Forms I/III	Raw data	3	0.176	0.337	0.392	3	0.12	0.276	0.413
	SNV	1	0.299	0.371	0.266	2	0.201	0.34	0.298
	MSC	1	0.299	0.372	0.266	2	0.203	0.346	0.296
	1st der.	1	0.196	0.253	0.467	1	0.292	0.495	0.452
	SNV/1st der.	1	0.181	0.23	0.637	1	0.284	0.448	0.313
	MSC/1st der.	1	0.198	0.227	0.641	1	0.293	0.491	0.342
Forms I/V	Raw data	4	0.383	1.039	0.724	4	0.421	1.016	0.896
	SNV	1	0.46	0.608	0.485	2	0.575	0.767	0.446
	MSC	1	0.458	0.605	0.485	2	0.575	0.767	0.449
	1st der.	3	0.344	0.66	0.588	1	0.644	0.812	0.932
	SNV/1st der.	2	0.488	0.748	0.687	1	0.664	0.808	0.994
	MSC/1st der.	2	0.470	0.640	0.726	1	0.686	0.833	1.725
Forms III/V	Raw data	3	0.376	0.741	0.31	3	0.446	0.744	0.385
	SNV	1	0.414	0.515	0.404	3	0.439	0.726	0.481
	MSC	1	0.41	0.509	0.401	3	0.444	0.714	0.476
	1st der.	2	0.397	0.553	0.279	2	0.448	0.672	0.344
	SNV/1st der.	1	0.402	0.539	0.279	2	0.449	0.704	0.377
	MSC/1st der.	2	0.358	0.514	0.278	2	0.451	0.702	0.356

Table 4.1 Results of low content binary analysis using different pre-processed NIR regions: 6970–6540 cm^{-1} and 5120–5000 cm^{-1} for 0–15% form I in form III; 6504–6230 cm^{-1}, 6132–6060 cm^{-1} and 4964–4850 cm^{-1} for 0%–15% form III in form I; 6960–6830 cm^{-1}, 5084–5050 cm^{-1} and 4558–4516 cm^{-1} for 0%–15% form I in form V; 6750–6300 cm^{-1} and 6160–6046 cm^{-1} for 0–15% form V in form I; 6900–6520 cm^{-1} and 5100–4990 cm^{-1} for 0–15% form V in form III and 6485–6174 cm^{-1} and 4982–4862 cm^{-1} for 0–15% form III in form V

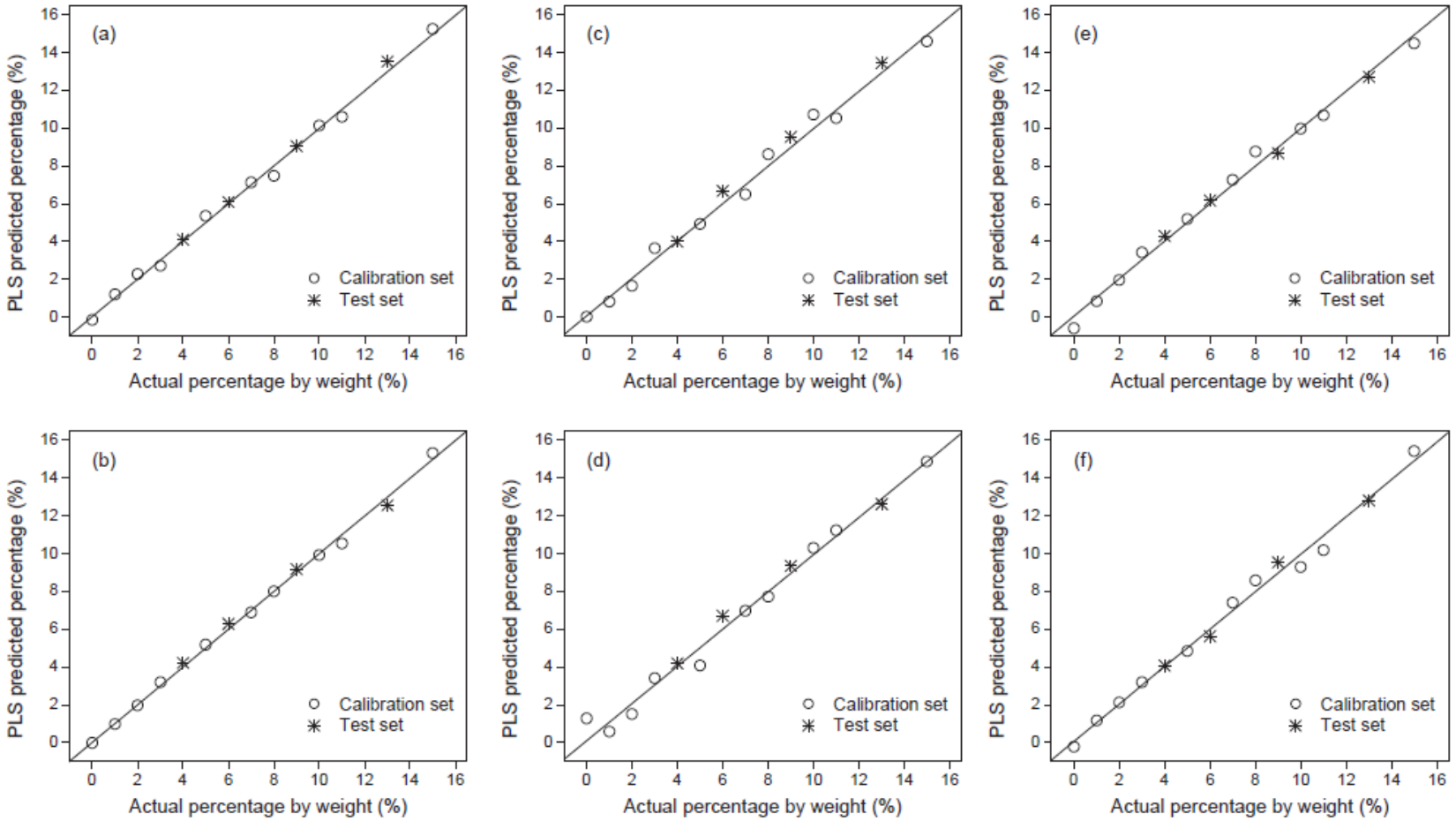

Fig. 4.9 Predicted vs actual percentage for binary mixtures analysed in the 0–15% composition range by NIR spectroscopy. (a) 0–15% form I in form III, SNV pre-processing; 6970−6540 cm−1 and 5120–5000 cm−1 range. (b) 0–15% form III in form I; SNV pre-processing; 6504−6230 cm−1, 6132−6060 cm−1 and 4964–4850 cm−1 range. (c) 0–15 % form I in form V; SNV pre-processing; 6960−6830 cm−1, 5084−5050 cm−1 and 4558–4516 cm−1 range. (d) 0–15% form V in form I; SNV pre-processing; 6750−6300 cm−1 and 6160–6046 cm−1 range. (e) 0–15% form III in form V; SNV and 1st derivative; 6485−6174 cm−1 and 4982–4862 cm−1 range. (f) 0–15% form V in form III; 1st derivative; 6900−6520 cm−1 and 5100–4990 cm−1 range. The solid lines represent the data fit with a linear regression model.

Analysis of ternary mixtures of sulfathiazole forms I, III, and the amorphous phase

NIR spectroscopy was chosen to be used in the analysis of sulfathiazole ternary mixtures (forms I, III, and the amorphous phase) over XRPD and IR spectroscopy due to its history of obtaining better results in binary analysis containing amorphous sulfathiazole, and in ternary systems containing sulfathiazole forms I, III, and V.[19] Since the spectra do not show a single relatively intense peak that is characteristic of each polymorph the chemometric method is likely be more successful than univariate techniques. Partial least squares analysis (PLS) was applied to two different ternary sample sets to the NIR regions of 6980 – 5800 cm^{-1} and 5130 – 4000 cm^{-1}. The first sample set focused on low content analysis of the sulfathiazole solid phases (Figure 4.10) (Table 4.2). The other sample set was designed to focus on the analysis of sample through the whole range (0-100%) of content between form I, form III, and the amorphous phase (Figure 4.11) (Table 4.3). As with the binary analysis, many external factors can interfere with the spectra creating background noise, and reducing the accuracy of the data obtained. For solid samples the systematic variation is due to, among others factors, light scattering and differences in path length and may often constitute a major part in the variation of the sample spectra. Because of this pre-processing of the data is needed. Pre-treatment of the data shows an improvement in the calibration models throughout the study. As with all ternary systems, the component that produces the most varied spectrum is the most distinguishable, and will be the easiest to quantify. This is observed throughout both ternary data sets, where calibration models quantifying form III show a greater accuracy with a lower RMSEC, RMSECV, RMSEP, and LOD.

Due to each pre-treatment having an effect on the accuracy in quantifying all components used in ternary analysis it is difficult to determine the best model. Where some pre-treatments may increase the sensitivity of one component, it may mask another lowering the detection of the other component. This is observed in the whole content ternary analysis of forms I, III, and the amorphous phase, where the best LOD results for the amorphous phase and form I is obtained using a combined pre-treatments of SNV and the 1st derivative (LOD of 1.48% and 1.88% respectively). Whereas the best pre-treatment used

for the detection of form III is SNV, having a LOD of 0.386%. This also seen in the low content ternary analysis, where the best pre-treatments used for the detection of form III was the 2nd derivative of raw data (LOD of 0.56%). Whereas the best pre-treatment for the amorphous phase and form I was obtained using MSC data, having a LOD of 1.09% and 4.98% respectively. This can make choosing the best model task dependent, and at the user's discretion. Because many of the transformations in this study include 3 components, the whole content ternary analysis was chosen using the model that gave the lowest LOD average of all 3 components. This was SNV combined with the 1st derivative, having a LOD of 1.48% for the amorphous phase, 1.88% for form I, and 1.47% for form III.

Amorphous					
Pre-treatment	**Loadings**	**RMSEC (%)**	**RMSECV (%)**	**RMSEP (%)**	**LOD (%)**
Raw data	5	1.864	3.929	3.395	2.768
Raw data, 1st derivative	2	2.915	3.954	2.589	4.084
Raw data, 2nd derivative	3	2.813	4.891	2.903	2.837
SNV	4	1.82	2.873	3.277	1.163
SNV, 1st derivative	2	2.67	3.565	2.245	1.478
SNV, 2nd derivative	2	3.405	4.910	3.106	1.673
MSC	4	1.818	2.886	3.453	1.091
MSC, 1st derivative	3	2.251	3.690	2.330	1.343
MSC, 2nd derivative	2	3.785	5.595	3.498	1.131

Form I					
Pre-treatment	**Loadings**	**RMSEC (%)**	**RMSECV (%)**	**RMSEP (%)**	**LOD (%)**
Raw data	5	1.421	3.516	2.697	5.995
Raw data, 1st derivative	2	2.363	3.078	1.735	7.817
Raw data, 2nd derivative	3	2.810	4.341	2.008	8.613
SNV	4	1.268	3.169	2.974	5.437
SNV, 1st derivative	2	2.111	2.922	2.024	7.353
SNV, 2nd derivative	2	2.611	3.855	2.1065	6.484
MSC	4	1.247	2.857	2.910	4.984
MSC, 1st derivative	3	2.139	4.394	2.228	7.214
MSC, 2nd derivative	2	2.757	4.100	2.1346	6.395

From III (Commercial)					
Pre-treatment	**Loadings**	**RMSEC (%)**	**RMSECV (%)**	**RMSEP (%)**	**LOD (%)**
Raw data	5	1.254	3.130	2.233	0.747
Raw data, 1st derivative	2	1.529	2.087	2.297	0.761
Raw data, 2nd derivative	3	1.448	2.622	2.281	0.555
SNV	4	1.293	2.956	1.159	1.162
SNV, 1st derivative	2	1.616	2.169	1.947	3.845
SNV, 2nd derivative	2	1.800	2.368	2.144	4.458
MSC	4	1.391	3.205	1.309	1.357
MSC, 1st derivative	3	1.378	2.550	1.443	1.764
MSC, 2nd derivative	2	2.106	2.935	2.586	5.567

Table 4.2 Results of low content ternary analysis using different pre-processed NIR data

Amorphous					
Pre-treatment	**Loadings**	**RMSEC (%)**	**RMSECV (%)**	**RMSEP (%)**	**LOD (%)**
Raw data	4	3.159	4.101	4.1723	3.453
Raw data, 1st derivative	3	2.83	3.565	2.340	4.285
Raw data, 2nd derivative	2	3.373	3.844	2.696	3.507
SNV	2	2.975	3.474	2.319	6.800
SNV, 1st derivative	3	2.528	3.495	2.271	1.481
SNV, 2nd derivative	2	3.447	4.056	2.210	2.740
MSC	2	3.032	3.842	2.588	6.803
MSC, 1st derivative	3	2.521	3.737	1.669	1.580
MSC, 2nd derivative	2	3.479	4.106	2.0536	2.411

Form I					
Pre-treatment	**Loadings**	**RMSEC (%)**	**RMSECV (%)**	**RMSEP (%)**	**LOD (%)**
Raw data	4	2.66	3.490	2.647	9.257
Raw data, 1st derivative	3	2.043	2.448	1.589	9.632
Raw data, 2nd derivative	2	2.389	2.736	1.842	11.254
SNV	2	2.517	2.909	1.887	2.174
SNV, 1st derivative	2	2.080	2.925	1.806	1.877
SNV, 2nd derivative	2	3.242	3.841	1.598	3.112
MSC	2	2.676	3.086	1.992	1.776
MSC, 1st derivative	3	1.860	3.355	1.232	3.212
MSC, 2nd derivative	2	3.251	3.864	1.574	2.969

Form III (Commercial)					
Pre-treatment	**Loadings**	**RMSEC (%)**	**RMSECV (%)**	**RMSEP (%)**	**LOD (%)**
Raw data	4	1.967	2.704	2.41	4.309
Raw data, 1st derivative	3	1.972	2.515963	2.41	5.590
Raw data, 2nd derivative	2	2.120	2.41836	2.065	8.719
SNV	2	1.911	2.564	2.303	0.386
SNV, 1st derivative	2	1.905	2.245	2.305	1.473
SNV, 2nd derivative	2	1.313	1.484	1.897	1.726
MSC	2	1.958	2.233	2.353	0.530
MSC, 1st derivative	3	1.542	1.770	2.266	1.22
MSC, 2nd derivative	2	1.427	1.607	1.874	1.89

Table 4.3 Results of whole content ternary analysis using different pre-processed NIR data

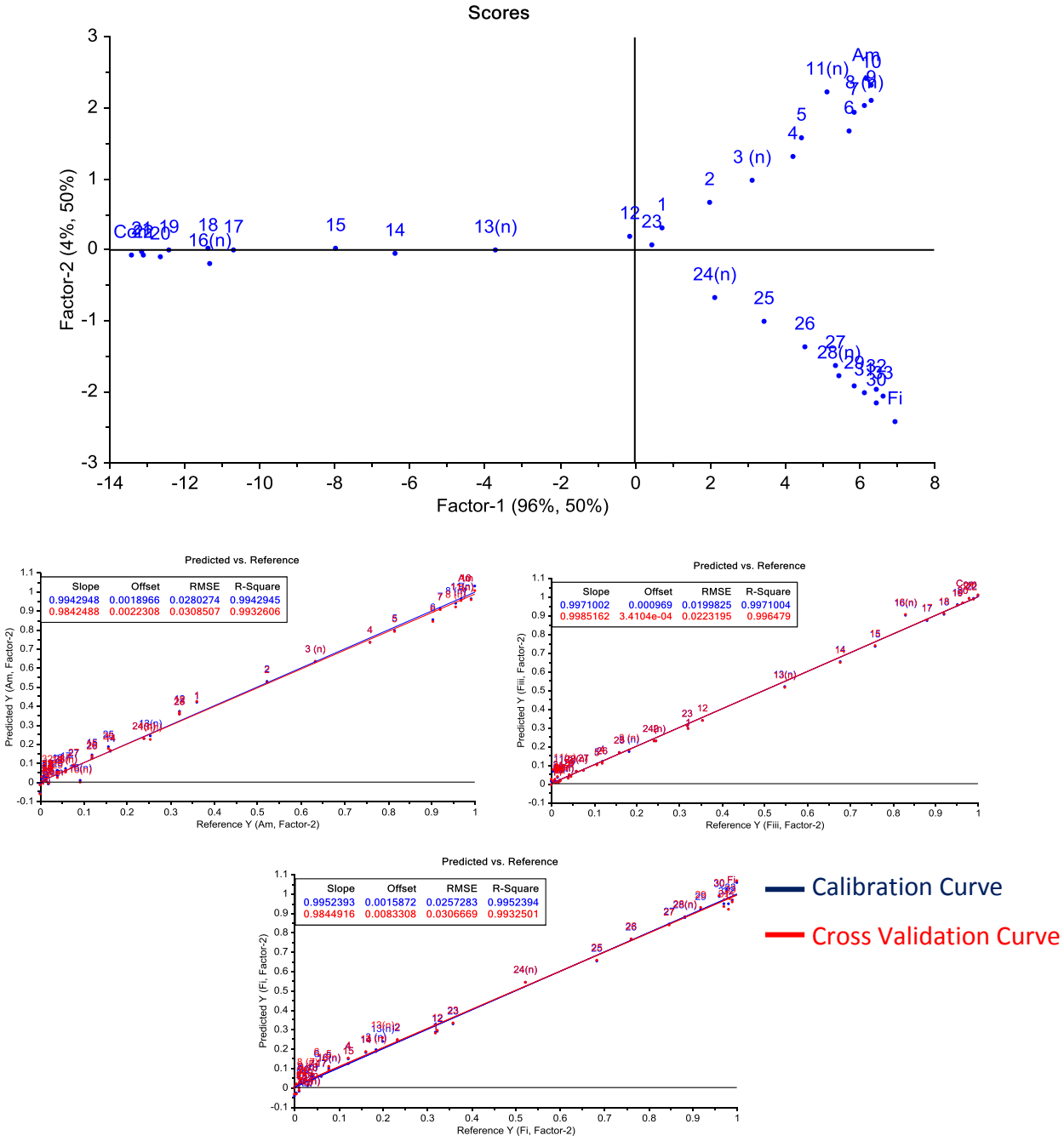

Fig. 4.10 PLS analysis of low content ternary mixtures pre-treated using SNV, showing the score plot (a) and calibration plots for forms I (b), III (c), and the amorphous phase (d)

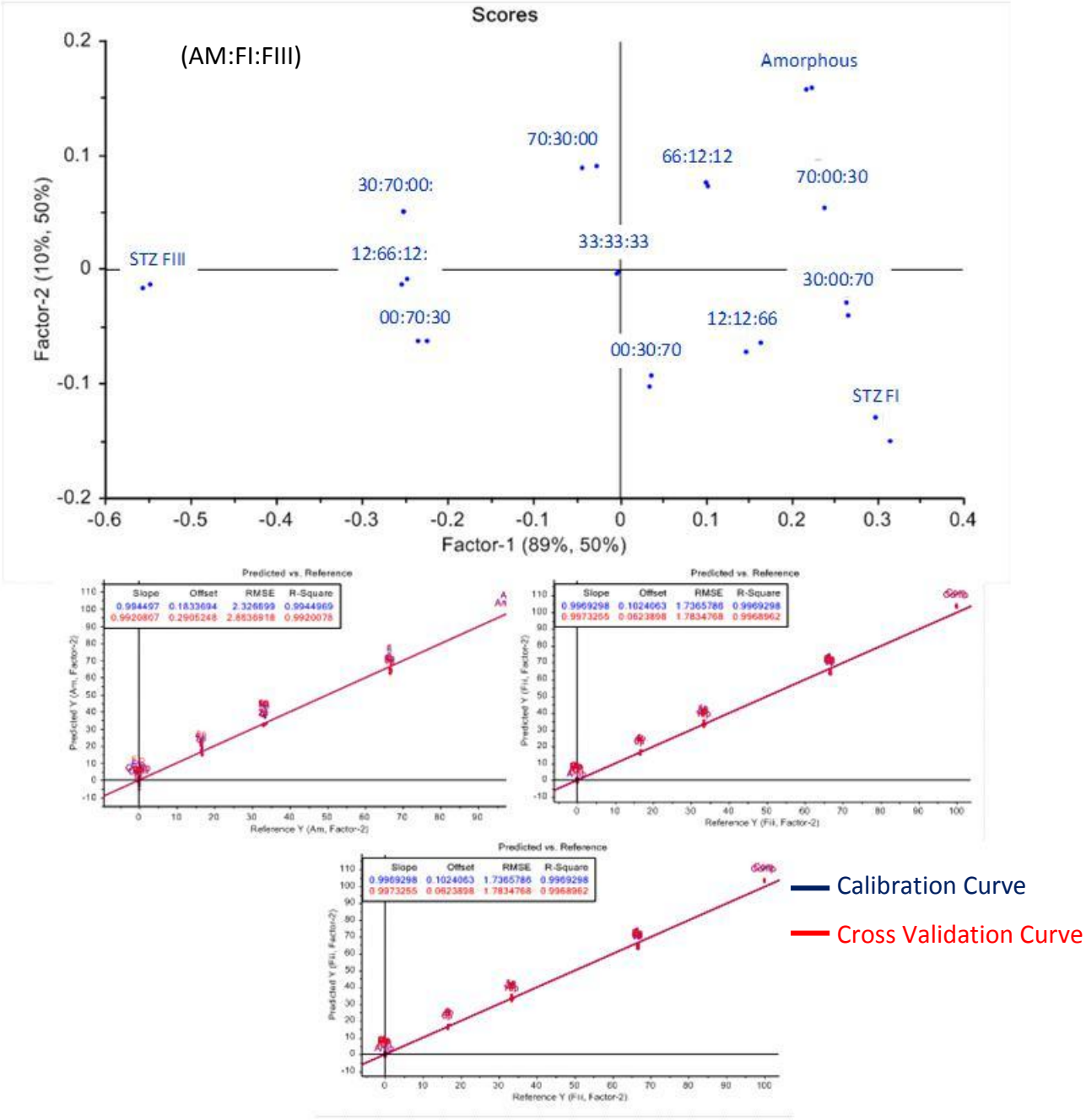

Fig. 4.11 PLS analysis of whole content ternary mixtures pre-treated using SNV, showing the score plot (a) and calibration plots for forms I (b), III (c), and the amorphous phase (d)

Effect of cryo-milling on sulfathiazole forms I and III

XRPD is regarded as the gold standard method for determining the crystallinity of a sample. Since XRPD patterns of amorphous materials usually exhibit a diffuse halo without observable sharp peaks it was chosen as the leading method to monitor the amorphisation of sulfamerazine. The XRPD patterns of the cryo-milled sulfathiazole polymorphs forms I and III at various milling times are shown in figure 4.12. The 2θ peaks at 10.9°, 16.0°, 17.7°, 18.9°, 20.9° and 22.0° are specific to form I, while peaks at 15.4°, and 22.2° are specific to form III. The XRPD patterns of both forms showed a rapid decrease in the diffraction peak intensities within the first 30 minutes of milling. The diffraction peaks of form III disappeared after 150 minutes, while in the case of form I, amorphisation was complete after 45 minutes. Thus cryo-milling of both forms led to amorphous materials as observed by XRPD. No polymorphic conversion was observed during cryo-milling of forms I and III for up to 180 minutes. This suggested that the transformation from crystalline material to the amorphous phase was direct. The NIR spectra of the sulfathiazole polymorphs measured after various milling times are shown in figure 4.13. The changes observed in the NIR spectra were in agreement with the XRPD results. In the NIR spectra of form III the intensities of the bands around 6410, 6370, 4916, and 4900 cm^{-1} which are specific to form III decreased during milling. At the same time bands at 6890, 6680, 5070, 5010 and 4530 cm^{-1} that are indicative of amorphous sulfathiazole increased in intensity. It is noted that the decreasing intensity of NIR bands around 6410 and 6370 cm^{-1} is a good indication of crystallinity decrease for sulfathiazole form III. The NIR spectrum of amorphous sulfathiazole is similar to that of form I. Nevertheless, the conversion of form I into the amorphous phase could be monitored by a general broadening of NIR bands and the disappearance of the peaks at 6152, 6104, 5080, 4900 and 4690 cm^{-1}. The bands in the spectrum of amorphous sulfathiazole are broader than those of crystalline samples due to the greater range of molecular environments that are available in the amorphous state.

The milling time for the amorphisation via milling of many pharmaceuticals such as indomethacin is independent of its polymorphic form.[108] Other pharmaceuticals such ranitidine hydrochloride (form 1 and form 2) show a slight dependence on the starting polymorph.[109] It has also been suggested that the ease of milling crystalline powders to an

amorphous form should be strongly related to molecular volume and the glass transition temperature (T_g). The latter is expected to be directly related to lattice energy.[96] It is difficult to compare the molecular volumes and densities of the indomethacin polymorphs as those reported on the Cambridge data base have all been measured at different temperatures. However in agreement with prediction forms I and II of ranitidine hydrochloride have molecular volumes of 437.8 and 437.7 $Å^3$ respectively and indistinguishable densities of 1.33 $Mg.m^{-3}$. On the other hand the very different results reported here for sulfathiazole are also in agreement with prediction as sulfathiazole forms I and III have molecular volumes of 169.5 and 162.4 $Å^3$ and lattice energies of -24.6 and - 24.75 $kcal.mol^{-1}$ respectively.[81] Recent work has suggested that fully amorphous sulfathiazole was difficult to obtain either by extended milling times at room temperature or by spray drying methods.[110] This body of work demonstrates the advantages of lower temperature milling (cryo-milling). The T_g of melt-quenched sulfathiazole and of cryo-milled form III have been reported to be 62.0 and 55.8°C, respectively,[90, 106] and we have measured *T*g for form I to be 54.7 °C.

Though the low content focused ternary analysis gave better results, the whole content focused PLS ternary models were used to follow the transformation of forms I and III during cryo-milling. This was to give a truer interpretation in the transformation that occurred in the cryo-milling of sulfathiazole polymorphs. Because the cryo-milling of both forms showed no transition to other polymorphs, the time profile data was confirmed using binary analysis. From the time profiles in figure 4.14, it can be clearly seen that the transformation to the amorphous phase of sulfathiazole is dependent on the polymorph used as a starting material.

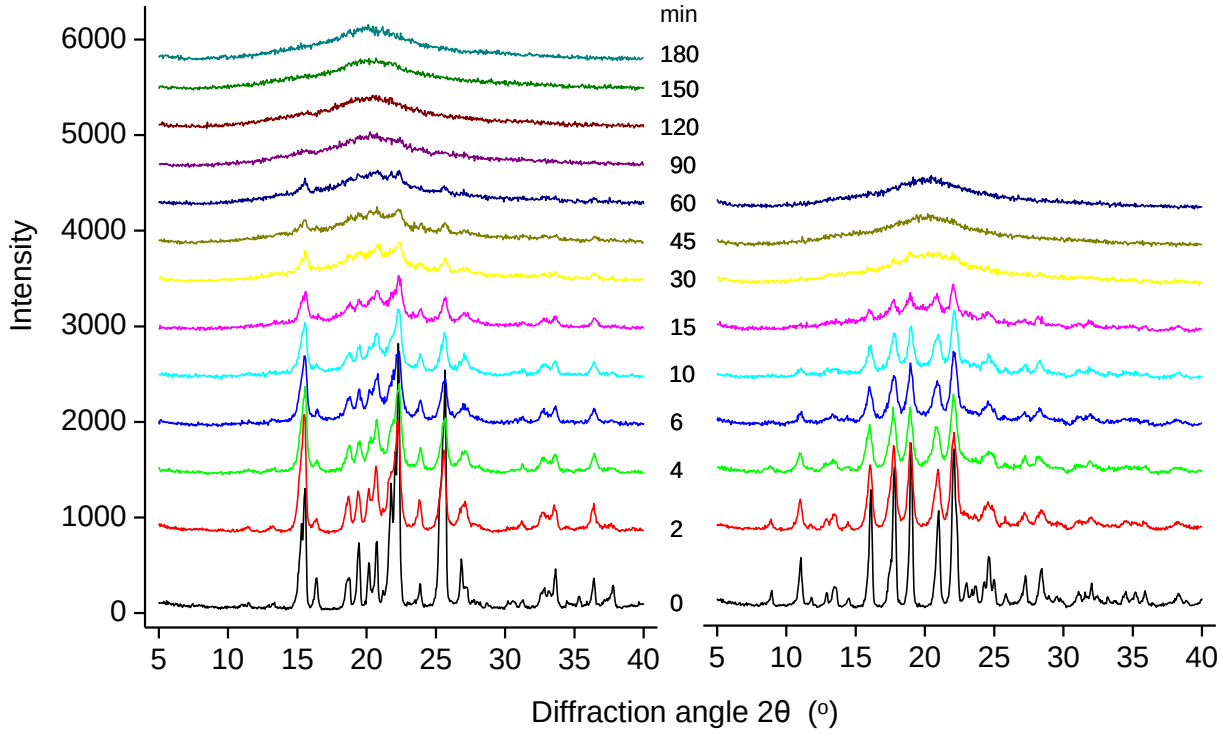

Fig. 4.12 XRPD patterns showing the amorphisation of FI (left) and FIII (right) via cryo-milling

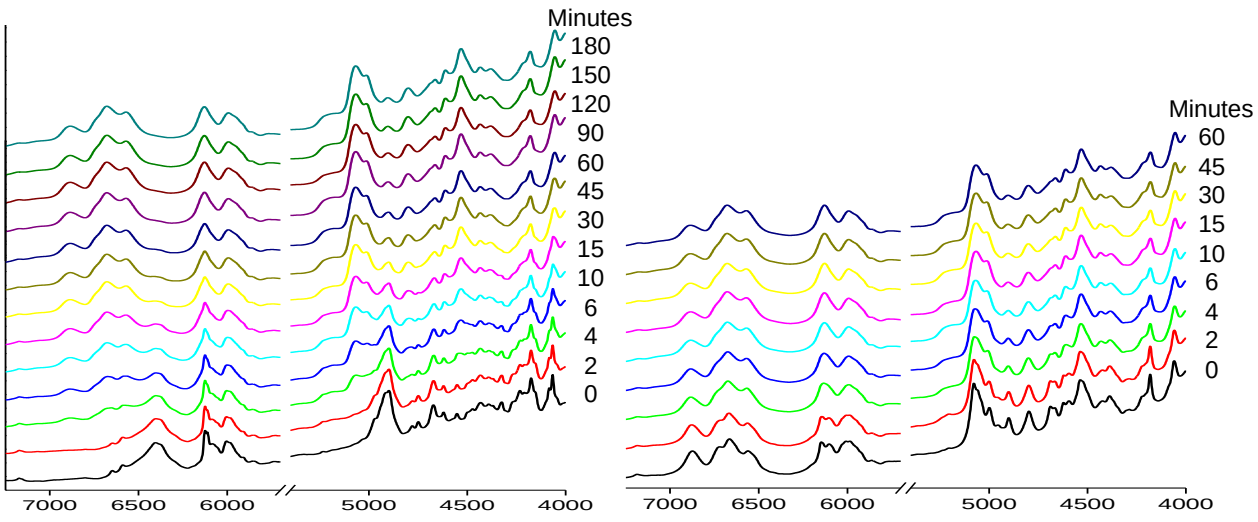

Fig. 4.13 NIR spectra showing the amorphisation of FI (left) and FIII (right) via cryo-milling

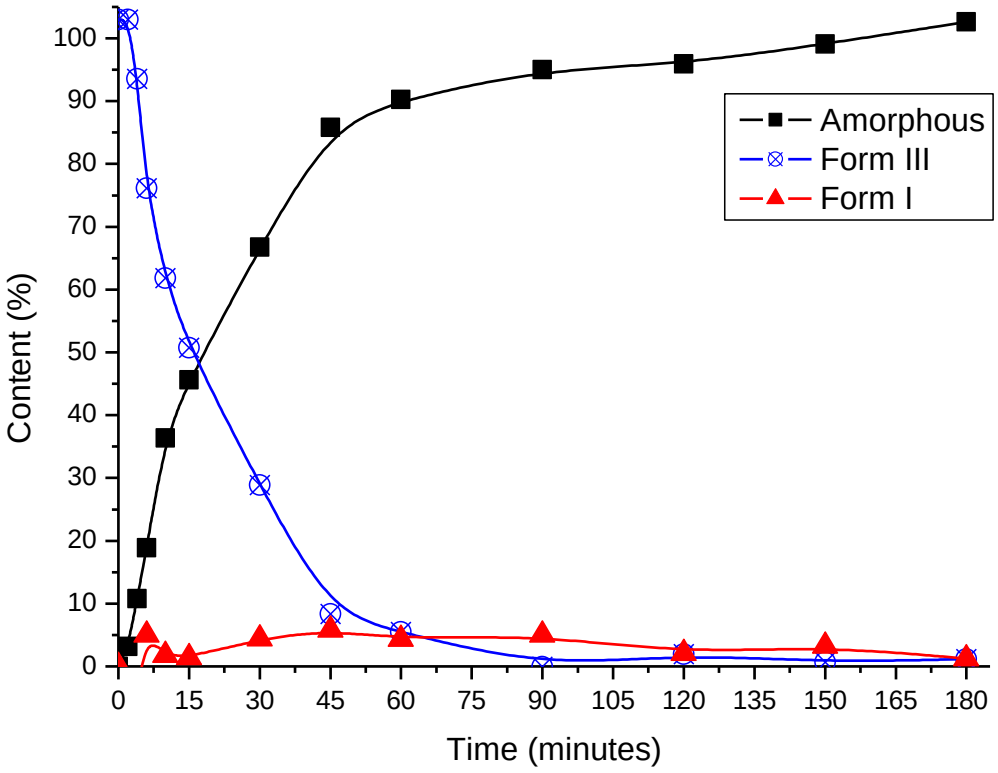

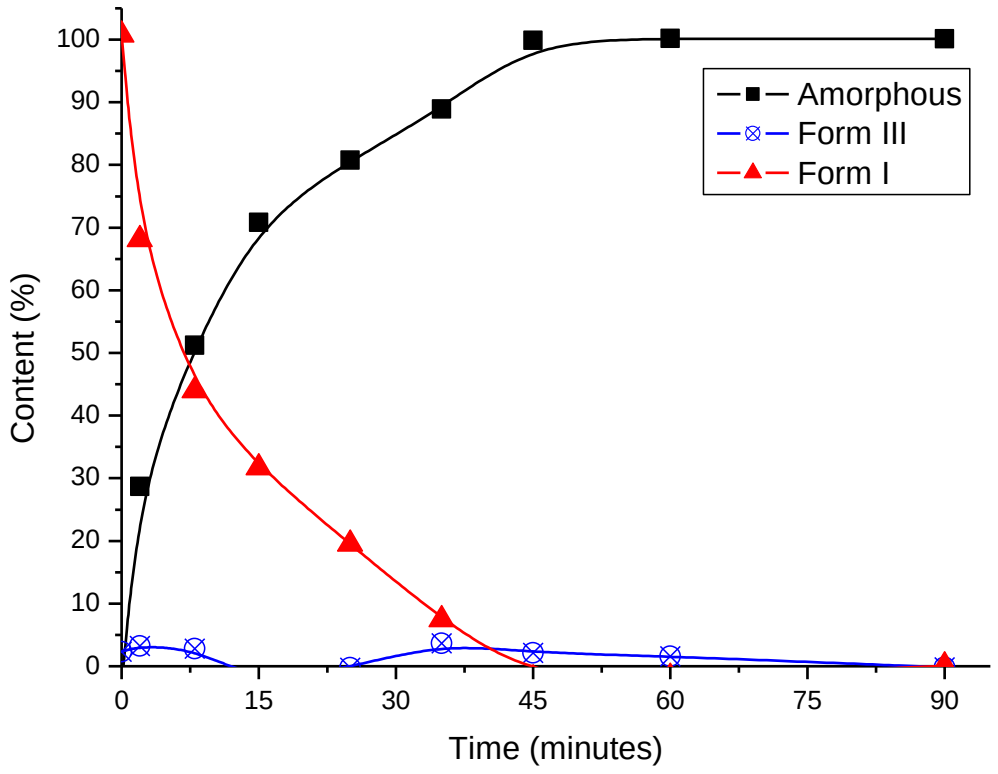

Fig. 4.14 Solid-state form composition of amorphous SMZ samples prepared by cryomilling FIII (top) and FI (bottom) *vs.* time cryo-milled

The effects of cryo-milling on both forms I and III were also examined using SEM (Figure 4.15). The particle surface can be clearly observed as rough and distorted granules with uniform particle sizes.

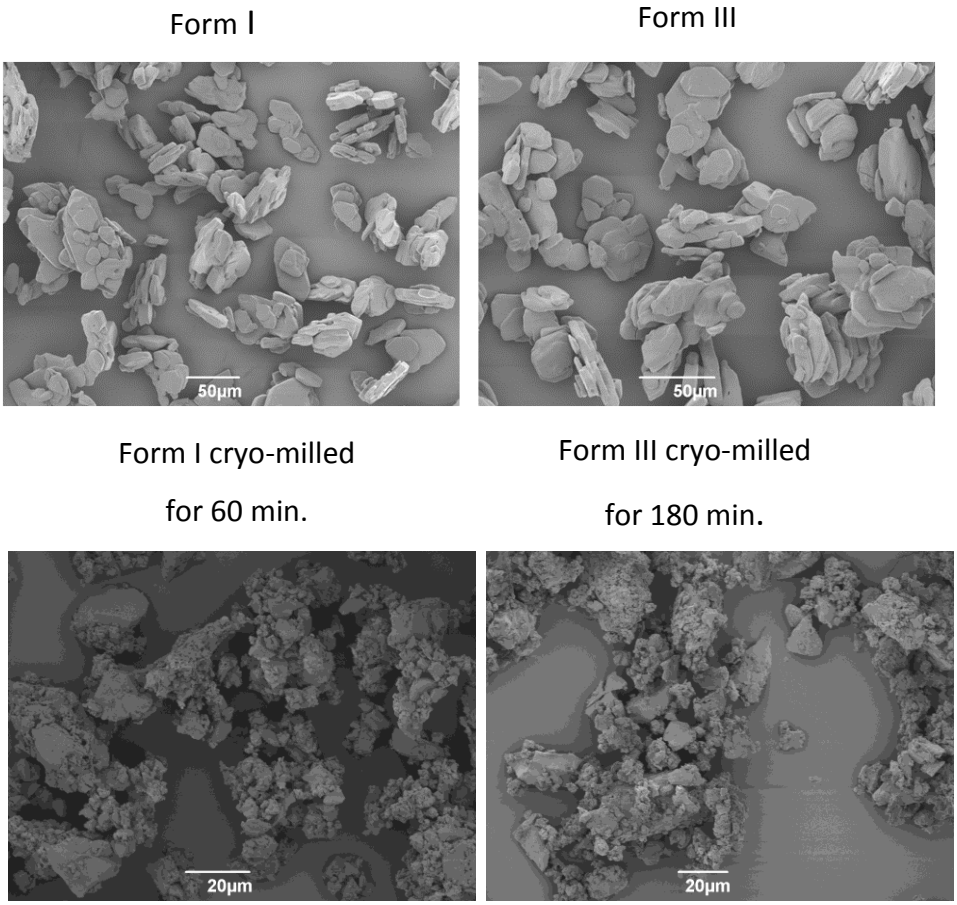

Fig. 4.15 SEM images of FI and FIII before and after cryo-milling

The stability of the amorphous phase of sulfathiazole was examined by the postdoctoral researcher Yun Hu. This was done by storing the samples under vacuum over silica gel at 4°C and 22°C and at 22°C in a humidity chamber at 35% RH. Here samples of the amorphous phase showed no signs of crystallinity to just over 14 days, when stored under vacuum at 4^{o}C. This is an increase in shelf-life, where samples of the amorphous phase stored on bench overnight have signs of crystallisation (Figure 4.16). After 14 days the sample would crystallise to a polymorphic mixture of forms I and III. It was also shown that Form I samples milled for 30 minutes and stored at 4°C for 14 days showed some crystallisation back to form I with characteristic 2θ peaks at 16.0, 17.7, and 18.9° (Figure 4.17). However, form I samples cryo-milled for 45 and 60 minutes remained amorphous

when stored at 4°C. It thus appears that in the case of form I when dislocation is less complete after 30 minutes cryo-milling time the ordered material present has a catalytic effect on recrystallisation. In contrast, amorphous samples prepared by cryo-milling both forms showed considerable recrystallisation when stored for 14 days at 22°C under vacuum. The cryo-milled form I sample was found to have mostly crystallized back to form I, while amorphous prepared from form III samples had partially recrystallised back to the mixtures of forms II and III with a small amount of form I.

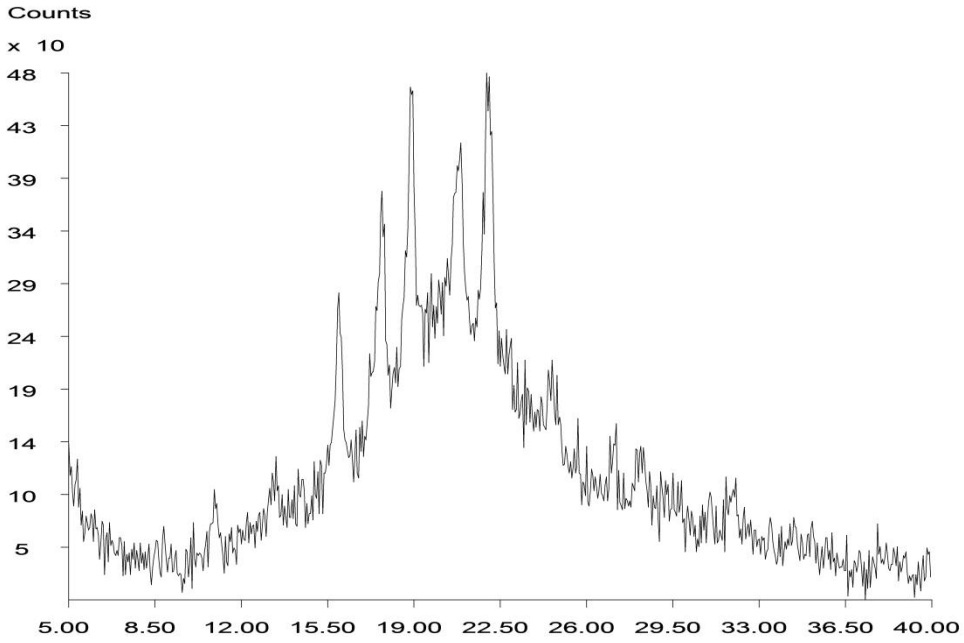

Fig. 4.16 Samples of amorphous sulfathiazole (Form I cryo-milled for 60 minute) stored on bench overnight

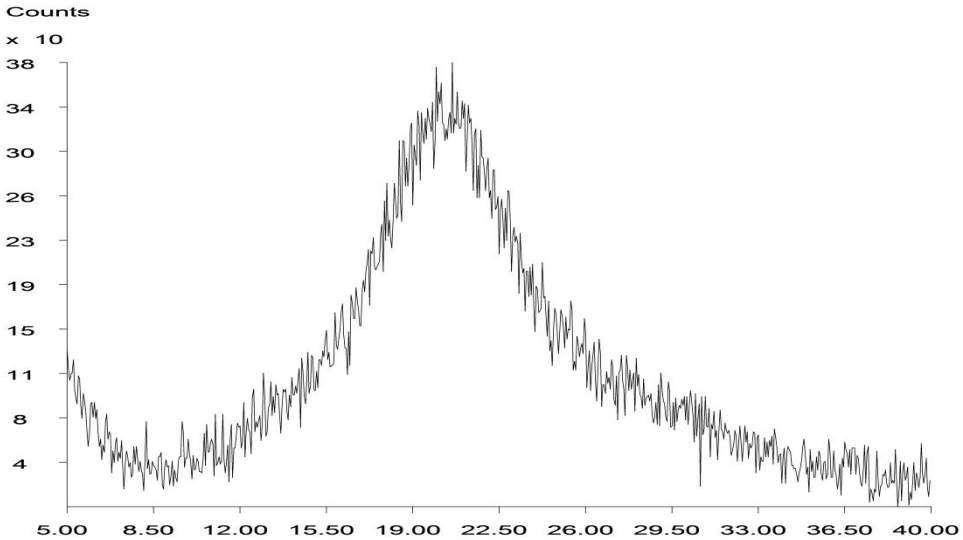

Fig. 4.17 Samples of amorphous sulfathiazole (Form I cryo-milled for 60 minute) stored at under vacuum 4^{o}C after 14 days

However, the powder patterns of forms III and IV are very similar and the presence of some form IV cannot be excluded. It is interesting that the starting crystal form affected the physical stability of cryo-milled amorphous materials. Because of the possible crystallisation of forms II and IV from the amorphous phase, the multivariate binary and ternary analysis cannot be used to monitor the shelf life of the amorphous sulfathiazole, and its crystallisation. The recrystallisation of an amorphised fraction can occur towards the starting form or towards another polymorph which is kinetically easier to reach.[111] Thus while amorphous samples may have an intrinsic tendency to crystallise back to the initial state because of the presence of residual crystalline particles of the starting form spontaneous or catalysed crystallisation to other more stable forms is also possible. The relative thermodynamic stability of sulfathiazole polymorphs has been proposed to be III ≈ IV > II > I.[45, 90] Therefore according to Ostwald's Rule of Stages, amorphous sulfathiazole should initially produce form I as it is the least stable form, followed by a stepwise conversion, through the other metastable forms, to the thermodynamically most stable form.[112]

Other reports of the recrystallisation behaviour of amorphous forms produced by milling vary. For example Chieng et al.[109] have reported the spontaneous recrystallisation of amorphous ranitidine hydrochloride back to the original crystal form only, but that seeding with a different form could induce crystallisation of that form, and Crowley and Zografi,[108] who examined the recrystallisation of amorphous indomethacin reported results that are similar to those reported here for sulfathiazole. Amorphous solids often readily absorb moisture. It is well established that water and other solvents absorbed by an amorphous solid lowers the T_g of the solid, thus acting as plasticizers and increasing molecular mobility and recrystallisation rates.[108, 113] The behaviour of amorphous samples stored under 35% RH at 22^{o}C for 7 days was also investigated. We tried to measure the T_g of the amorphous samples prepared from both forms after equilibration at 35% RH for 3 hours (Figure 4.18). However, it is difficult to disern a T_g from the DSC for the amorphous samples due to the overlap with the recrystallisation exotherms. The water content of the amorphous samples was determined by TGA to be between 1.28 to 1.34%. The rapid absorption of water is evident from the water peaks around 7070 and 5200 cm^{-1} in the NIR spectra.[50, 51]

Furthermore, it was observed that the absorbed water promoted crystallisation. Even more importantly, it was also found that the composition of the resulting crystalline material was not the same as for samples stored under vacuum. It was found that from amorphous samples prepared from form I crystallised into the mixtures of forms II and III/IV with very small amounts of form I, while that from form III crystallised into the mixtures of forms I, II and III. As already discussed above, XRPD does not distinguish forms III and IV in mixtures. It is also difficult to distinguish these two polymorphs using NIR spectroscopy, as their spectra are quite similar.[89] Therefore III/IV is used to indicate that some form IV may be present in mixtures containing form III. The relative amount of form I is much lower in the milled form I samples, and higher in the milled form III samples compared to that of samples stored under vacuum over silica gel, as shown by the intensity of the XPRD 2θ peaks at 17.7 and 18.9 and the shift in the band around 6900 cm^{-1} to 6878 cm^{-1} and the intensity changes to the peak at 5080 cm^{-1} in the NIR spectra. This is also in agreement with a recent report which described the effect of relative humidity on amorphous sulfathiazole prepared by spray drying.[114]

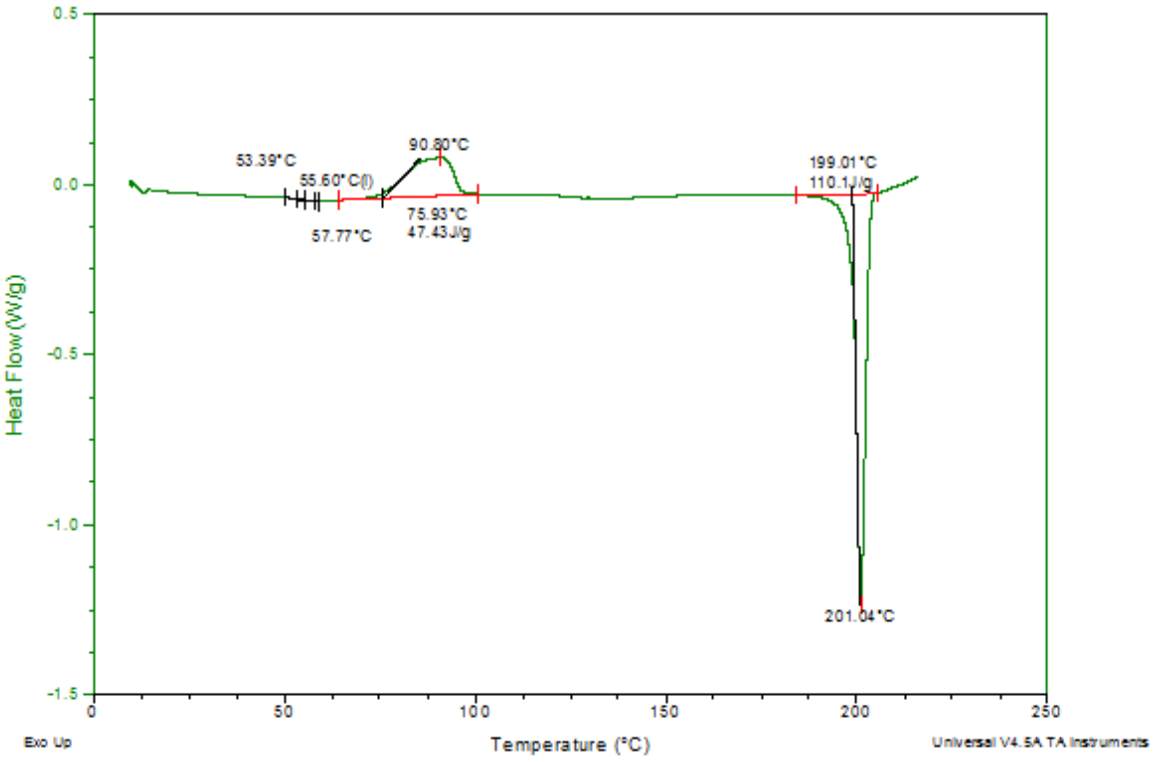

Fig. 4.18 DSC of amorphous sulfathiazole

Discussion

Cryo-milling was found to be an effective method of preparing the amorphous sulfathiazole without degradation (as seen in the melt quench method). The pure samples of the amorphous phase were used to create calibration models, giving a novel method to analyse the transformation between different sulfathiazole polymorphs during cryo-milling. Calibration models also allowed a successful comparison of different analytical techniques such as XRPD, NIR and IR spectroscopy for whole content and low content analysis.

Chapter Five

Conclusions

Sulfamerazine

The full transformation to the amorphous phase of sulfamerazine (FA) has been successfully completed for the first time via the melt quench method and by cryo-milling of both FI and FII (22.5 and 120 minutes respectively). FA prepared using FI as a starting material was found to be more stable than that using FII.

The availability of sufficient sample of pure amorphous phase of sulfamerazine provided the opportunity to instigate a novel study into FA stability and crystallisation. From the stability studies of FA prepared from cryo-milling FI at different times, it was found that the cryo-milling time has an effect on the recrystallisation of FA. Here it was found that samples cryo-milled for less than 60 minutes recrystallise to polymorphic mixtures of FI and FII, whereas samples cryo-milled for 60 minutes or longer recrystallise exclusively to FII. Though storage temperature played a role in the shelf life of FA, with shelf life increasing from hours at room temperature storage to days at 4^{o}C storage, storage temperature had no effect on the crystallisation pathway of FA. Using the pure samples of FA, FI and FII binary and ternary mixtures were prepared to create regression models for novel multivariate analysis. In the binary analysis LOD values ranged from 0.530% to 6.712% and for ternary analysis the LOD values ranged from 0.682% to 6.152%. The ternary regression model was successfully used to create novel time profiles illustrating the recrystallisation of FA, and the solid state transformations that occur to FI and FII during the room temperature and cryo-milling processes.

Sulfathiazole

Low level calibration models were able to detect and quantify different polymorphs of sulfathiazole. In these calibration models, binary mixtures of all known sulfathiazole polymorphs that could be obtained in pure polymorphic form were used. To the best of our knowledge, calibration models for binary mixtures of forms I / V and forms III / V or for low levels of form III in form I have not been previously described. Low levels of sulfathiazole

forms I, III and V in binary mixtures can be accurately quantified by NIR spectroscopy coupled with chemometrics, with LOD and LOQ values ranging from 0.4%–1.5% and 1.1–4.6%, respectively. However, careful selection of analytically useful data regions is required. Although satisfactory models could be developed for the low content quantification by XRPD, it is clear that NIR spectroscopy exhibits higher accuracy on the basis of RMSE values except for the determination of low levels of form I in I / V mixtures, where the XRPD method gave slightly lower RMSE values. Furthermore, NIR spectroscopy gives significantly lower LOD and LOQ values than XRPD. Combined with the convenient "in glass bottle" sampling method, the present results provide further justification of the effectiveness of NIR spectroscopy for polymorph analysis.

For the first time commercial sulfathiazole (form III) and prepared form I could be made fully amorphous by cryo-milling for 150 and 45minutes, respectively, as determined using the NIR chemometric approach with a ternary analysis model. No transformation between forms I and III observed during the cryo-milling process. It was found that the recrystallisation of the amorphous phase that was prepared from form III and kept under vacuum at room temperature was more complex than that of amorphous sulfathiazole obtained from form I. Moisture not only increased the crystallisation rates of amorphous sulfathiazole, but also gave similar polymorphic mixtures for both samples. The crystallisation of amorphous sulfathiazole obeys Ostwald's rule more effectively in the presence of moisture. NIR spectroscopy combined with multivariate methods allowed novel analysis allowing the detection and quantification of the crystalline disorder generated by cryo-milling of both sulfathiazole forms I and III.

Throughout this work NIR has shown great accuracy and sensitivity in detecting changes to the solid phases of the different polymorphs of both sulfa-drugs (sulfamerazine and sulfathiazole). This was able to be done 'in bottle', reducing environmental exposure to samples. This allowed the generation of accurate calibration models that were successfully used to give further insight into their solid state transformations. A PLS method was used to process the NIR spectroscopic data to create calibration models. This allowed the simultaneous quantification of multiple components throughout the experiments. It also allowed spectroscopic data to be pre-treated which was found to greatly increase the accuracy of the calibration models. To summarise, NIR spectroscopy coupled with

chemometrics gives an accurate and detailed insight to the solid state transformations of sulfathiazole and sulfamerazine.

Electronic information

Disc contains the calibration models used throughout this work.

References

1. Roy, S.; Alexander, K. S.; Riga, A. T.; Chatterjee, K. *J. of Pharm. Sci.* **2003,** 92, (4), 747-759.
2. Hu, Y.; Macfhionnghaile, P.; Caron, V.; Tajber, L.; Healy, A. M.; Erxleben, A.; McArdle, P. *J. of Pharm. Sci.* **2013,** 102, (1), 93.
3. Chattoraj, S.; Bhugra, C.; Telang, C.; Zhong, L.; Wang, Z.; Sun, C. C. *Pharm. Res.* **2012,** 29, (4), 1020.
4. Zhang, G. G. Z.; Gu, C.; Zell, M. T.; Burkhardt, R. T.; Munson, E. J.; Grant, D. J. W. *J. Pharm. Sci.* **2002,** 91, (4), 1089.
5. Beckmann, W. *Eng. Life Sci.* **2003,** 3, (3), 113.
6. Bauer, J.; Spanton, S.; Henry, R.; Quick, J.; Dziki, W.; Porter, W.; Morris, J. *Pharm.Res.* **2001,** 18, (6), 859.
7. Larsen, S.; Hansen, E. T.; Hoffmeyer, L.; Rastrup-Andersen, N. *Acta Crystallogr. n. Sect. C* **1993,** 49, (12), 2184.
8. Hansen, E.; Rastrup Andersen, N.; Ringborg, L. H. *EP0679154 B1* **1995**.
9. Malvina, O.; Christos, K. Identification and Stability of Calcipotriol Pseudopolymorphs in Pharmaceutical Creams. *Essay* **2001**
10. McCrone, W. *Physics and Chemistry of the Organic Solid State* **1965,** 2, 725.
11. Chikhalia, V.; Forbes, R. T.; Storey, R. A.; Ticehurst, M. *Euro. J. of Pharm. Sci* **2006,** 27, (1), 19.
12. Yu, L. *Acc. of Chem. Res.* **2010,** 43, (9), 1257.
13. Chan, H. K.; Doelker, E. *Drug Dev. and Indt. Pharm.* **1985,** 11, (2-3), 315.
14. Haleblian, J.; McCrone, W. *J. of Pharm. Sci* **1969,** 58, (8), 911.
15. Mitscherlich, E. *Ann. Chem. Physiq.* **1822,** 19, 350.
16. Santen, R. A. *J. Phys. Chem.* **1984,** 88, 5768.
17. Ostwald, W. *Zeit. für Phys. Chem.* **1897,** 22, 289.
18. Févotte G., Calas J., Puel F., Hoff C. *Int. J. Pharm* **2004** 273 (1-2), 159-169,
19. Hu, Y.; Erxleben, A.; Ryder, A. G.; McArdle, P. *J. of Pharm. Sci and Biomed. Anal.* **2010,** 53, (3), 412.
20. Chalus, P.; Roggo, Y.; Walter, S.; Ulmschneider, M. *Talanta.* **2005**, 1294.
21. Roggo, Y.; Chalus, P.; Maurer, L.; Lema-Martinez, C.; Edmond, A.; Jent, N. *J. of Pharm. Sci and Biomed. Anal.* **2007,** 44, (3), 683.
22. Markovich, R.; Pidgeon, C. *Pharma. Res.* **1991,** 8, (6), 663.
23. Hennigan, M. C.; Ryder, A. G. *J. of Pharm. Sci and Biomed. Anal.* **2013,** 72, (0), 163.
24. Li, Y.; Chow, P. S.; Tan, R. B. *Int.J. of Pharm.* **2011,** 415, (1-2), 110.
25. Craig, D. Q. M., Characterization of Polymorphic Systems Using Thermal Analysis. In Polymorphism, Wiley-VCH Verlag GmbH & Co. KGaA: **2006**; 43.
26. Giron, D. *Thermo. Acta* **1995,** 248, 1.
27. Munroe, A.; Croker, D.; Rasmuson, A. C.; Hodnett, B. K. *Cryst. Eng.Comm.* **2011,** 13, (3), 831.
28. Yu, L.; Stephenson, G. A.; Mitchell, C. A.; Bunnell, C. A.; Snorek, S. V.; Bowyer, J. J.; Borchardt, T. B.; Stowell, J. G.; Byrn, S. R. *J. of Am. Chem. Soc.* **2000,** 122, (4), 585.
29. Barham, A. S.; Omar, A. M. E.; Roos, Y. H.; Hodnett, B. K. *Cryst. Gro. & Des.* **2006,** 6, (8), 1975.
30. De Jong, S. *J. of Chemometr.* **1990,** 4, (6), 441.
31. Sundberg, R. *Scand. J. of Stats.* **1999,** 26, (2), 161.
32. Pearson, K. *Philo. Mag. Ser. 6* **1901,** 2, (11), 559.
33. Helland, I. S. *Comm. in Stats. ; Sim. and Comp.* **1988,** 17, (2), 581.
34. Wentzell, P. D.; Vega Montoto, L. *Chemometr. and Intel. Lab. Sys.* **2003,** 65, (2), 257.
35. Wold, S.; Antti, H.; Lindgren, F.; Öhman, J. *Chemometr. and Intel. Lab. Sys.* **1998,** 44, (1–2), 175.
36. Savitzky, A.; Golay, M. J. E. *Anal. Chem.* **1964,** 36, (8), 1627.

37. Larive, C. K.; Sweedler, J. V. *Anal. Chem.* **2013,** 85, (9), 4201.
38. Dhanoa, M. S.; Lister, S. J.; Sanderson, R.; Barnes, R. J. *J.NIR Spec* **1994,** (2) 43
39. Li, W.; Worosila, G. D.; Wang, W.; Mascaro, T. *J. of Pharma Sci.* **2005,** 94, (12), 2800.
40. Press, E.; Kennerstein, M. *Arch. of Disease. in Child.* **1943,** 18, (93), 50.
41. Lesch, J. E. *Oxford univrsity Press* **2007**, 51
42 McArdle, P.; Gilligan, K.; Cunningham, D.; Dark, R.; Mahon, M. *Cryst Eng Comm* **2004,** 6, (53), 303
43. Gong, Y.; Collman, B. M.; Mehrens, S. M.; Lu, E.; Miller, J. M.; Blackburn, A.; Grant, D. J. *J. of Pharm. Sci.* **2008,** 97, (6), 2130.
44. Anwar, J.; Tarling, S. E.; Barnes, P. *J. of Pharm. Sci.* **1989,** 78, (4), 337.
45. Chan, C. F.; Anwar, J.; R., C.; Barnes, P.; Wilson, R. M. *J. Appl. Cryst.* **1999,** 32, 436.
46. Apperley, D. C.; Fletton, R. A.; Harris, R. K.; Lancaster, R. W.; Tavener, S.; Threlfall, T. L. *J. of Pharm. Sci.* **1999,** 88, (12), 1275.
47. Macrae, C. F.; Bruno, I. J.; Chisholm, J. A.; Edgington, P. R.; McCabe, P.; Pidcock, E.; Rodriguez-Monge, L.; Taylor, R.; van de Streek, J.; Wood, P. A. *J. Appl. Cryst.* **2008,** 41, (2), 466.
48. Taylor, R.; Macrae, C. F. *Acta Crystallogr., n. Sect. B* **2001,** 57, (6), 815.
49. Chieng, N.; Rehder, S.; Saville, D.; Rades, T.; Aaltonen, J. . *J. of Pharm. and Biomed. Anal.* **2009,** 49, (1), 18.
50. Heinz, A.; Savolainen, M.; Rades, T.; Strachan, C. J. *Euro. J. of Pharm. Sci.* **2007,** 32, (3), 182.
51. Savolainen, M.; Jouppila, K.; Pajamo, O.; Christiansen, L.; Strachan, C.; Karjalainen, M.; Rantanen, J. *J. of Pharm. And Pharma.* **2007,** 59, (2), 9.
52. Farr, M. M.; Wehr, E. E. *J. of Parasit.* **1945,** 31, 353.
53. Forbes, G. B.; Perley, A.; Dehlinger, J. *J. of Pediac.* **1946,** 28, 24.
54. Lehr, D. *J. of the Am. Med. Ass.* **1948,** 137, (13), 1150.
55. McGee, J. C.; Priest, W. S. *J. of the Am. Med. Ass* **1948,** 137, (15), 1315.
56. Hossain, G. M. G. Acta Crystallogr. n. *Sect. E Struct. Rep. Online* **2006,** 62, (6), 2166.
57. Acharya, K. R.; Kuchela N. K., *J. of Crys. and Spec. Res.* **1982,** 12, (4), 10.
58. Caira, M. R.; Mohamed, R. *Acta Crystallogr. n. Sect. B: Struct. Sci.* **1992,** B48, (4), 492.
59. Deo, N.; Tiwari, R. K.; Singh, T. P. *J Sci Res* **1980,** 2, (2), 3.
60. Kawakami, K.; Asami, Y.; Takenoshita, I. *J. of Pharm. Sci.* **2010,** 99, (1), 76.
61. Kurotani, M.; Hirasawa, I. *Chem. Eng. Res. and Des.* **2010,** 88, (9), 1272.
62. Gu, C. H.; Young, V. J.; Grant, D. J. *J. of Pharm. Sci.* **2001,** 90, (11), 1878.
63. Lee, S.; Choi, A.; Kim, W.-S.; Myerson, A. S. *Cryst. Gro & Des.* **2011,** 11, (11), 5019.
64. Lee, M.-J.; Seo, D.-Y.; Wang, I.-C.; Chun, N.-H.; Lee, H.-E.; Jeong, M.-Y.; Kim, W.-S.; Choi, G. J. *J. of Pharm. Sci.* **2012,** 101, (4), 1578.
65. Sun, C.; Grant, D. J. *Pharma. Res.* **2001,** 18, (3), 274.
66. Blinc, R.; Seliger, J.; Zidansek, A.; Zagar, V.; Milia, F.; Robert, H. *ssNMR* **2006,** 30, (2), 61.
68. Cao, X.; Sun, C.; Thamann, T. J. *J. of Pharm. Sci.* **2005,** 94, (9), 1881.
69. Blagden, N. *Powder Tech.* **2001,** 121, 46.
70. Yu, L. *Adv. Drug Del. Rev.* **2001,** 48, (1), 27.
71. Otte, A.; Zhang, Y.; Carvajal, M. T.; Pinal, R. *Cryst. Eng. Comm.* **2012,** 14, (7), 2560.
72. Zhang, Y.; Pinal, R.; Carvajal, T. *Comm.* **2010,** Purdue University.
73. Fosbinder, R. J.; Walter, L. A. *J. of the Am. Chem. Soc.* **1939,** 61, (8), 2032.
74. Cooper, F. B.; Gross, P.; Hagan, M. L. *J. of Clinic. Invest.* **1942,** 21, (3), 281.
75. Swann, J. P. *PDA J. of Pharm. Sci.and Tech. / PDA* **1999,** 53, (3), 148.
76. Goodman, L.; Gillman, A. *New York: Macmillan* **1965**, 1145.
77. Durrett, J. *History Office Files, FDA* **1940,** 3.
78. Stockman, F.; Campbell, W.; Klumpp, T.; Kirk, J. *Hyak Report, AF 13191* **1941,** 4, (2), 7.
79. Olsen, O. L., G. *Hyak Report, AF 13191* **1942,** 6.
80. Bingham, A. L.; Hughes, D. S.; Hursthouse, M. B.; Lancaster, R. W.; Tavener, S.; Threlfall, T. L. *Chem. Comm.* **2001**, (7), 603.

81. McArdle, P.; Hu, Y.; Lyons, A.; Dark, R. *Cryst. Eng. Comm.* **2010,** 12, (10), 3119.
82. Abu Bakar, M. R.; Nagy, Z. K.; Rielly, C. D.; Dann, S. E. *Int. J. of Pharma.* **2011,** 414, (1–2), 86.
82. Blagden, N.; J. Davey, R.; F. Lieberman, H.; Williams, L.; Payne, R.; Roberts, R.; Rowe, R.; Docherty, R. *J. of the Chem. Soc. Fara. Tran.* **1998,** 94, (8), 1035.
84. Grove, D. C.; Keenan, G. L. *J. Am. Chem. Soc.* **1941,** 63, 97.
85. Miyazaki, H. *Jap. J. of Pharma. Chem.* **1947,** 19, 359-365.
86. Mesley, R. J. *J. of Phar. and Pharma.* **1971,** 23, (9), 687-694.
87. Hughes, D.; Hursthouse, M.; Lancaster, B.; Tavener, S.; Threlfall, T.; Turner, P. *Acta Crystallogr.,Sect. C* **1999,** 55, 1831.
88. Lagas, M.; Lrk, C. F. *Int. J. of Pharma.* **1981,** 8, (1), 11.
89. Zeitler, J. A.; Newnham, D. A.; Taday, P. F.; Threlfall, T. L.; Lancaster, R. W.; Berg, R. W.; Strachan, C. J.; Pepper, M.; Gordon, K. C.; Rades, T. *J of Pharma. Sci.* **2006,** 95, (11), 2486.
90. Parmar, M. M.; Khan, O.; Seton, L.; Ford, J. L. *Cryst. Gro. & Des.* **2007,** 7, (9), 1635.
91. Shakhtshneider, T. P.; Boldyrev, V. V. *Drug Dev. and Indt. Pharm.* **1993,** 19, (16), 2055.
92. Shakhtshneider, T. P.; Vasilchenko, M. A.; Politov, A. A.; Boldyrev, V. V. *J of Therm. Anal.* **1997,** 48, (3), 491.
93. Boldyrev, V. V.; Shakhtshneider, T. P.; Burleva, L. P.; Severtsev, V. A. . *Drug Dev. and Indt. Pharm* **1994,** 20, (6), 1103.
94. Aaltonen, J.; Rantanen, J.; Siiria, S.; Karjalainen, M.; Jørgensen, A.; Laitinen, N.; Savolainen, M.; Seitavuopio, P.; Louhi-Kultanen, M.; Yliruusi, J. *Anal. Chem.* **2003,** 75.
95. Kordikowski, A.; Shekunov, T.; York, P. *Pharm. Res.* **2001,** 18, (5), 682.
96. Lin, Y.; Cogdill, R. P.; Wildfong, P. L. *J. of Pharm. Sci.* **2009,** 98, (8), 2696.
97. Kruger, G. J.; Gafner, G.; *Acta Crystallogr, n. Sect. B* **1972,** 28, 272.
98. Kruger, G. J.; Gafner, G.; *Acta Crystallogr, n*. *Sect. B* **1971,** B27, 326.
99. Gelbrich, T.; Hughes, D. S.; Hursthouse, M. B.; Threlfall, T. L. *Cryst. Eng. Comm.* **2008,** 10, (10), 1328.
100. Patel, A. D.; Luner, P. E.; Kemper, M. S. *J. of Pharm. Sci.* **2001,** 90, (3), 360.
101. Höskuldsson, A. *Basic Theory, Vol. 1* **1996**.
102. Geladi, P.; Kowalski, B. R. *Anal. Chim. Acta* **1986,** 185, (0), 1.
103. Otsuka, M.; Kato, F.; Matsuda, Y. *Analyst* **2001,** 126, (9), 1578.
104. Rantanen, J.; Wikstrom, H.; Rhea, F. E.; Taylor, L. S. *App. Spec.* **2005,** 59, (7), 942.
105. Luner, P. E.; Majuru, S.; Seyer, J. J.; Kemper, M. S. *Pharm. Dev. and Tech.* **2000,** 5, (2), 231.
106. Pöllänen, K.; Häkkinen, A.; Huhtanen, M.; Reinikainen, S.-P.; Karjalainen, M.; Rantanen, J.; Louhi-Kultanen, M.; Nyström, L. *Analy. Chim. Acta* **2005,** 544, (1–2), 108.
107. Helland, I. S.; Naes, T.; Isaksson, T. *Chemometr. Intell. Lab. Syst* **1995,** 29, 233.
108. Crowley, K. J.; Zografi, G. *J. of Pharm. Sci.* **2002,** 91, (2), 492.
109. Chieng, N.; Rades, T.; Aaltonen, J. *J. of Pharm. Sci. and Biomed. Anal.* **2011,** 55, (4), 618.
110. Caron, V.; Tajber, L.; Corrigan, O. I.; Healy, A. M. *Mol. Pharma.* **2011,** 8, (2), 532.
111. De Gusseme, A.; Neves, C.; Willart, J. F.; Rameau, A.; Descamps, M. *J. of Pharm. Sci.* **2008,** 97, (11), 500.
112. Blagden, N.; Davey, R. J.; Lieberman, H. F.; Williams, L.; Payne, R.; Roberts, R.; Roweb, R.; Docherty, R. *J. of Chem. Soc., Fara. Tran.* **1998,** 94, (8), 1035.
113. Andronis, V.; Yoshioka, M.; Zografi, G. *J. of Pharm. Sci.* **1997,** 86, (3), 346.
114. Bianco, S.; Caron, V.; Tajber, L.; Corrigan, O. I.; Nolan, L.; Hu, Y.; Healy, A. M. *AAPS Pharm. Sci. Tech.* **2012,** 13, (2), 647.